Space Programs Summary No. 37-28, Volume III

for the period May 1, 1964 to June 30, 1964

The Deep Space Network

jpl

JET PROPULSION LABORATORY
CALIFORNIA INSTITUTE OF TECHNOLOGY
PASADENA, CALIFORNIA

July 31, 1964

Space Programs Summary No. 37-28, Volume III

for the period May 1, 1964 to June 30, 1964

The Deep Space Network

JET PROPULSION LABORATORY
CALIFORNIA INSTITUTE OF TECHNOLOGY
PASADENA, CALIFORNIA

July 31, 1964

Preface

The *Space Programs Summary* is a six volume, bimonthly publication designed to report on JPL space exploration programs, and related supporting research and advanced development projects. The subtitles of all volumes of the *Space Programs Summary* are:

Vol. I. The Lunar Program (Confidential)

Vol. II. The Planetary–Interplanetary Program (Confidential)

Vol. III. The Deep Space Network (Unclassified)

Vol. IV. Supporting Research and Advanced Development (Unclassified)

Vol. V. Supporting Research and Advanced Development (Confidential)

Vol. VI. Space Exploration Programs and Space Sciences (Unclassified)

The *Space Programs Summary,* Volume VI consists of an unclassified digest of appropriate material from Volumes I, II, and III and a reprint of the space science instrumentation studies of Volumes I and II.

W. H. Pickering, *Director*
Jet Propulsion Laboratory

Space Programs Summary No. 37-28, Volume III

Prepared under Contract No. NAS 7-100, National Aeronautics & Space Administration

Contents

I. Introduction

The Deep Space Network (DSN) is a precision communication system which is designed to communicate with, and permit control of, spacecraft designed for deep space exploration. The DSN consists of the Deep Space Instrumentation Facility (DSIF), the Space Flight Operations Facility (SFOF), and the DSN Ground Communication System (GCS).

The DSIF utilizes large antennas, low-noise phase-lock receiving systems and high-power transmitters located at stations positioned approximately 120 deg around the Earth to track, command and receive data from deep space probes. Overseas stations are generally operated by personnel of the respective countries. The DSIF stations are:

I.D. No.	Name	Location
11	Goldstone, Pioneer	Goldstone, California
12	Goldstone, Echo	Goldstone, California
13	Goldstone, Venus (R&D)	Goldstone, California
14	Goldstone, Mars (under construction)	Goldstone, California
41	Woomera	Island Lagoon, Australia
42	Canberra (under construction)	Canberra, Australia
51	Johannesburg	Johannesburg, South Africa
61	Madrid (under construction)	Madrid, Spain
71	Spacecraft Monitoring	Cape Kennedy, Florida

The SFOF is located in a three-story building at the Jet Propulsion Laboratory in Pasadena, California, and utilizes operations control consoles, status and operations displays, computers, data processing equipment for analysis of spacecraft performance and space science experiments, and communication facilities to control space flight operations. This control is accomplished by generating trajectories and orbits, and command and control data, from tracking and telemetry data received from the DSIF in near real time. The SFOF also reduces the telemetry, tracking, command and station performance data recorded by the DSIF into engineering and scientific information for analysis and use by the scientific experimenters and spacecraft engineers.

The DSN Ground Communication System consists of: voice, normal and high data rate teletype circuits provided by the NASA World-Wide Communications Network between each overseas station and the SFOF; and teletype and voice circuits between the SFOF, Goldstone stations and Cape Kennedy, and a microwave link between the SFOF and Goldstone, provided by the DSN.

The DSN has facilities for simultaneously controlling a newly launched spacecraft and a second one already in flight and, within a few months, will be able to control simultaneously either two newly launched spacecraft plus two in flight, or the operations of four spacecraft in flight at the same time. The DSIF is equipped with 85-ft antennas having gains of 53 db at 2300 Mc and a system temperature of 55°K, making it possible to receive significant data rates at distances as far as the planet Mars. To improve the data rate and distance capability, a 210-ft antenna is under construction at the Goldstone Mars Station and two additional antennas of this size are scheduled for installation at overseas stations.

It is the policy of the DSN to continuously conduct research and development of new components and systems and to engineer them into the DSN to maintain a state-of-the-art capability.

The DSN is a NASA facility, managed by JPL through a contract between NASA and the California Institute of Technology. The Office of Tracking and Data Acquisition is the cognizant NASA office.

II. Tracking Station Engineering and Operations

A. Project Engineering

1. Surveyor

The command and data console (CDC) at the Pioneer site has been checked out and temporary cables laid to the DSIF. This enabled CDC/DSIF compatibility tests to be carried out during the latter half of June 1964. A prototype version of the *Surveyor*/CDC system tester has been installed adjacent to the CDC and will be used to simulate the spacecraft during these tests.

A series of tests was recently made at Goldstone to obtain experimental data on:

(1) Best procedure for first acquisition of *Surveyor* by the DSIF.

(2) Typical times involved in carrying out this procedure.

For this purpose, the *Surveyor* S-band test transponder was installed in a helicopter together with a suitable power supply and antenna. A flight path was developed for the helicopter which simulated the first pass of *Surveyor* at Johannesburg. This was varied slightly during the tests in order to simulate a variation in time and azimuth of first visibility.

The helicopter flight path was adjusted to give an effective angular tracking rate of about 0.06 deg/sec, which is the maximum rate expected for *Surveyor*. The transponder transmitter power output and the Goldstone Duplicate Standard (GSDS) transmitter power output were adjusted to present signal power levels at both receivers which were typical of the levels expected during an actual mission.

On each run, the helicopter pilot gave an estimated "10 sec to go" call before he appeared above the local horizon, and this point was used as the starting point for the subsequent acquisition procedure given in Table 1. The times taken to accomplish each step of the acquisition procedure are given in Fig. 1. Of the 16 runs made by the aircraft, acquisition was not completed on Runs 1, 2, and 4 due to procedural confusion. In all remaining cases, the procedure was completed and two-way lock established in less than 3 min. On Runs 7 through 16, Event 3 was omitted as it proved possible to lock the ground

Table 1. Acquisition procedure 1

Step	Servo 1	Servo 2	Exciter	Receiver 1	Receiver 2
1	On point (aided track mode)	On alert at switchover panel (servo on Receiver 2)	(Transmitter on SAA)	Search low half of spectrum (receiver on SAA)	Search high half of spectrum (receiver on SAA)
2				If Receiver 1 acquires first, VCO information is used by Receiver 2 to acquire	Acquires spacecraft *Mark 1*
3	When Receiver 2 is in lock, switches to automatic *Mark 2*		Switches Receiver 1 from SAA to SCM	Acquires spacecraft on SCM	
4		Switches servo from SAA to SCM when Receiver 1 AGC voltage is approximately 2.5 to 3.0 v greater than Receiver 2 AGC *Mark 3*			
5			Starts frequency search, stops when receivers drop lock *Mark 4*		
6	Switches to aided track when receivers drop lock	Switches servo to Receiver 2			Reacquires spacecraft *Mark 5*
7	When Receiver 2 is in lock, switches to automatic *Mark 6*			Reacquires spacecraft *Mark 7*	
8		Switches servo from SAA to SCM when Receiver 1 AGC voltage is approximately 2.5 to 3.0 v greater than Receiver 2 AGC *Mark 8*			
9			Switches transmitter from SAA to SCM *Mark 9*		

transmitter on to the transponder receiver with the servo in auto-track on the SAA antenna.

Fig. 1 also shows that, on most runs, Event 7 was accomplished before Event 5; i.e., Receiver 1 on the S-band Cassegrain monopulse (SCM) feedhorn and bridge system could be locked up before Receiver 2 on the SAA. This may have been due to higher operator efficiency or to the stronger signal available from Receiver 1 connected to the SCM.

It is also apparent that the longest time between events occurred between Event 6 and Event 8 corresponding to the operation of switching from auto-track on the S-band acquisition aid (SAA) to auto-track on the SCM. This depends on the tracking performance in the SAA mode and requires that the angle error be sufficiently small to be within the S-curve of the SAA mode before the transfer can be made.

These tests were made with the full GSDS S-band configuration which includes two receiver channels and two angle channels. Further tests will be required to evaluate the constraints of the L- to S-band configuration at Johannesburg.

2. *Pioneer*

Meetings were held at JPL with Ames and STL at which times detailed information was furnished on DSIF receiver characteristics, cable requirements, rack

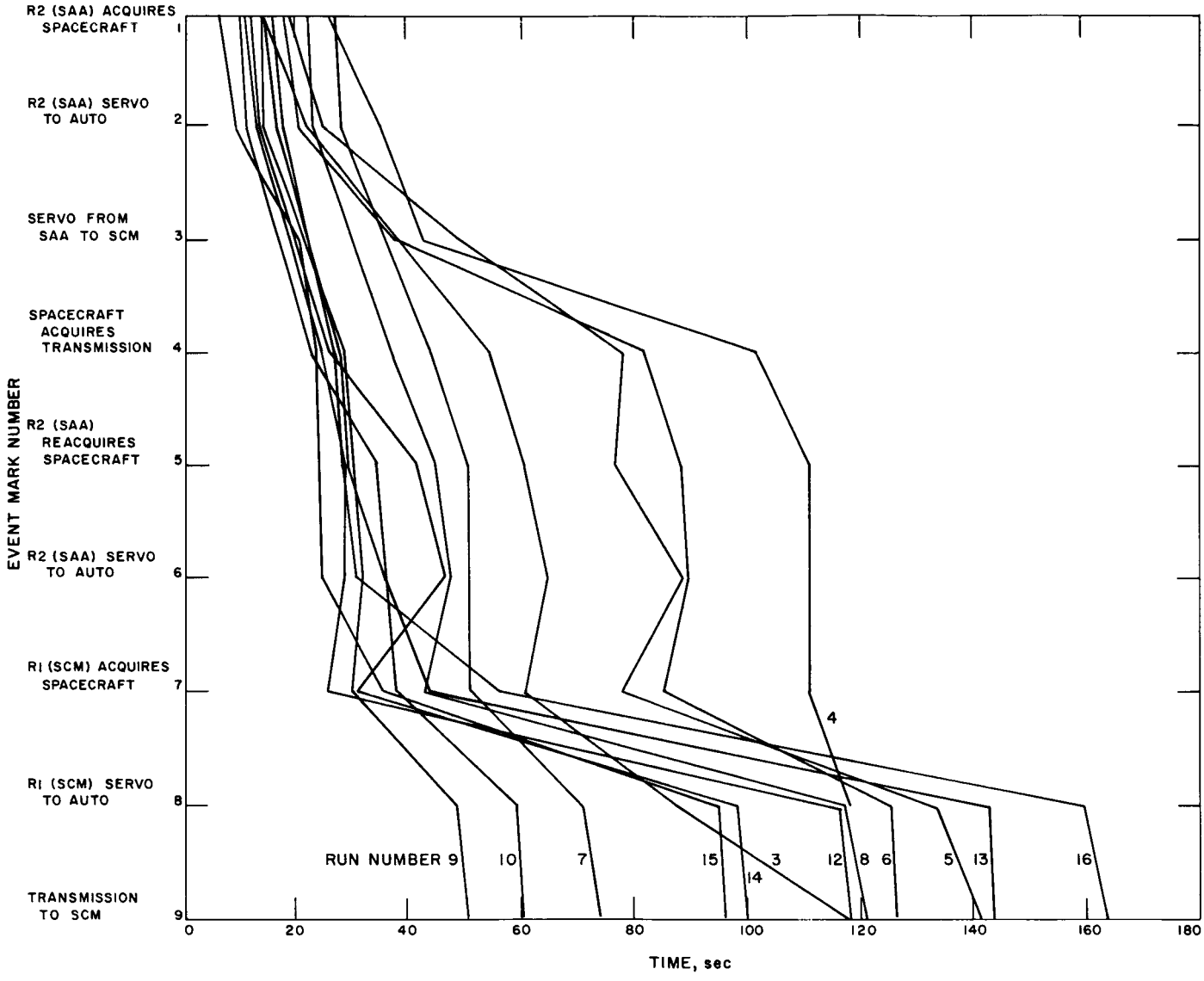

Fig. 1. *Surveyor* transponder tests: acquisition time versus event mark number

installation, exhaust ducting, primary power, computer and recorder characteristics, and radio frequency interference (RFI). The information provided will be formally transmitted to Ames in the form of minutes of the meeting.

The location of the Ames/*Pioneer* equipment at Goldstone is now planned to be in the main control building in the area adjacent to the *Surveyor* equipment. Installation problems are under study.

Loan of the S-band feasibility model receiver to STL for compatibility testing has been rescheduled for September.

An Ames/*Pioneer*–DSIF interface document (prepared by Ames) has been received and is under review.

3. *Ranger* Block III

The effect at L-band of the presence of the S-band cone and acquisition feed has been investigated and the resulting gain changes and pointing error appear to be negligible. The DSIF *Ranger* Block III interface organizational support equipment (OSE) functional specification has been updated with the most recent performance numbers and will be available for the *Ranger* 7 mission.

4. Mariner C

The DSIF/*Mariner C* telecommunications compatibility tests were conducted at Goldstone in late May and early June 1964. (See B, "Systems Analysis," for details.)

5. Lunar Orbiter

A series of meetings was held during the weeks of May 11 and May 18, 1964, with technical representatives of Langley Research Center and the Boeing Company. The primary purpose of these meetings was to introduce the Lunar Orbiter Project (LOP) personnel to the DSIF philosophy, design, and operations.

B. Systems Analysis

1. DSIF/Mariner C Tests

Compatibility tests were conducted at Goldstone during the period from May 25 to June 10, 1964, between the DSIF S-band ground system and the *Mariner C*, type approval model radio system.

The tests were conducted over a signal path link between the Pioneer site and the Goldstone Spacecraft Test Facility.

The objectives of the tests were to evaluate the performance of the *Mariner C* telecommunication system operating with the DSIF S-band system. The performance of pertinent ground equipment such as the read–write–verify (RWV), the teletype encoder, the receiver and transmitter, the ranging subsystem, and the telemetry demodulator and decommutator was evaluated; and calculated system parameters such as threshold signal strengths and carrier modulation losses were verified.

The majority of the tests indicated nominal performance. The results after the data reduction and evaluation will be reported in a subsequent *SPS*.

2. Suitcase Telemetry System

The systems study of the suitcase telemetry feasibility experiment has been completed and is undergoing review.

3. Mariner C Occultation Experiment

Systems analysis support is being given to the Communications Elements Research Section of JPL in the preparation of the DSIF systems design for this experiment. Simulation of spacecraft signal dynamics and resultant ground system response and the determination of the expected phase jitter of the S-band doppler extraction subsystem are under investigation. Tests are to be continued after the *Ranger 7* launch schedule.

4. Station Control and Monitor Console: Phase II

A program is underway to provide a station control and monitor (SCAM) console at the DSIF Stations to display information for the station manager that will provide him with an over-all evaluation of the station S-band system performance. This information should provide an indication of nonstandard situations which would be detrimental to the performance of the station and acquisition of data.

Phase II of this program has now been initiated to expand the capability of the Phase I SCAM. This will involve the utilization of the on-site digital instrumentation system (DIS) to monitor specific station and spacecraft parameters, to analyze these data, and to provide a continual assessment of station status and performance.

Phase II is being conducted in two parts:

(1) A systematic study of requirements including:
  (a) The determination of the required system parameters.
  (b) Methods for calculating system performance from observables.
  (c) Methods of comparison with predicted values including alarm requirements.

(2) Program implementation including:
  (a) DIS computer programming.
  (b) Hardware procurement (printer, etc.).

5. L-band Calibration

A description of an active calibration program of the L-band RF system was given in a previous *SPS*. Under Phase I of that program, the present DSIF L-band ground radio subsystem parameter values are listed as follows:

a. Antenna, diplexer, and feed lines. Antenna gains and temperatures given in the following tabulation are

measured at the output of the feed or microwave bridge and are given for right-hand circular polarization. Diplexer losses are given through the respective transmit or receive leg. Line losses include line between feed and diplexer, and between feed/diplexer or feed, and low-noise amplifier or transmitter.

Station	Parameter	Nominal	Tolerance
11 (Pioneer)	Receiving gain, db	45.7	±0.8
	Receiving axial ratio, db	0.7	±0.3
	Receiver line loss, db	0.3	±0.2
	Antenna temperature, °K	33	±8
12 (Echo)	Receiving gain, db	45.7	±0.8
	Transmitting gain, db	45.2	±0.9
	Receiving axial ratio, db	0.7	±0.3
	Transmitting axial ratio, db	1.3	±0.1
	Receiver diplexer loss, db	0.25	±0.05
	Transmitter diplexer loss, db	<0.05	
	Receiver line loss, db	0.3	±0.2
	Transmitter line loss, db	0.6	±0.2
	Antenna temperature, °K	33	±8
DSIF 41[1] and DSIF 51 (Woomera and Johannesburg; GSDS feed)[1]	Receiving gain, db	43.7	±0.9
	Transmitting gain, db	41.9	±0.9
	Receiving axial ratio, db	2.7	±0.1
	Transmitting axial ratio, db	3.0	±0.4
	Receiver diplexer loss, db	0.25	±0.05
	Transmitter diplexer loss, db	<0.05	
	Receiver line loss, db	0.3	±0.2 −0.0
	Transmitter line loss, db	0.6	±0.2
	Antenna temperature, °K	43	+0 −10
DSIF 59 (Mobile Tracking Station)	Receiving gain, db	25.8	±0.75
	Transmitting gain, db	26.4	±0.6
	Receiving axial ratio, db	0.6	±0.3
	Transmitting axial ratio, db	2.7	±0.3
	Receiver diplexer loss[2], db	0.4	±0.1
	Transmitter diplexer loss[2], db	0.4	±0.1
	Receiver line loss[2], db	0.4	±0.1
	Transmitter line loss[2], db	0.4	±0.1
	Antenna temperature, °K	100	±20

[1]A slightly modified tracking feed will be utilized at DSIF 41 (Woomera) to provide support for other programs (Blue Scout Junior). Its performance will be at least that of the GSDS feed.

[2]Based on total line and diplexer loss of 0.8 ±0.2 db for both transmitting and receiving.

b. System noise temperature and figure. Temperatures and gains are given in the following tabulation:

Station	Parameter	Nominal	Tolerance
DSIF 11 (Pioneer)	Cold sky system noise temperature, °K	95	+35 −15
DSIF 12 (Echo)	Cold sky system noise temperature, °K	110	±30
DSIF 41 and DSIF 51 (Woomera and Johannesburg)	Cold sky system noise temperature, °K	240	+25 −65
DSIF 59 (Mobile Tracking Station)	System noise figure, db	7.2	+0.5 −1.2

c. Typical receiver system threshold. Measurements are given in the following tabulation:

Station	Parameter	Nominal	Measurement
DSIF 11 and DSIF 12 (Pioneer and Echo)	System threshold with cold sky condition (20 cps $2B_{I.O}$), dbm	−165.0	±1.5
DSIF 41 and DSIF 51 (Woomera and Johannesburg)	System threshold with cold sky condition (20 cps $2B_{I.O}$), dbm	−162.0	±1.5
DSIF 59 (Mobile Tracking Station)	System threshold with cold sky condition (20 cps $2B_{I.O}$), dbm	−155	±1.5

A calibrated transmitter signal source, for use as a power level standard, has been sent to the overseas sites for calibration and evaluation of the various systems. Through the use of this calibrated signal source, Johannesburg detected and corrected a discrepancy in their receiver calibration. This error was caused by an improperly shielded test transponder, which is normally used for the receiver calibration. In an effort to reduce system errors and to maintain accuracy of the receiver calibrations, the calibrated transmitter will be periodically shipped to the various overseas stations and used for signal level reference.

C. System Engineering and Integration

1. Venus Site 100-kw Mariner C System Status

a. RF and microwave. A detail block diagram has been prepared for the exciter; all major components, modules, test equipment, power supplies, etc., have been ordered. The exciter system fabrication and assembly is on schedule. The power amplifier-cone assembly has been delivered. All modification work on the power supply, heat exchanger, and control circuitry has been completed.

b. RWV command unit. The command unit assembly has been ordered and is scheduled for delivery to Goldstone by November 20, 1964.

c. System instrumentation. A tape recorder and multichannel test recorder are being arranged to provide instrumentation of the *Mariner C* transmitter system.

d. General. All phases of the program implementation are on schedule.

2. Mission-Dependent Equipment (MDE) Transfer Rack

The Project Implementation Plan and the functional specification for the transfer rack have been written and submitted for management review. This rack will be utilized to provide a rapid transfer of DSIF connections from one program to another. The *Pioneer* prototype MDE transfer rack is scheduled for completion in September 1964.

3. System Documentation

a. System Signal Interface Document. Work is continuing on the compilation of data for the system cable interface document. A new method of presenting the information has been devised and is currently being implemented. Each connector from any subsystem that is used as system interface is being compiled on a separate sheet identified by the rack assembly number and the jack number on that rack. Each pin of the connector is identified along with its function and a simplified schematic representation of the circuitry to which the connector is attached.

b. Operational Procedures Manual. A DSIF Operational Procedures Manual, designated DZW-1000-OP, was published and distributed on May 20, 1964. Its purpose is to provide a standard instruction and reference document for all mission-independent procedures in use throughout the DSIF. The manual consolidates those redundant procedures which, in the past, have appeared in various internal documents for each planned mission.

c. Documentation standards. Work is in progress to establish documentation standards for the DSIF. These documentation standards (hardware) fall into two separate areas: that of defining the framework of documentation requirements and that of defining the specific requirements for the S-band system. The documentation system will be further described in future issues of the *SPS*.

Reference designations have been assigned to all major S-band equipment units. Equipment layouts have been completed for the Pioneer staging area, Butler building, Canberra control room, Pioneer and Canberra hydromechanical building, and antenna upper and lower electronics rooms. A systems documentation block diagram for the Canberra Station is being revised.

The DSIF procedure for cable identification has been revised to reflect current systems designation information (DSIF-STD 1001-C). JPL Specification 8913, a general requirements specification for DSIF cabling and wiring, is being reviewed for comments made by cable fabricators. A systems interconnecting cable diagram is being prepared. A control document for the preparation of test plans for subsystem testing is undergoing final review.

In its initial issue, the Operational Procedures Manual comprised an Introduction and eight separate procedures, similar to chapters. Listed below are brief descriptions of the eight standard procedures:

(1) General Information: describes the organization and functions of the DSIF.

(2) Data Requirements: outlines the data requirements of each station, and of the SFOF, for a typical mission.

(3) Standard Reporting: prescribes the procedures to be used by the DSIF in reporting mission information to the SFOF and JPL.

(4) Standard L-Band Acquisition and Tracking: provides detailed instructions for acquisition and tracking of a spacecraft using present day L-band hardware.

(5) Standard L-Band Recording: establishes typical recording procedures and channel utilization for standard L-band operation.

(6) Labeling and Shipment of Data: furnishes explicit instructions for preparing mission data for shipment to the SFOF.

(7) Communications: furnishes a general description of the DSN Communications System, and includes some procedures particularly applicable to the DSIF.

(8) Voice Communication: regulates and standardizes the techniques to be used.

Later issues of the manual will contain S-band acquisition, tracking, and recording procedures as the procedures become firm.

4. DSIF Reliability Program

A DSIF Failure Review Board has recently been organized for reviewing and initiating corrective action on all critical DSIF failures. The board meets biweekly and consists of five permanent members, with specialists being called as consultants as the need arises.

At the present time, all operational DSIF Stations are reporting equipment failures on a weekly basis. Reports are analyzed and follow-up action initiated by the DSIF reliability engineer. A monthly failure report summary is generated and distributed to all DSIF cognizant engineers.

A number of GSDS equipments have demonstrated high failure-rate histories. Trouble and failure reports have pointed out a number of DSIF units with recurring failures.

a. CEC oscillographs. Over the past 3 yr, the CEC 5-123 oscillograph has demonstrated an exceptionally high failure rate. Frequent loss of drive transmissions, lamps, and galvanometers has been reported at all stations. Equipment redesign is underway to correct these areas.

b. Coaxial connectors. The reliability of DSIF coaxial connectors is presently under survey. Failure reports indicate that the major reasons for connector loss or damage are improper assembly and failure to gage all connectors fabricated at the stations. Gages have been requisitioned, and an instruction program is being outlined to teach technicians and engineers the correct methods to be used for coaxial connection manufacturing.

5. DSIF Quality Assurance Program

A three-point DSIF quality assurance program has been established providing for: (1) initial vendor inspection, (2) in-process inspection, and (3) receiving inspection of DSIF hardware. The program allows responsibility of quality assurance to be retained by the DSIF cognizant engineers.

Quality assurance inspection of DSIF hardware is provided by the JPL System and Procedures Group. After receiving a request from a DSIF cognizant engineer, the quality assurance group conducts inspections of prospective vendors' facilities, evaluating both equipment and procedures and estimating the capability of the vendor to adequately produce reliable equipment. A vendor survey report is given to the cognizant engineer.

Two full-time inspectors at Goldstone are currently providing inspection services on the backlog of newly arriving DSIF hardware.

6. DSIF Standards Laboratory Program

A project implementation plan for a DSIF Standards Program was published and has been approved. A comprehensive program was presented for establishment and operation of a certified DSIF primary standards facility and an operational secondary facility at Goldstone. A series of secondary standards facilities located at all other DSIF Stations was also recommended.

Authorization was given and implementation has begun for the DSIF Primary and Secondary Facility located at Goldstone.

This facility has the responsibility for certifying the integrity of all operating secondary standards equipment and for providing the services of test equipment repair and calibration. Overseas Stations Facility will be implemented at a later date.

7. Spacecraft Test Facility

The Phase I version of the Goldstone Spacecraft Test Facility was completed on May 22 as scheduled, and was immediately occupied by *Mariner C* personnel preparing for DSIF compatibility tests. The facility consists

of a 12- by 18-ft shielded enclosure with a 12-ft ceiling height, erected toward one end of a reinforced 60- by 30-ft concrete pad (Figs. 2 and 3).

The associated facilities are:

(1) Air conditioning: 5-ton capacity, electrically filtered.

(2) Power: 120/208 v, 60 cycles, three phases each of 25-amp capacity, filtered and terminated inside the enclosure.

(3) Communications outside enclosure: one phone plus 30-pair cable terminations.

(4) Communications inside enclosure: one phone, one data line plus intercom to Pioneer Butler building, Pioneer control room, and Pioneer collimation tower.

A 4-ft-diameter antenna is mounted on a 20-ft tower adjacent to the enclosure and connected to it by a 40-ft length of ½-in.-diameter Spiroline. The Pioneer collimation tower carries two back-to-back S-band antennas: one directed toward the Pioneer DSIF antenna and the other toward the test facility.

Table 2. Summary of test results

P_{in}, dbm	P_T = 0 dbm		P_T = 30 dbm		P_T = 40 dbm	
	P_RAV, dbm	L_PAV, db	P_RAV, dbm	L_PAV, db	P_RAV, dbm	L_PAV, db
−0	−108	108	−108	108	−109	109
−10	−117	107	−117	107	−118.5	108.5
−20	−127	107	−126.6	106.6	−128.5	108.5
−30	−138	108	−136.6	106.6	−138.5	108.5
−40	−149	109	−147.3	107.3	−149	109
−50	−161	111	−157.3	107.3	−159	109
−53	—	—	−160.6	107.6	−162	109
−56	—	—	−164	108	−164.5	108.5
−57	—	—	−164.5	107.5	−165.5	108.5
−58	—	—	−165.5	107.5	−166.5	108.5
−59	—	—	−166	107	—	—
−60	—	—	—	—	—	—

Average total path loss = −108.0 db
Gain of GSDS antenna = +53.0 db
Average net path loss = −161.0 db
P_T = transmitter power, dbm
P_{in} = power input to Spiroline termination, dbm
P_RAV = average power received at DSIF receiver, dbm
L_PAV = average path loss, db

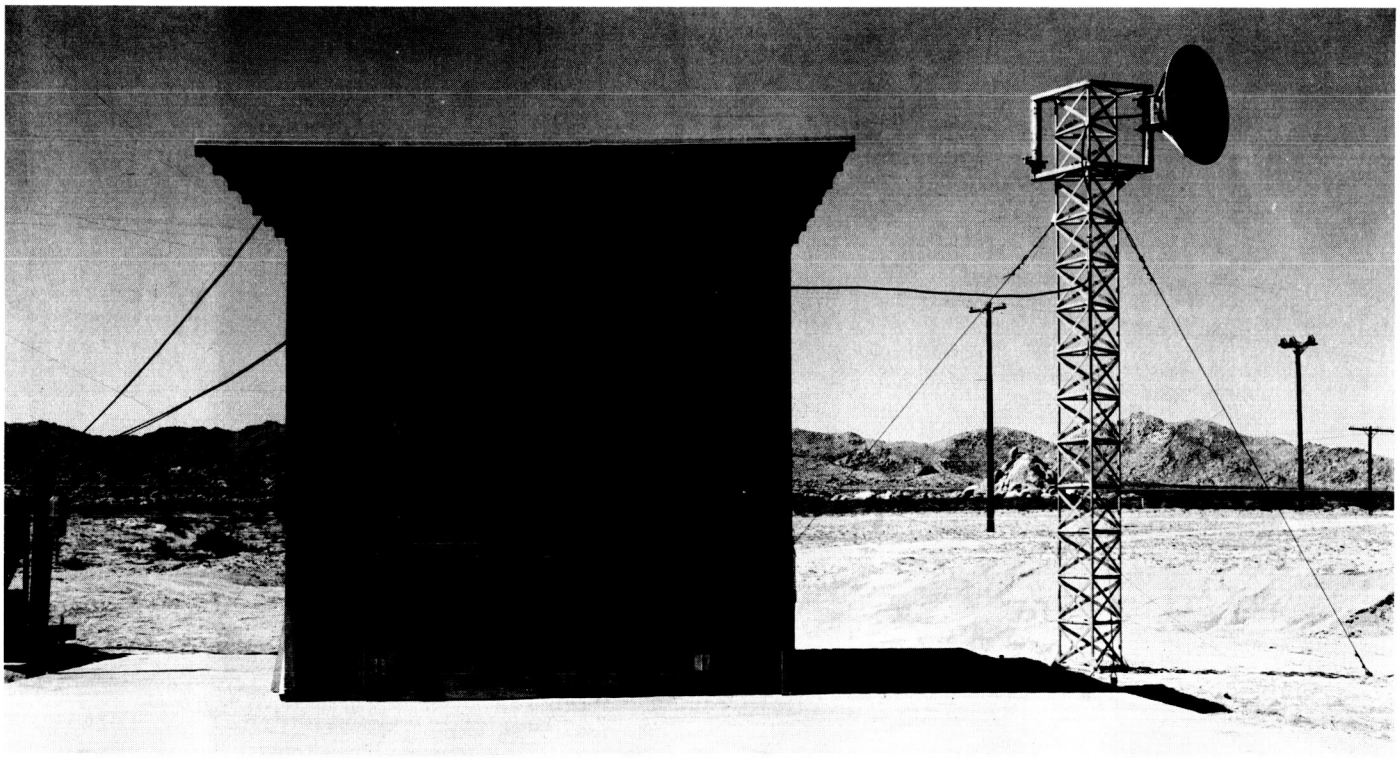

Fig. 2. Spacecraft Test Facility

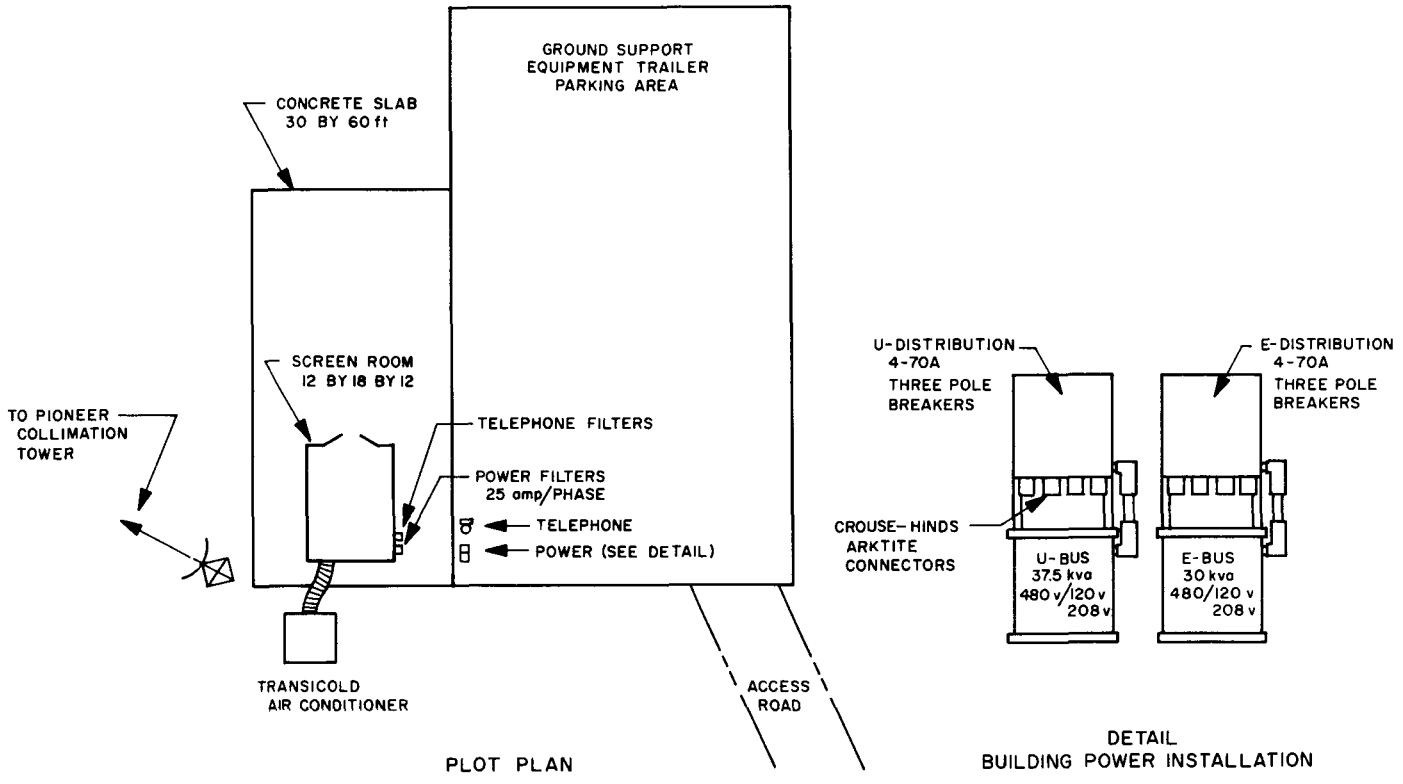

Fig. 3. Plot plan of Spacecraft Test Facility

The facility was designed to simulate planetary space loss of 260 to 270 db between a spacecraft transmitter and the DSIF antenna, when used in conjunction with a 50-db pad and up to 60 db of variable attenuation inside the enclosure.

The following tests were conducted to verify the performance of the facility. Signal sources at various power levels were connected through suitable attenuators to the Spiroline terminal inside the enclosure. The attenuation was increased in 10-db steps until the DSIF receiver threshold was reached and the system dropped out of lock. The following data were recorded:

(1) Transmitter power (P_T).

(2) Power input to the Spiroline termination (P_{in}).

(3) AGC voltage recorded at the Pioneer receiver (V_{AGC}).

(4) Power received at the maser input (P_R).

The results are summarized in Table 2. These show that the average net path loss between the Spiroline termination at the test facility and the GSDS antenna is 161 db. The attenuation inside the enclosure between the transmitter and the line termination depends on the transmitter power. With a 10-w transmitter and 100-db attenuation, the power received at the Pioneer site was below the receiver threshold. The total loss in the transmission path under these conditions was 261 db.

The power received at the maser input is plotted as a function of input power at the Spacecraft Test Facility (Fig. 4).

The phase stability of the re-radiated signal from the collimation tower was checked by locking up the receiver and putting the servos in the auto-track mode at a signal level of −138 db. The servos retained lock satisfactorily, although further tests of this kind are needed to further substantiate these data. In particular, two-way lock tests with a transponder are required. (*Mariner C* tests will provide these data.)

The DSIF exciter was energized and a signal transmitted from the Pioneer site to the test facility. The

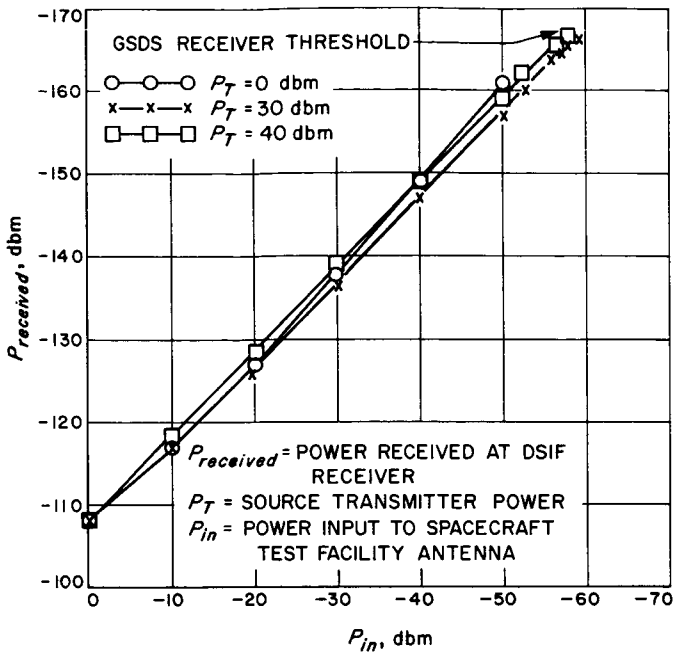

Fig. 4. Radio path calibration

received signal strength was measured with the following results:

Power transmitted, dbm	+34
Power received, dbm	−75
Total path loss, db	109
DSIF antenna gain, db	51
Total net path loss, db	160

This agrees with the net path loss measured in the other direction within the limits of experimental error.

These test results are considered to verify the feasibility of this approach to the problem of simulating lunar or planetary space loss. Further testing under more rigidly controlled conditions with accurately calibrated antennas and attenuators is required to establish the exact path loss and its variation with time. The influence of atmospheric conditions along the radio path and effect of vehicles moving on the roadway are also factors to be considered.

A demonstration of the requirements for a screen room at the Spacecraft Test Facility was provided by setting an output level from the test transmitter in the screen room so that the DSIF transmitter at the Pioneer site was at threshold. A signal level approximately 30 db stronger than the threshold level was measured, when the door to the screen room was opened.

Testing will continue as soon as the *Mariner C* tests are complete. The present enclosure will be expanded to the 20- by 20- by 18-ft size required for *Surveyor*.

8. Spacecraft Monitoring Station

A Project Implementation Document applicable to the Spacecraft Monitoring Station was completed and is undergoing review.

D. Goldstone Operations

The major installation of Pioneer site S-band equipment was accomplished during the latter part of April, and operational testing of subsystems, integrated as a complete system, was performed in May and June. The change in the *Ranger 7* launch date allowed additional time for Echo site technical personnel to assist at Pioneer, and for a longer test period on the Canberra Cassegrain cone and hyperbola installed on the Echo antenna. Concurrently, installation and testing of the *Surveyor* ground support equipment progressed to an advanced stage, and the Echo L-band equipment for *Ranger 7* continued to be maintained in operational readiness.

1. Equipment

a. Pioneer site. With the bulk of the first S-band system contained in the S-band annex building (Ref. 1), operational and interface testing is progressing. In general, the tests have been conducted on the radio frequency subsystem (transmitter and receiver), the ranging subsystem, the telemetry equipment, and the command read–write–verify (RWV) equipment. Miscellaneous tests have also been conducted on other subsystems and assemblies as required. In addition to the system operation testing and subsystem interface correlation, the S-band system has been tested for compatibility with the spacecraft transponder. Tests involving the use of the antenna and the S-band servo equipment were conducted using a spacecraft transponder installed in a helicopter.

The screen room, formerly located near the base of the Echo collimation tower (Ref. 2), was moved to a new location near the Goldstone Antenna Range site. A microwave link,using back-to-back antennas on the Pioneer collimation tower, linked the spacecraft equipment in the screen room (Fig. 5) to the Pioneer antenna. Essentially, the tests were to determine the compatibility of the S-band system with the *Mariner C* equipment. A *Mariner C* transponder and associated data handling equipment were used in the tests, which included acquisition, two-way lock, telemetry data transmission, and receipt of and simulated action to command signals transmitted from Pioneer. Two major tests were conducted:

(1) Operation of the Mark I ranging subsystem with the S-band system and the spacecraft.

(2) Telemetry Mode I data transmission interfaces from the spacecraft engineering data encoder, through Pioneer to SFOF, and over the data ground lines.

The RF subsystem tests are performed at various signal levels down to threshold. The operational testing of the subsystem includes functional operation of the ranging equipment and the command modulation. Some panel rearrangement has been made as a result of these tests; however, the final configuration of the S-band system is well established.

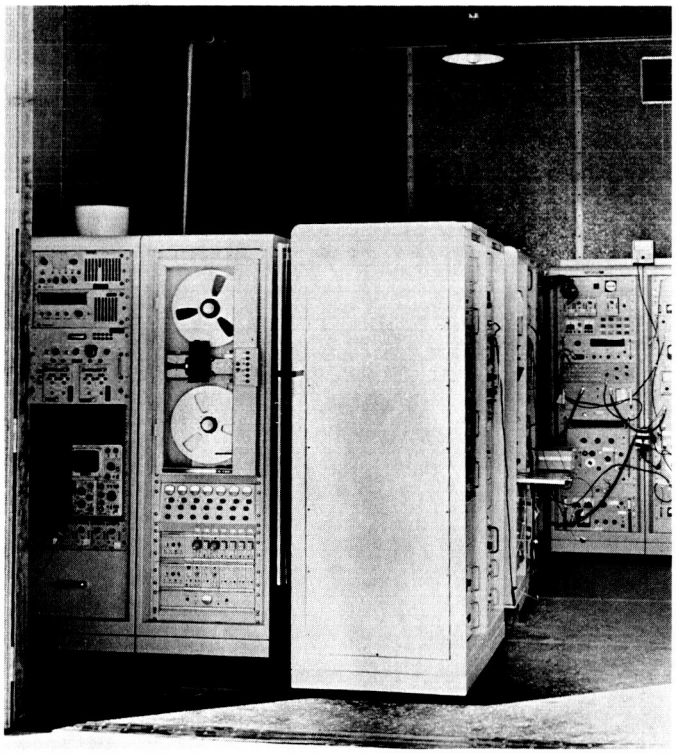

Fig. 5. *Mariner* C spacecraft test equipment in screen room

The first traveling wave maser/closed cycle refrigerator assembly has been accepted, and maser personnel have performed a cold/warm/cold recycle to demonstrate local maintenance capability. Goldstone and overseas maser personnel, for additional operator/maintenance experience, are participating in all S-band system tests involving the maser and parametric amplifier.

Ancillary equipment has been tested with the transmitter and receiver during simulated trackings using the helicopter. System tests and testing of individual subsystems and assemblies have been performed concurrently. Overseas equipment is integrated into these tests; after complete operational testing and performance evaluation, the satisfactory equipment is shipped to the various stations. Extensive testing has been done on the command RWV subsystem and the Mark I ranging subsystem, which continue to be tested as part of the over-all system tests.

Two schools attended by Goldstone and overseas personnel were:

(1) FR-1400 Recorder School conducted by manufacturer representatives at Echo during the first 2 wk in May.

(2) *Mariner C*, Mission-Dependent, Ground Telemetry School which began on May 11 and is currently in session. Part of the curriculum includes participation in the S-band campatibility tests.

Addition testing space became necessary for completion of the overseas S-band systems. An additional interim building (Fig. 6), the Manned Space Flight Net (MSFN) annex, has been erected west of the MSFN wing on the Pioneer control building. Initially, the annex will be used for S-band system tests of overseas scheduled equipment. Upon completion of the S-band tests, it will be used to house and test the equipment which will be used for the Manned Space Flight Program.

b. Venus site. The 100-kw capability of the Venus site will be used to provide command transmissions for the *Mariner C* vehicle (Ref. 3). The Cassegrain cone assembly (Fig. 7), which contains the final 100-kw klystron power amplifiers, has arrived at Goldstone and will be tested on the Venus antenna. The DSIF/*Mariner*

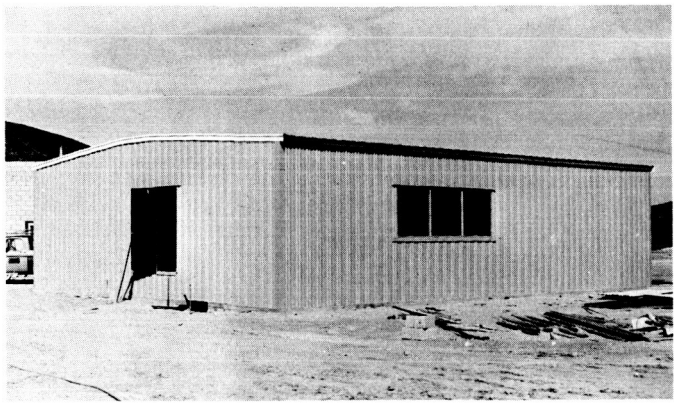

Fig. 6. MSFN annex building

transmitter system is designed as a self-contained assembly, independent of the Venus site except for the use of the high-voltage power supply to the 100-kw klystrons. Removal of the Venus 2388-Mc cone and installation of the *Mariner C* 2115-Mc cone, or vice versa, is planned to take approximately 6 hr.

Trailer-mounted teletype telemetry monitoring equipment, for use during net integration and operational readiness tests and the *Ranger 7* mission, was installed near the Echo control building. Essentially, this equipment will monitor and record the quality of the teletype telemetry transmitted from the Echo site to the Space Flight Operations Facility (SFOF).

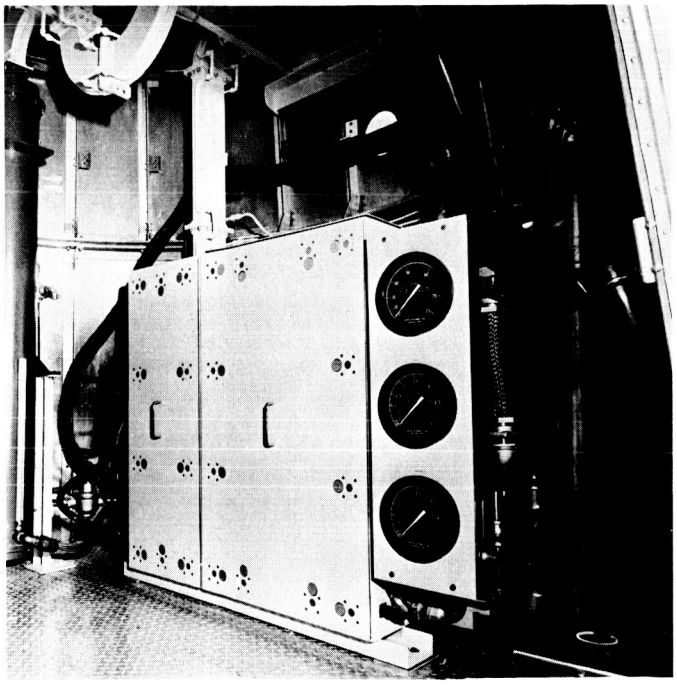

Fig. 7. *Mariner* C 100-kw transmitter in cone

Operational readiness of the RCA video equipment for *Ranger 7* is being maintained, with some internal equipment modifications already accomplished. No major changes, however, have been necessary. Interface and compatibility tests with the L-band receiver were started in June and will continue until the *Ranger 7* mission is completed.

In the interim period between the *Ranger 6* flight and extensive preparations for *Ranger 7*, the Echo antenna was used for tracking feed tests and Canberra Cassegrain cone and hyperbola tests. The tracking feed tests included operational testing of the auto-track subsystem. One L-band dispersion test of the tracking feed, with the S-band cone in place on the antenna, was conducted to determine the cone's effect on the tracking performance.

2. Surveyor Project

a. Pioneer site. Installation of the *Surveyor* ground support equipment has been completed (Fig. 8), and assembly and subsystem operational and interface tests are in progress. Interface testing with the Pioneer S-band system began during the last 2 wk of June. A system tester, received in May, provides means for testing the compatibility of both *Surveyor* and the Pioneer S-band systems by injecting simulated spacecraft signals into the Pioneer antenna. The transponder, included as part of the system tester, was used for the helicopter tracking tests of the S-band system due to its capability of performing a two-way lock condition.

The *Surveyor* ground support equipment provides a control room capability for command control of the *Surveyor* spacecraft and receipt of telemetry data and video transmissions from the vehicle during flight and after the lunar landing. The command function provides for transmitting spacecraft commands via punched tape or manual keyboard, the latter to be used only in emergencies. Full functions of the DSIF/SFOF will be used for all transmitting, receiving, and data handling for the *Surveyor* Project.

3. Construction

a. Pioneer site. Construction of the S-band and the MSFN wings on the control building is advancing rapidly. The aerial view in Fig. 9 shows the progress made since

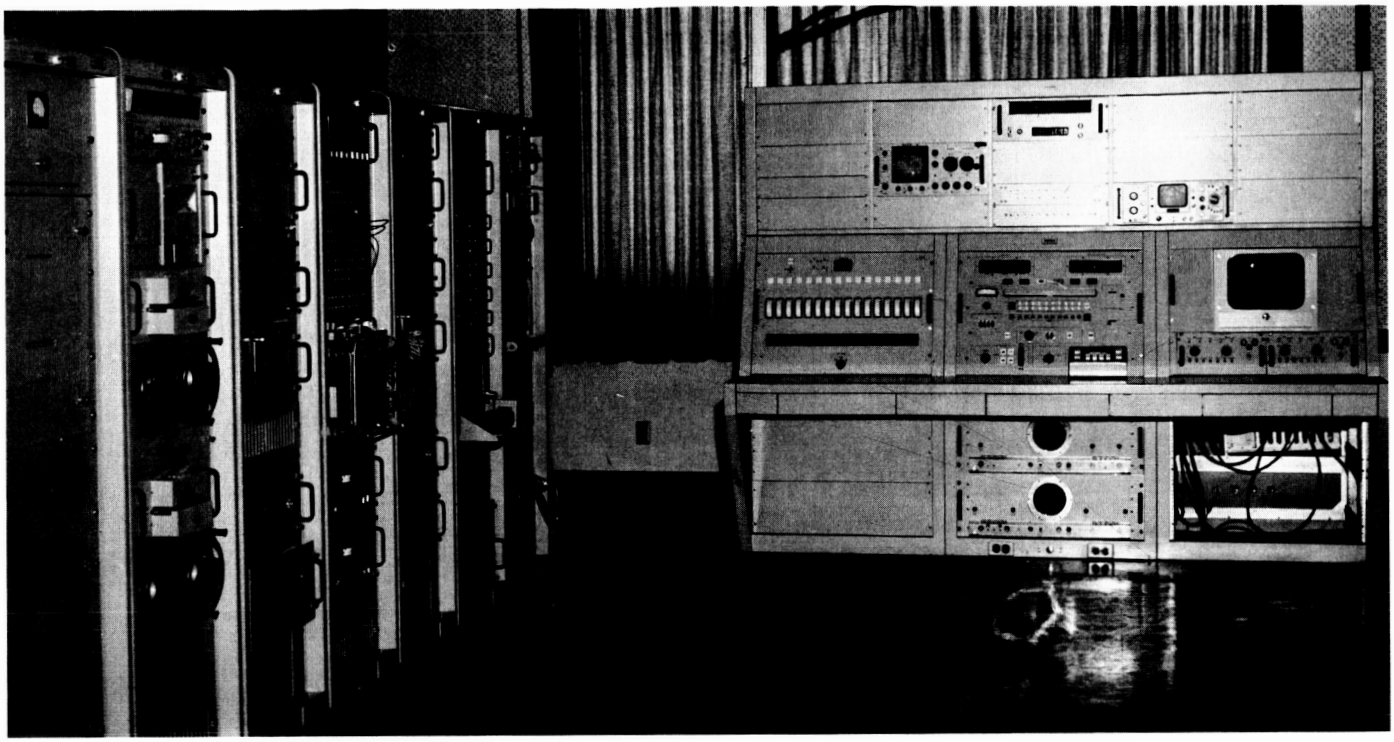

Fig. 8. *Surveyor* equipment control room

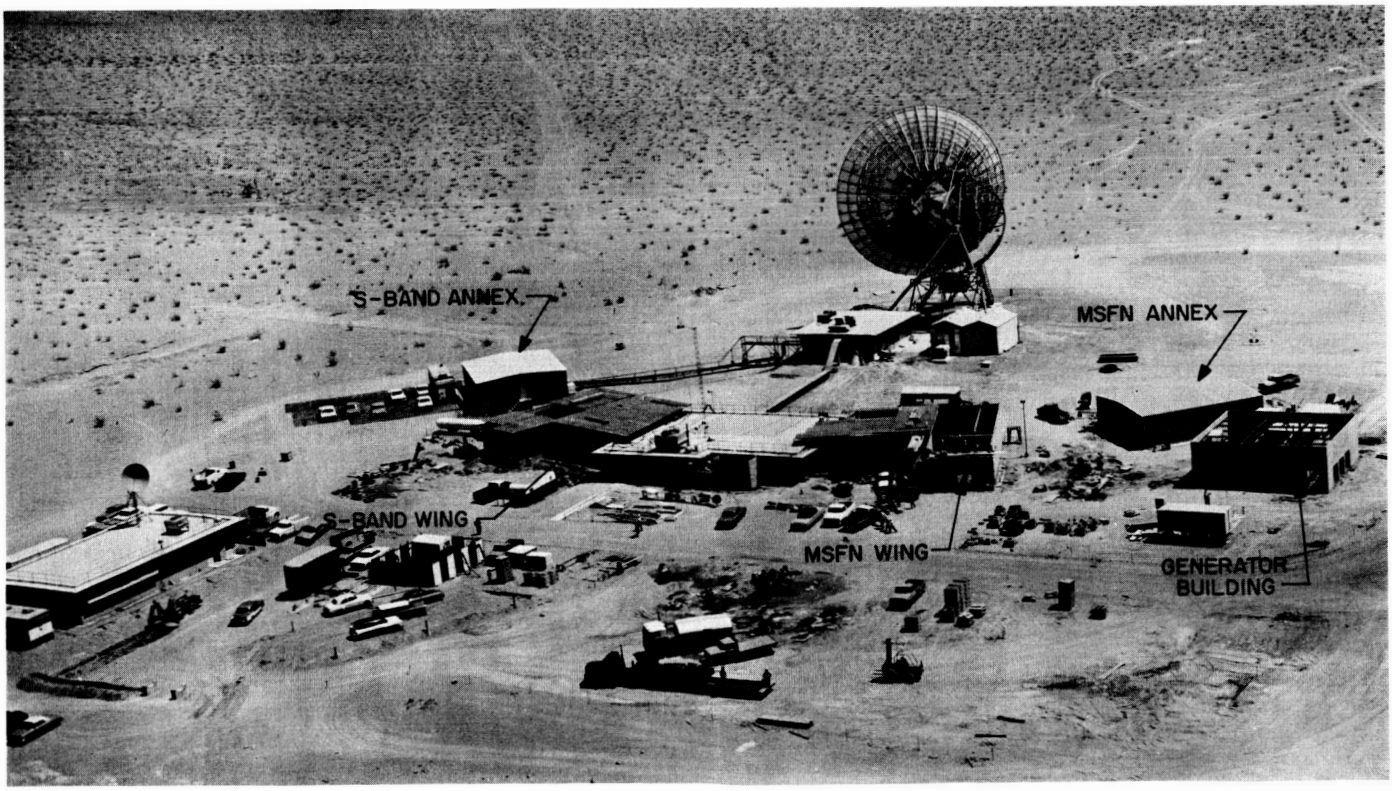

Fig. 9. Construction progress on control building wings

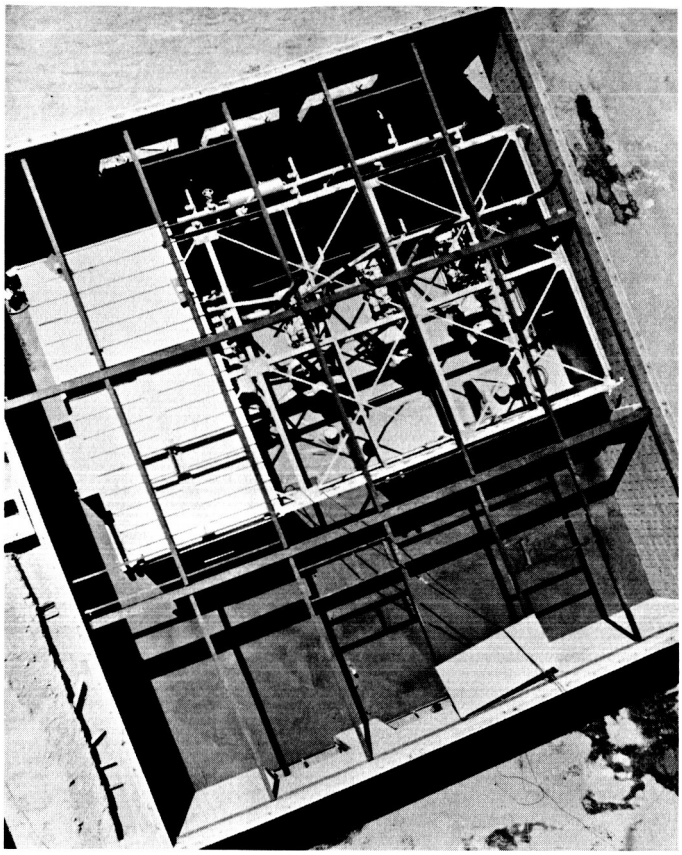

Fig. 10. Generator building constructed around current building

the previous report (Ref. 1). The MSFN annex (Fig. 6) is nearing completion with equipment installation scheduled to begin during the latter part of July. The new generator building, being constructed around the present building (Fig. 10), is approximately 65% complete.

b. Venus site. Installation of elevators in the transmitter building in order to allow ground testing of Cassegrain cone equipment is progressing satisfactorily. The elevator pits are being prepared for installation of the hydraulic hoists.

E. Determination of Geocentric Locations of DSIF Stations

This report presents the results of the latest determination of exact geocentric locations of the DSIF Stations positioned around the Earth. A re-evaluation of the accuracy of existing locations was prompted recently by NASA's adoption of a unique ellipsoid for the figure of the Earth, the "Kaula" or "165" spheroid, also known as the "NASA Earth Model" spheroid. Changes in geocentric positions came not only from the Kaula adjustments, but also from new survey data (Refs. 4 and 5).[1,2] In order to fully understand the new determinations, a brief description of geodesy is necessary and is included herewith as an integral part of this report.

1. Geodesy and the Figure of the Earth

Theoretically, the Earth can be best represented by an ellipsoid of revolution or spheroid (that is, the figure formed by an ellipse rotated about its minor axis, as shown in Fig. 11). Thus, any slice parallel to the equator yields a circle and any meridian is an ellipse. This figure can be defined by two quantities: the semi-major axis, a, of the ellipse and its flattening, f; a is the radius of the equator and f shows how closely the ellipse approaches a sphere.

[1] See also *Minutes of the Meeting of NASA Earth Model* at Marshall Space Flight Center, May 4, 1961.

[2] Private Communication. Memorandum from W. M. Kaula to NASA Earth Model Committee, June 20, 1963.

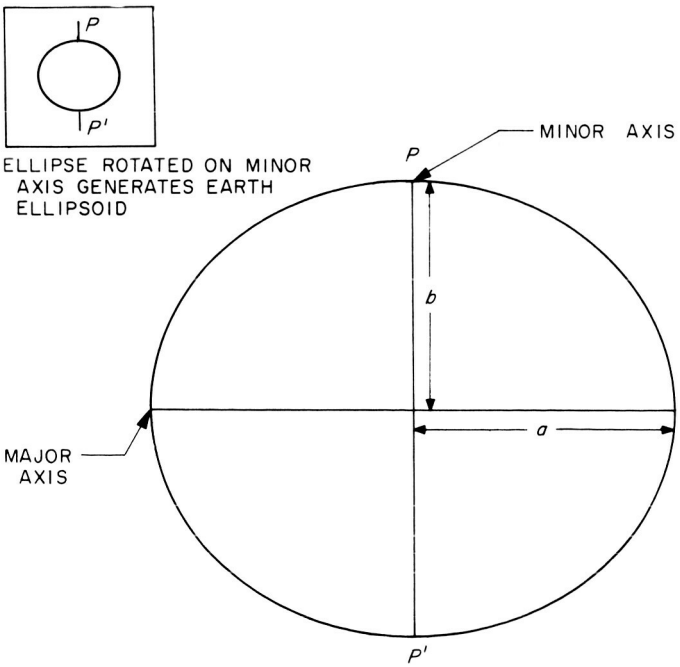

a = ONE-HALF OF THE MAJOR AXIS = SEMI-MAJOR AXIS
b = ONE-HALF OF THE MINOR AXIS = SEMI-MINOR AXIS
f = FLATTENING = $a-b/a$
PP' = AXIS OF REVOLUTION OF THE EARTH'S ELLIPSOID

Fig. 11. Elements of an ellipse

The representation of a point on the surface of the Earth is simply done by two angles (Fig. 12). Longitude is straightforward; latitude is slightly more complicated. In Fig. 12, the line PA is perpendicular to the ellipsoid at P. The angle it forms with the equator is called the geodetic latitude. This picture of Earth does not take into account the surface irregularities. However, one can include these by defining a third parameter, h, as the height above the spheroid. Thus, with three simple quantities, one can describe any point on the Earth. This is the simple theory, but it is not easily put into practice because the spheroid is a mathematical surface which does not correspond to any physical reality.

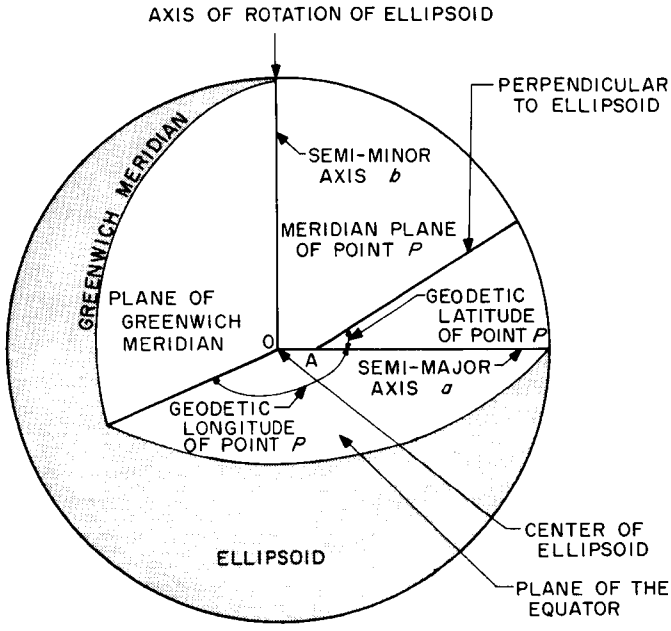

Fig. 12. Geodetic coordinates

In practice, the surveyor works with two surfaces: the spheroid, as described, and the geoid. The geoid is an equipotential surface where the force of gravity is equal to that at mean sea level. In other words, it would be the surface of the ocean if there were no continents. Due to the uneven mass distribution of the Earth, the geoid is an irregular surface and does not always correspond to the spheroid. Mass and gravity abnormalities cause geoid undulations, as seen in Fig. 13. Mass surpluses tend to pull the geoid up. Since the geoid is a gravity equipotential surface, the direction of gravity is always perpendicular to the geoid. As most leveling equipment is gravity oriented, the local vertical is perpendicular to the geoid. At any point, the angle between the normal to the geoid and the normal to the spheroid is called the deflection of the vertical. One should note that the deflection of the vertical is relative to the spheroid and will change if another spheroid is used.

The geoid, as one can see, is the physical reality that the surveyor must face. He determines the shape of the

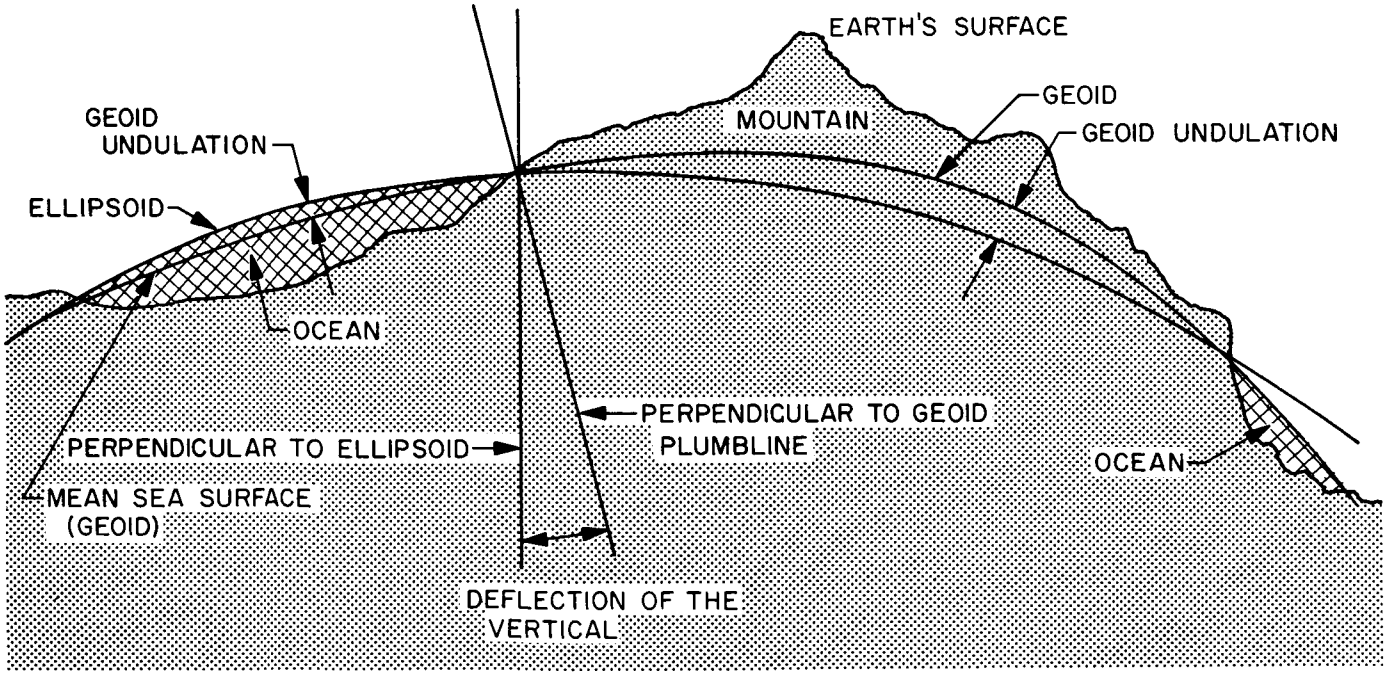

Fig. 13. Geoid/ellipsoid relationships

geoid by laying out survey nets either by triangulation, which consists of measuring the angles of juxtapositioned triangles, or by trilateration, in which the lengths of the sides of the triangles are measured. However, the surveyor must start with a known origin, called a datum. A datum consists of the latitude and longitude of the origin of an ellipsoid and of the geoid height at the origin. From the datum, the surveyor can compute by astronomic observations the deflections of the vertical at all his points. He then adjusts his origin by a least-squares fitting on the deflections. He thus obtains the spheroid which corresponds closest to the geoid (Fig. 14).

There are numerous datums throughout the world, the principal ones covering large areas such as the North American Datum or the European Datum.

There is one further problem with astro-geodetic datums in that their center of ellipsoid does not necessarily correspond to the center of the Earth (Fig. 15). This means that different datums are unconnected and offset from each other as well as from the center of the Earth. This makes it almost impossible to connect two points on two different datums with the accuracy needed for satellite tracking. A unified system is needed, and the Kaula system (adopted for the NASA Earth Model) meets the requirements. The unification is done in two steps:

(1) A best fitting ellipsoid for the entire Earth surface is determined. This is accomplished by measuring the curvatures of several long arcs and by satellite data. This center of ellipsoid is assumed to coincide with the center of the Earth.

(2) The principal datums are corrected and reoriented to be centered at the Earth's center. This is done by extensive gravimetric measurements. In the Kaula system, the adjustment is simply a translation of the ellipsoid center to the Earth's center without any rotation or change in the size of the ellipsoid.

This unified system allows computations of geocentric station locations which are consistent, since they are referenced to the same point. The station locations described herein are NASA Earth Model ellipsoid locations.

GEOID AND ELLIPSOID ARE ORIENTED SO THAT THE SUM OF THE SQUARES OF SEVERAL DEFLECTIONS OF THE VERTICAL SELECTED THROUGHOUT THE GEODETIC NETWORK IS MADE AS SMALL AS POSSIBLE

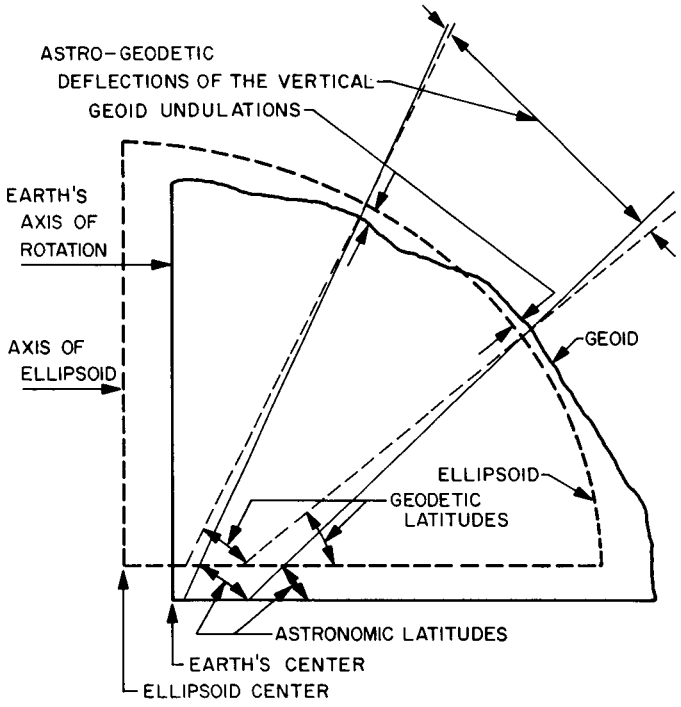

ORIENTATION OF ELLIPSOID CENTER WITH RESPECT TO EARTH'S CENTER

Fig. 14. Astro-geodetic datum orientation

2. *Positions of the DSIF Stations*

Table 3 presents the geodetic and geocentric positions of the DSIF Stations. All the positions refer to the center of rotation of the antenna (CORA), i.e., the intersection of the rotation axis, if it exists, or the intersection of the primary axis and the plane generated by the secondary axis. In the HA–Dec antenna, this is the intersection of the polar axis with the hour angle gear plane. The following is an explanation of the quantities in Table 3.

Column 1: DSIF Station number.

Column 2: Name and location of site.

Column 3: Diameter of parabolic dish.

Columns 4, 5: Geodetic latitude (ϕ_g) and geodetic longitude (λ_g). The latitude and longitude resulting from a mathematical transformation of the local surveying rectangular grid to an ellipsoidal coordinate system defined by the local datum. The local datum consists of an assumed ellipsoid and of the observed (and corrected) position of the true origin of the survey net.

Column 6: Height (h) The spirit level height above the local base mean sea level (i.e., above the geoid).

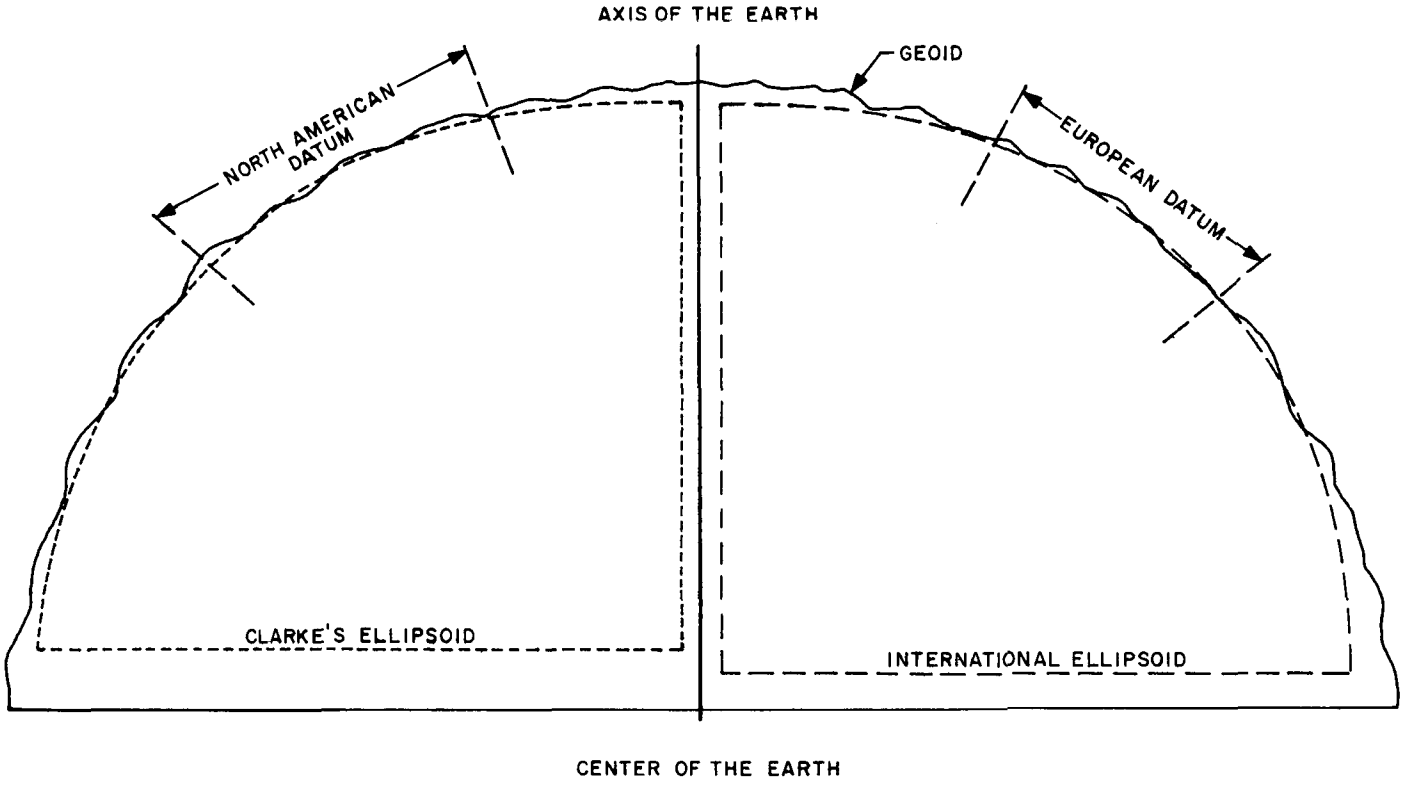

Fig. 15. The preferred datums are relative datums

Column 7: Geoidal height (N)

The height at the antenna of the local geoid above the assumed ellipsoid. This must be determined by detailed astrogeodetic survey.

Column 8:

The datums used are those given in Table 4. The symbols ΔX, ΔY, and ΔZ are the offsets required to move the center of the ellipsoid to the center of the Earth. The "165" ellipsoid is assumed to be centered at the Earth's center.

Columns 9–14: Geocentric position

The Earth centered coordinates of the stations were computed on an IBM 1620 in double precision, using the following equations:

$$e^2 = 2f - f^2$$

$$d = a(1 - e^2 \sin^2 \phi_g)^{-1/2}$$

$$x = (d + h + N) \cos \phi_g \cos \lambda_g + \Delta X$$

$$y = (d + h + N) \cos \phi_g \sin \lambda_g + \Delta Y$$

$$z = \left[d(1 - e^2) + h + N\right] \sin \phi_g \Delta Z$$

$$R_c = \text{geocentric radius} = (x^2 + y^2 + z^2)^{1/2}$$

$$\phi_c = \text{geocentric latitude} = \sin^{-1} \frac{z}{R_c}$$

$$\lambda_c = \text{geocentric longitude} = \tan^{-1} \frac{y}{x}$$

The axes are oriented with x in the direction (0°N, 0°E), y in the direction (0°N, 90°E), and z in the direction (90°N, 0°E). The geocentric latitude is positive north and negative south. Longitude is measured positive to the East.

Columns 15–17: Geodetic positions on NASA Earth model ellipsoid

The positions of the stations are referenced to the NASA Earth Model ellipsoid, the parameters of which are:

Semi-major axis = 6378165.0 m
Flattening = 1/298.3

These geodetic coordinates were computed on an IBM 1620 in double precision by dropping a normal from the geocentric position to the "165" ellipsoid. The height obtained is height above the spheroid.

a. Probable errors. All probable errors listed in Table 3 are simplifications of multi-digit numbers. Thus, 35.38950 ± 10 is meant to be 35.38950 ± .00010.

Table 3. Geodetic and geocentric positions of the DSIF Stations

Station			Local datum				
Station I.D.	Name	Size, ft	Geodetic latitude (°)	Geodetic longitude (°)	Height (m)	Geoid height (m)	Datum
1	2	3	4	5	6	7	8
11	Pioneer (Goldstone)	85	35.38950±10	243.15175±10	1037.5	−17±10	North American
12	Echo (Goldstone)	85	35.29986±10	243.19539±10	989.5	−17±10	North American
13	Venus (Goldstone)	85	35.24772±10	243.20599±10	1213.5	−17±10	North American
	Venus (Goldstone)	30	35.24725±10	243.20946±10	1201.3	−17±10	North American
14	Mars (Goldstone)	210	35.42528	243.12222	1150.0	−17±10	North American
41	Woomera (Australia)	85	−31.38314±5	136.88614±5	144.8	−15±15	Australian Central
42	Canberra (Australia)	85	−35.40111±5	148.98028±5	654.0	−15±16	Australian Central
51	Johannesburg (South Africa)	85	−25.88921±10	27.68570±10	1398.1	+ 7±14	Cape Kennedy
59	Mobile Tracking Station (South Africa)	10	−25.88563±10	27.70414±10	1543.8	+ 7±14	Cape Kennedy
61	Madrid (Spain)	85	40.4290	355.7510	800	−10±7	European
71	Launch (Cape Kennedy)	6	28.48713±10	279.42315±10	1.0	+ 5±9	North American

Geocentric position

	Spherical			Cartesian		
Station I.D.	Geocentric latitude (°)	Geocentric longitude (°)	Geocentric radius (m)	X (m)	Y (m)	Z (m)
1	9	10	11	12	13	14
11	35.20807 ± 24	243.15082 ± 24	6372034.1 ± 26.0	−2351417.9	−4645104.4	3673779.8
12	35.11863 ± 24	243.19446 ± 24	6372017.6 ± 26.0	−2350456.2	−4651994.8	3665638.8
13	35.06662 ± 24	243.20507 ± 24	6372259.9 ± 26.0	−2351183.3	−4655575.5	3661044.8
	35.06615 ± 24	243.20853 ± 24	6372247.8 ± 26.0	−2350911.1	−4655735.5	3660995.2
14	35.24377	243.12129	6372134.1	−2352813.1	−4641921.9	3677081.0
41	−31.21234 ± 26	136.88614 ± 26	6372531.7 ± 30.0	−3978574.5	3724890.2	−3302317.1
42	−35.21963 ± 26	148.98028 ± 26	6371668.6 ± 30.0	−4460904.9	268272.5	−3674619.6
51	−25.73876 ± 24	27.68559 ± 24	6375541.5 ± 26.0	5085470.9	2668300.5	−2768697.8
59	−25.73521 ± 24	27.70403 ± 24	6375695.2 ± 26.0	5084886.6	2670081.3	−2768407.9
61	40.2380	355.7505	6370086.8	4849350.9	−360325.1	4114847.2
71	28.32648 ± 24	279.42315 ± 24	6373291.3 ± 26.0	918518.6	−5534438.9	3024095.3

Geodetic position on NASA Earth model ellipsoid

Station I.D.	Geodetic latitude (°)	Geodetic longitude (°)	Height (m)
1	15	16	17
11	35.38951	243.15082	1000.5
12	35.29987	243.19446	952.4
13	35.24774	243.20507	1176.4
	35.24727	243.20853	1164.2
14	35.42529	243.12129	1113.0
41	−31.38314	136.88614	129.8
42	−35.40111	148.98028	639.0
51	−25.88957	27.68559	1425.3
59	−25.88599	27.70403	1578.0
61	40.4278	355.7505	870
71	28.48748	279.42315	−39.8

The probable errors given in Table 4 for ΔX, ΔY, and ΔZ are along the x-, y- and z-axes and are the major contributors to the error in these quantities. To find the probable errors of the geocentric spherical quantities, it was assumed that the errors in Kaula's offsets formed a sphere of error. The contributions from other causes were assumed minor. It was assumed also that the error in height was much smaller than the error in geoidal height (N). N is taken from free air geoid maps and the uncertainty is a measure of the interpolation errors.

The uncertainties given by Kaula for ΔX, ΔY, and ΔZ, although slightly optimistic, are probably a fair measure of the actual observation errors, but may neglect significant systematic errors due to incorrect adjustment of geodetic control connecting stations more than about 100 km apart.

The stations for which no uncertainties are given are approximate locations which will not become definite until the antennas are erected. The quantities listed under local datum (Columns 4–8) are the result of surveying done at the sites at different levels of accuracy. The following is a cursory examination of the basic survey at each station.

b. Goldstone.

Pioneer (DSIF 11) 85-ft HA–Dec. The coordinates presently in use are the results of a second-order survey contracted to Pafford and Associates in 1958. The survey originated at the first order points LEACH, Nelson, and IRWIN. Bollinger does not think that the survey was good second-order work, but in any case is no worse than third-order. Assuming third-order accuracy, the connection with the first-order net should be less than 10 to 15 ft in error. The nearest Pafford bench mark is at the Pioneer collimation tower; the survey to the antenna was done by JPL.

Echo (DSIF 12) 85-ft HA–Dec (P-4). The antenna was tied into the Pafford network by Bollinger.

Venus (DSIF 13) 85-ft Az–El. The preliminary location of the antenna was scaled from a topographic map before construction (coordinates unknown and no longer in use). After construction, a second-order survey from the first-order points Barstow (Lane Mountain) and Tiefort to the antenna was performed by a contractor. This survey is independent of the Pafford survey.

Venus (DSIF 13) 30-ft Az–El. The preliminary location of the antenna was scaled from a topographic map before construction. This location was approximately 2 sec in error in longitude. After construction, a second-order survey from the first-order point Barstow (Lane Mountain) and Tiefort to the antenna was performed by a contractor in connection with the survey to the Venus 85-ft antenna. This survey is independent of the Pafford survey.

All the geodetic coordinates are on the Clark spheroid of 1866. The error in the first-order net is not known.

There is presently in progress a first-order geodetic survey with astronomic observations and first-order leveling which will include all the antennas at Goldstone and four of the surrounding primary stations. At present, the elevations of the antennas are not well known. The location of the Mars station is preliminary.

c. South Africa (DSIF 51 and 59).

Triangulation. The survey marks of the DSIF 51 survey were coordinated by triangulation to third order trigonometrical control points. The locations of the collimation tower and the antenna were fixed by forward intersection only. The Mobile Tracking Station and

Table 4. Datums

Name of datum	Origin	Date of survey	Spheroid			Kaula's Offsets		
			Name	A(m)	1/f	ΔX(m)	ΔY(m)	ΔZ(m)
North American	Meades Ranch, Kansas	1927	Clarke 1866	6378206	295.0	−23 ± 26	+142 ± 22	+196 ± 22
Australian	"Maurice" net adjustment	1963	"165"	6378165	298.3	0 ± 30	0 ± 30	0 ± 30
Central Cape	Buffelsfontein, South Africa	1906	Clarke 1880	6378249	293.47	−109 ± 23	−70 ± 29	−289 ± 23
European	Potsdam, Germany	1924	International	6378388	297.0	−57 ± 23	−37 ± 29	−96 ± 23

Minitrack were coordinated to second- and third-order trigonometrical control points.

All observations were made with a Wild T-2, with the exception of the astronomical observations at the Mobile Tracking Station (T-3).

The internal consistency of the Hartebeesthoek survey is ±0.02 ft. The estimated probable errors in the survey are listed below.

From		To			
Station	Order	Station	Order	Distance, mi	Probable error, ft.
Cape Origin	First	Nooitgedacht I	First	1000	25-50 (10 m adopted)
Nooitgedacht I	First	Brit 22 and 44	Third	10	0.2
Brit 22 and 44	Third	Antenna	Third	1	0.05

Leveling. The level datum is Mean Sea Level (MSL) at the Cape. The leveling is of international precision leveling standard from the datum to Kruegersdorp, and by second-order vertical angle from Kruegersdorp to Brit 44. The elevation of the 85-ft antenna was obtained by vertical angles from Brit 44 to the collimation tower 7.2-ft mark and third-order leveling from the collimation tower to the antenna.

The level datum at Minitrack and the Mobile Tracking Station is "Peg A." This datum was set out by vertical angles from surrounding trigonometrical stations during the topographical survey and retained as the permanent datum in that area.

The internal leveling accuracy of the Hartebeesthoek survey is 2 in.

Probable error in leveling. Listed below are the probable errors in leveling in the topographical survey:

From	To	Method	Distance	Probable error, ft
Cape	Kruegersdorp	First order	1000 mi	2
Kruegersdorp	Brit 44	Second-order vertical angle	20 mi	0.5
Brit 44	Collimation tower	Third-order vertical angle	6550 ft	0.3
Collimation tower	"F"	Third-order level	5000 ft	0.05
"F"	Antenna	Second-order level	100 ft	0.01
Antenna	CORA	Vertical tape	50 ft vertical	0.08

Geodetic coordinates. The geodetic location of "Antenna Center" was computed from survey coordinates on the Clarke 1880 spheroid, Cape Datum. Calculations by two different methods and conversion tables yielded essentially identical results. The position of the reference point on the antenna [intersection of the polar axis and the plane of the hour angle gear, i.e., the center of rotation of the antenna (CORA)], was measured relative to T2296 to within 0.1 ft.

d. Woomera (DSIF 41). The area around Woomera is well surveyed, and has undergone survey covering a 120-mi² area extending north and west from Island Lagoon.

The original geodetic survey of Australia was done on the Clark 1858 spheroid with a Sydney origin. This is now known to be a poorly fitting, badly oriented spheroid which yields errors at Woomera on the order of 1200 ft.

The Australia Division of National Mapping has recently completed a new geodetic survey of Australia and has computed interim results based on 150 isostatically reduced La Place Stations. The adopted spheroid is the NASA "165" spheroid.

Preliminary results computed in 1962 were based on 54 La Place Stations with a mean error of ±0.″32 latitude and ±0.″15 longitude.

The estimated coordinates of the Maurice Trigonometric Station in South Australia were adopted as the origin for the 1962 computation.

In 1963, the coordinates of all the geodetic stations were reduced from a continental adjustment. The Maurice Station has now been given the corrected coordinates.

"165" spheroid: "Central" origin, 1963

Latitude: −32° 51′ 14.″015

Longitude: +138° 30′ 34.″102

The final reduction and official adoption of the new spheroid and origin is planned for 1965, but it is unlikely that the datum will be changed by future observation in Australia by ½ sec of arc in either coordinate.

On May 5, 1963, JPL adopted the "165-Central" position for the Woomera antenna. The coordinates were rigorously computed in September 1963.

The antenna was located by second-order triangulation to a nearby (2 mi) first-order line.

The MSL base is at Port Augusta. The elevation base for the Woomera range is at the Pimba railway station, 15 mi from the DSIF Station.

e. Canberra (DSIF 42). All the surveying for the DSIF project in Paddy's River Valley has been done relative to the false origin of the 1000-ft grid system. From the adopted coordinates of Tidbinilla trigonometric station, the coordinates of the Mount Stromlo geodetic station were calculated and the field survey run from Mount Stromlo into Paddy's River Valley. All survey work is done relative to the false origin, but the system is tied to the Stromlo Station. The error at the sites in the survey from Stromlo is less than ½ ft. The grid system is oriented by the Stromlo meridian on a plain projection at 2000-ft elevation above MSL. The preliminary antenna location was determined by adopting the "Central" coordinates for Stromlo and computing the offset to the antenna.

f. Madrid (DSIF 61). Approximate position was taken from a small scale topographic map. The location given is for site "K," the proposed first site.

g. Spacecraft Monitoring Station (DSIF 71). No information on the survey is available. The initial data listed is assumed to be the position on the North American Datum.

F. Stereographic Projection Generator and Stereographic Plotter

1. Introduction

In the past, the use of stereographic station projections has proved to be a valuable aid in visualizing tracking problems and analyzing space trajectory/antenna relationships. However, the production of originals for these projections for the DSIF Stations has always been a laborious and time-consuming task. Previously, parameters were computed and given to a draftsman, who in turn plotted the curves manually. With establishment of new DSIF antenna sites and the necessity for revisions on the older plots, it became clear that some means of simplifying and expediting the production of stereographic station projections was needed.

As a result, a Fortran Computer Program has been written for the SDS 920 computer to output (on magnetic tape) X–Y coordinates for the hour angle and declination angle intersections superimposed on the corresponding coordinates of the azimuth-elevation system for an arbitrary station location. The second half of the program reads the computed data from magnetic tape and automatically plots these intersections. An added feature is the capability of superimposing stereographic representations of probe trajectories on the plot.

2. Operation

a. Stereographic projection generator (Fig. 16). The stereographic projection generator program may be conveniently separated into three sub-programs: Az–El generator, HA–Dec generator, and the land mask portion. A control program, at the beginning, interrogates an IBM card for a negative, zero, or positive number which designates the desired program.

b. Negative, Az–El generator. The input information includes the file number, station number, angle type (Az–El), station latitudes, and a value called "check." "Check" controls the number of elevation circles generated. Computation is begun at azimuth equal to 0 deg and elevation equal to 0 deg. Elevation is then incremented at 5-deg intervals while azimuth is held constant. After incrementing each time, the date are output on magnetic tape and a comparison is made between elevation and "check." If equal, the elevation is reset to 0 deg, and the azimuth is increased 5 deg and so on until azimuth reaches to 360 deg, at which time the program control is transferred out of the Az–El generator and awaits a new program designator.

c. Zero, HA–Dec generator. The inputs to the HA–Dec generator are file number, station number, angle type (HA–Dec), station latitude, and two quantities, delta hour angle and delta inclination, which determine the spacing of the points. At the start of computation, the sine of station latitude is examined to determine the station hemisphere. Declination starts at 90 deg and is decremented by ΔDec until elevation becomes negative. At this time, hour angle is decremented by ΔHA and declination is reset to 90 deg. This procedure continues until all hour circles have been generated. Program control is then transferred out of the HA–Dec generator and awaits a new program designator.

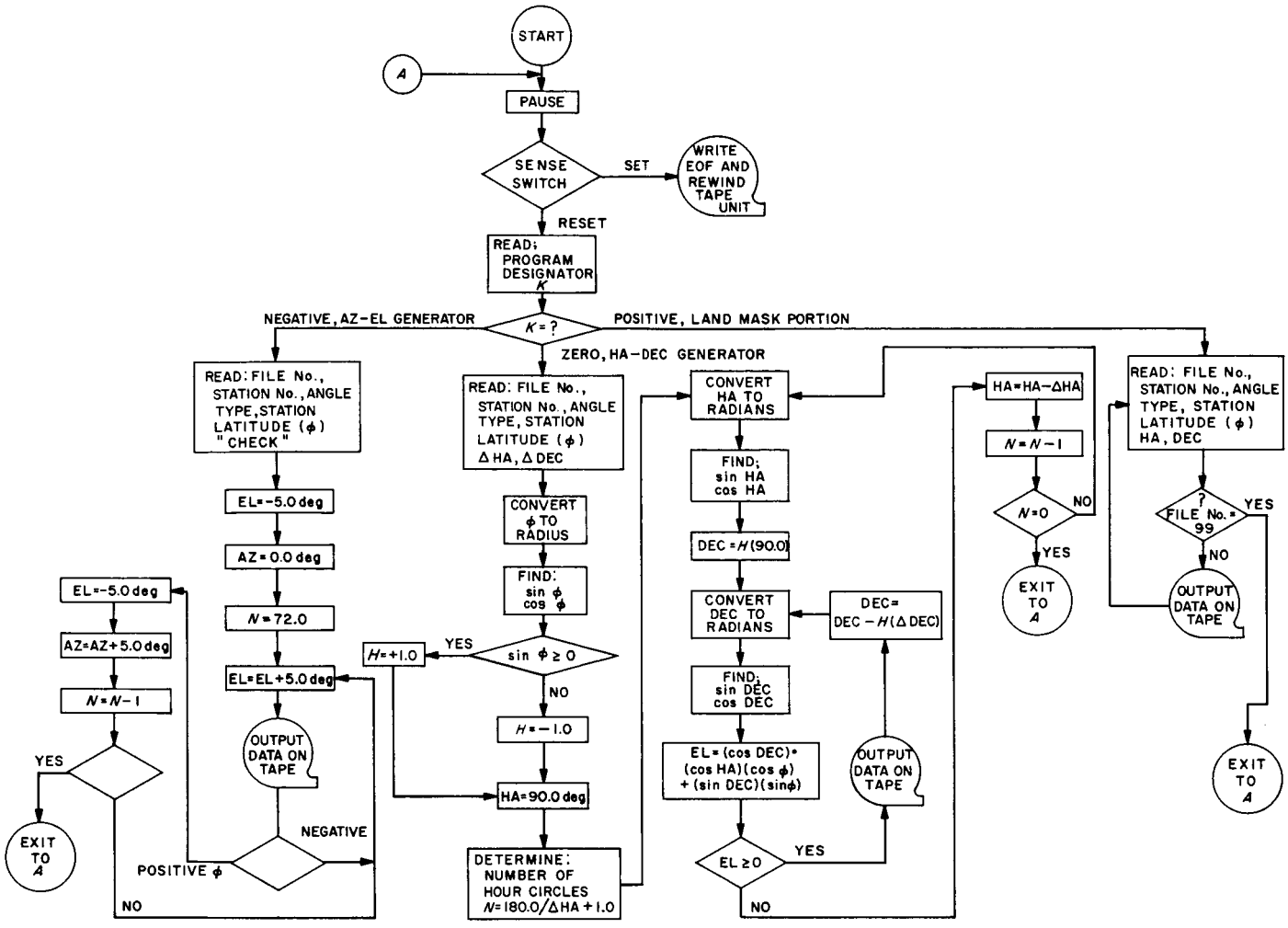

Fig. 16. Stereographic projection generator

d. Positive, land mask portion. The land mask portion simply reads IBM cards with manually punched data and writes the information on magnetic tape. To terminate the land mask portion, a card is inserted with 99 in the file number field which transfers control to the beginning of the program. When all computation is complete, a sense switch is set, causing an end-of-file to be written on the magnetic tape. The tape is then rewound.

e. Stereographic plotter (Fig. 17). The stereographic plotter program basically reads magnetic tape, converts the data to Baudot code, and automatically plots X–Y points. The program is initiated by two inputs: file number and the desired radius of the plot. Tape is read until the "actual" file number corresponds to the "input" file number. The angle type (Az–El or HA–Dec) is interrogated, after which the appropriate conversion routine is called to derive the desired X–Y coordinates. Now that a point has been computed, the plotter is tested for a ready signal. If ready, the point is examined for maximum magnitude. With all conditions met, the data is converted to the proper Baudot code, character for character, and is output to the plotter.

3. Equipment Facility

The computer complex used for this program is located at the Goldstone Space Communications Station, Echo site, and consists of:

(1) An SDS 920 computer, with a 4096-word memory and 24-bit word length.

(2) A Burroughs card reader.

(3) Two low-density tape units.

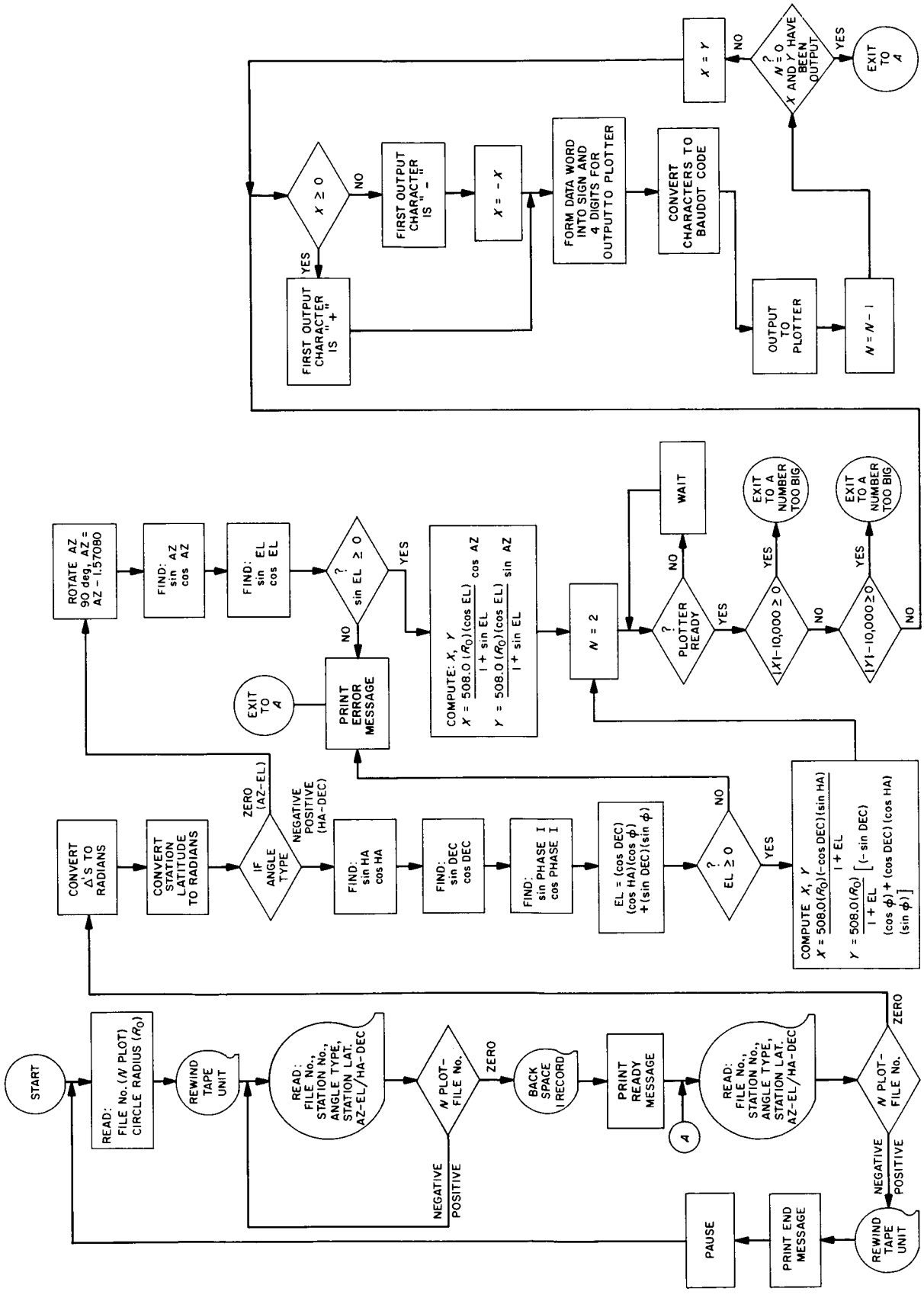

Fig. 17. Stereographic plotter

(4) Interface electronics to an on-line plotter.

(5) A Benson-Lehner, Model J, point plotter.

4. Other Capabilities

The capability of superimposing stereographic representations of probe trajectories on the plots has proven to be a valuable aid in preflight analysis of tracking problems. The trajectory program (Ref. 6) has been adapted for compatibility with the stereographic plotter program.

G. *Agena* Aspect-Angle Program

The function of this computing routine is to define the relationship of a DSIF Station's line-of-sight vector to the control axes of an attitude controlled *Agena* vehicle. Since the vehicle's transmitting antenna system is fixed relative to the control axes, this allows one to determine the orientation of the line-of-sight in the antenna pattern, and thus the expected signal strength.

The governing assumptions are:

(1) That the yaw axis is along the local vertical.

(2) That there is zero yaw angle of attack.

Two aspect angles are defined:

(1) PHA–angle between the roll axis and the negative line of sight.

(2) PSA–angle that the projection of the line-of-sight vector on the roll plane makes with the yaw axis, positive in the direction toward the positive pitch axis.

$$\cos(PHA) = -\frac{\boldsymbol{\rho}\cdot(\mathbf{R}\times\mathbf{V}\times\mathbf{R})}{\rho R^2 V\cos\Gamma}$$

$$\tan(PSA) = \frac{\boldsymbol{\rho}\cdot(\mathbf{V}\times\mathbf{R})}{(\boldsymbol{\rho}\cdot\mathbf{R})V\cos\Gamma}$$

where:

$\mathbf{R}$ = geocentric inertial radius vector of the vehicle

$\boldsymbol{\rho}$ = station-to-vehicle line-of-sight vector = $\mathbf{R} - \mathbf{r}_s$ ($\mathbf{r}_s$ = geocentric inertial radius vector of the tracking station)

$\mathbf{V}$ = geocentric inertial velocity vector of the vehicle

Γ = inertial path angle of the vehicle

ρ, R, V are corresponding absolute magnitudes.

The routine has been programmed in Fortran II and is composed of 47 Fortran statements including numerical checking commands.

References

1. "S-Band Construction", *SPS 37-27*, Vol. III, pp. 5–9, Jet Propulsion Laboratory, Pasadena, California, May 31, 1964.

2. "*Ranger* 6 Proof Test Model", SPS 37-25, Vol. III, p. 6, Jet Propulsion Laboratory, Pasadena, California, January 31, 1964.

3 "Klystron Amplifier Subsystem", *SPS 37-25*, Vol. III, pp. 18–19, Jet Propulsion Laboratory, Pasadena, California, January 31, 1964.

References (Cont'd)

4. Fischer, I., "An Astrogeodetic World Datum From Geoidal Heights Based on The Flattening $F = 1/298.3$," *Journal of Geophysical Research*, Vol. 65, No. 7, July 1960.

5. Kaula, W. M., "A Geoid and World Geodetic System Based on a Combination of Gavimetric, Astrogeodetic, and Satellite Data," *Journal of Geophysical Research*, Vol. 66, No. 6, (Note 702) June 1961.

6. "Trajectory Program for On-Site Computers," *SPS 37-25*, Vol. III, pp. 13–14, Jet Propulsion Laboratory, Pasadena, California, January 31, 1964.

III. Space Flight Operations Facility

A. SFOF Operations Group

The Space Flight Operations Facility (SFOF) operations group concentrated its efforts primarily in support of *Ranger* and *Mariner* tests. Orientation of personnel continued on a reduced scale, while the scheduling activities became more complex as the demands for SFOF support continuously increased. A support systems unit has been added to provide additional SFOF support capabilities.

1. SFOF Tests

The decision to move *Ranger* Block III flight operations to the SFOF resulted in a curtailment of the SFOF internal testing program. Commencement of *Mariner* testing closely followed that of *Ranger*, which made it necessary to integrate internal testing with these project tests. Operational use of equipment was evaluated and the requirements for reconfiguration were formulated. In several instances, equipment which had received satisfactory ratings in initial tests proved to be less than satisfactory until modifications were made. However, as a result of the *Ranger* and *Mariner* tests, the SFOF support of space flight operations is progressing rapidly and should be fully responsive to the requirements of the first actual space flight operations conducted in the SFOF.

2. Orientation of Personnel

Early in May the orientation program emphasis switched from mission-dependent and mission-independent personnel who will work in the SFOF to a public-information-type orientation slanted toward visitors, news media, and other outside groups. However, *Surveyor* project personnel have begun their orientation program, and their participation increased significantly toward the end of June.

3. Scheduling

The *Ranger* and *Mariner* testing programs have increased the scheduling requirements, since much of the

SFOF equipment is used by both projects and some testing is conducted concurrently. Rigid scheduling procedures have been mandatory in order to satisfy all the requirements placed on the SFOF.

4. Display

Display alterations have been held to a minimum considering the requirements of the many project tests. The capability to more easily display negative values and decimals has been added to the semiautomatic display boards in all areas. Requirements for certain parameters to be displayed were not firm, and several changes were required. The operations of the Eidophor projectors proved to be marginal, and steps were taken to more fully train display maintenance technicians to perform the more complicated repairs on this equipment. A program of modifying the remote time displays is in progress and is close to completion. This program is expected to result in more reliable operation.

5. Support Systems Unit

In order to improve the support that the SFOF operations group provides, a support systems unit was organized. It is the responsibility of this unit to provide the necessary assistance required in technical and operational areas of the SFOF in preparation for, and in support of, space flight tests and missions. This includes providing technical area assistants, establishing and maintaining access control to the operational areas of the SFOF, controlling the utilization of the SFOF, and other duties that may be necessary to ensure a smooth operation. Personnel have been assigned to this unit and have actively participated in the *Ranger* and *Mariner* tests. Training classes were conducted on the use and operation of equipment, standard operating procedures within the facility, and duties in each of the technical areas.

6. Other Support Activities

In order to bring the SFOF equipment and personnel to a *go* status, a check list system was initiated. This ensures that, with proper execution of the system, the SFOF will be ready to fully support an operation at any specified time. This check list system is an extension of the standard operating procedures program. An IBM card method was initiated for maintaining communications assignments and closed circuit television patching and switching. This same IBM card method was adapted to updating and printing an SFOF directory.

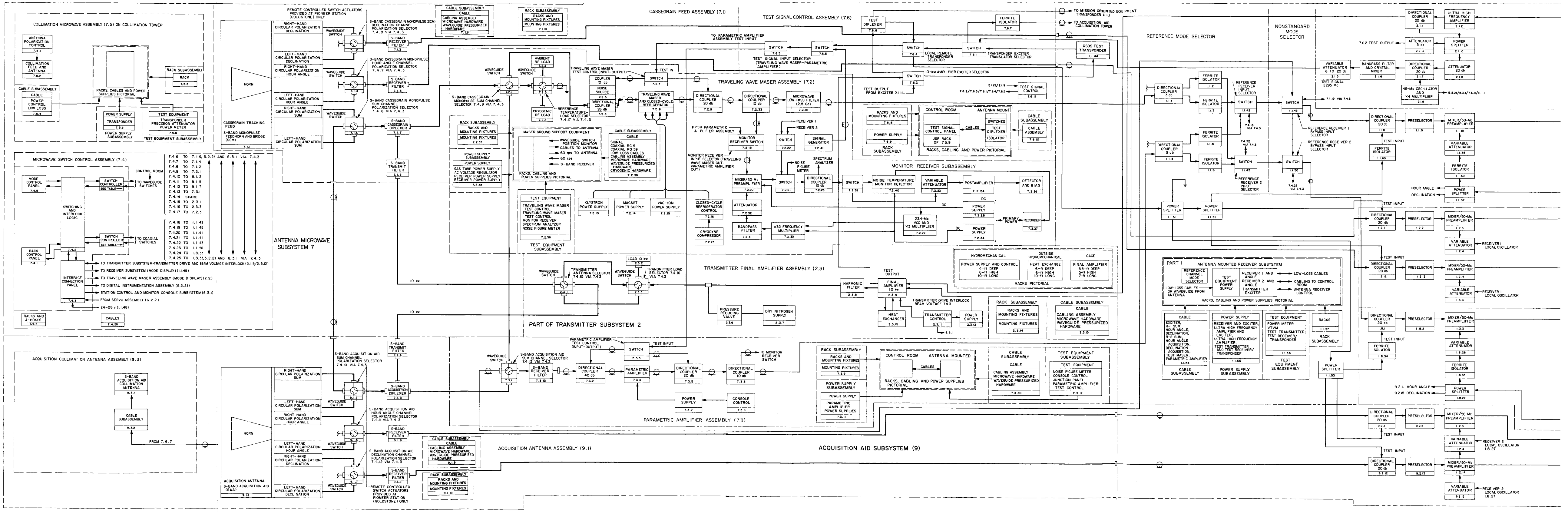
COLLIMATION MICROWAVE ASSEMBLY (7.5) ON COLLIMATION TOWER
ANTENNA POLARIZATION CONTROL 7.5.1
COLLIMATION FEED AND ANTENNA 7.5.2
CABLE SUBASSEMBLY
CABLE POWER CONTROL LOW LOSS 7.5.4
RACK SUBASSEMBLY
RACK 7.5.3
RACKS, CABLES AND POWER SUPPLIES PICTORIAL
POWER SUPPLY
TRANSPONDER 7.5.3
POWER SUPPLY SUBASSEMBLY
TEST EQUIPMENT
TRANSPONDER PRECISION ATTENUATOR POWER METER 7.5.5
TEST EQUIPMENT SUBASSEMBLY
MICROWAVE SWITCH CONTROL ASSEMBLY (7.4)
MODE CONTROL PANEL 7.4.3
SWITCH CONTROLLER (SEE TABLE)
CONTROL ROOM
TO WAVEGUIDE SWITCHES
SWITCHING AND INTERLOCK LOGIC
7.4.6 TO 7.1.5, 5.2.2† AND 8.3.1 VIA 7.4.3
7.4.7 TO 7.1.4
7.4.8 TO 7.1.2
7.4.9 TO 7.2.1
7.4.10 TO 9.1.2
7.4.11 TO 9.1.5
7.4.12 TO 9.1.7
7.4.13 TO 7.3.1
7.4.14 SPARE
7.4.15 TO 2.3.1
7.4.16 TO 2.3.3
7.4.17 TO 7.2.3
7.4.18 TO 1.1.42
7.4.19 TO 1.1.45
7.4.20 TO 1.1.41
7.4.21 TO 1.1.41
7.4.22 TO 1.1.43
7.4.23 TO 1.1.50
7.4.24 TO 1.8.33
7.4.25 TO 1.8.33, 5.2.2† AND 8.3.1 VIA 7.4.3
SWITCH CONTROLLER (SEE TABLE)
TO COAXIAL SWITCHES
INTERFACE CONNECTION PANEL 7.4.5
RACK CONTROL PANEL 7.4.1
RACKS AND J-BOXES 7.4.4
CABLES 7.4.36
TO TRANSMITTER SUBSYSTEM-TRANSMITTER DRIVE AND BEAM VOLTAGE INTERLOCK (2.1.5/2.3.12)
TO RECEIVER SUBSYSTEM (MODE DISPLAY) (1.1.49)
TO TRAVELING WAVE MASER ASSEMBLY (MODE DISPLAY) (7.2)
TO DIGITAL INSTRUMENTATION ASSEMBLY (5.2.21)
STATION CONTROL AND MONITOR CONSOLE SUBSYSTEM (8.3.1)
FROM SERVO ASSEMBLY (6.2.7)
24-28 v (1.1.48)
ANTENNA MICROWAVE SUBSYSTEM 7
CASSEGRAIN TRACKING FEED
S-BAND MONOPULSE FEEDHORN AND BRIDGE (SCM) 7.1.1
HORN
REMOTE CONTROLLED SWITCH ACTUATORS PROVIDED AT PIONEER STATION (GOLDSTONE) ONLY
RIGHT-HAND CIRCULAR POLARIZATION DECLINATION
LEFT-HAND CIRCULAR POLARIZATION DECLINATION
RIGHT-HAND CIRCULAR POLARIZATION HOUR ANGLE
LEFT-HAND CIRCULAR POLARIZATION HOUR ANGLE
RIGHT-HAND CIRCULAR POLARIZATION SUM
LEFT-HAND CIRCULAR POLARIZATION SUM
WAVEGUIDE SWITCH
S-BAND CASSEGRAIN MONOPULSE SECOM DECLINATION CHANNEL POLARIZATION SELECTOR 7.4.8 VIA 7.4.3
S-BAND CASSEGRAIN MONOPULSE HOUR ANGLE CHANNEL POLARIZATION SELECTOR 7.4.7 VIA 7.4.3
S-BAND CASSEGRAIN MONOPULSE SUM CHANNEL POLARIZATION SELECTOR 7.4.6 VIA 7.4.3
S-BAND RECEIVER-EXCITER 7.1.3
S-BAND RECEIVER FILTER 7.1.8
S-BAND CASSEGRAIN DIPLEXER 7.1.7
S-BAND TRANSMIT FILTER 7.1.6
CABLE SUBASSEMBLY
CABLING ASSEMBLY MICROWAVE HARDWARE WAVEGUIDE PRESSURIZED HARDWARE 7.1.9
RACK SUBASSEMBLY
RACKS AND MOUNTING FIXTURES
MOUNTING FIXTURES 7.1.10
CASSEGRAIN FEED ASSEMBLY (7.1)
S-BAND CASSEGRAIN MONOPULSE SUM CHANNEL SELECTOR 7.4.9 VIA 7.4.3
RACK SUBASSEMBLY
RACKS AND MOUNTING FIXTURES
MOUNTING FIXTURES 7.2.37
POWER SUPPLY SUBASSEMBLY
POWER SUPPLY
GAS TUBE POWER SUPPLY
AC VOLTAGE REGULATOR
RECEIVER POWER SUPPLY
RECEIVER POWER SUPPLY 7.2.30
AMBIENT RF LOAD 7.2.4
CRYOGENIC RF LOAD 7.2.4
REFERENCE TEMPERATURE SENSOR SELECTOR 7.4.7 VIA 7.4.3
TRAVELING WAVE MASER TEST CONTROL (INPUT-OUTPUT)
COUPLER 10 db
NOISE SOURCE 7.2.5
DIRECTIONAL COUPLER 26 db 7.2.6
TEST IN
SWITCH 7.2.7
TRAVELING WAVE MASER (TWM) AND CLOSED-CYCLE REFRIGERATOR 7.2.8
TRAVELING WAVE MASER ASSEMBLY (7.2)
MASER GROUND SUPPORT EQUIPMENT
WAVEGUIDE SWITCH POSITION MONITOR
CABLES TO ANTENNA
60 cps TO ANTENNA
60 cps
S-BAND RECEIVER
RACKS, CABLING AND POWER SUPPLIES PICTORIAL
CABLE SUBASSEMBLY
CABLE
SIGNAL COAXIAL RG 9
COAXIAL RG 59
LOW-LOSS CABLES
CABLING ASSEMBLY MICROWAVE HARDWARE WAVEGUIDE PRESSURIZED HARDWARE
CRYOGENIC HARDWARE 7.2.38
TEST EQUIPMENT SUBASSEMBLY
TRAVELING WAVE MASER TEST CONSOLE
TRAVELING WAVE MASER TEST CONTROL
MONITOR RECEIVER SPECTRUM ANALYZER
NOISE FIGURE METER 7.2.36
KLYSTRON POWER SUPPLY 7.2.13
MAGNET POWER SUPPLY 7.2.14
VAC-ION POWER SUPPLY 7.2.15
CLOSED-CYCLE REFRIGERATOR CONTROL 7.2.16
CRYODYNE COMPRESSOR 7.2.17
DIRECTIONAL COUPLER 20 db 7.2.9
DIRECTIONAL COUPLER 10 db 7.2.33
MICROWAVE LOW-PASS FILTER (2.5 GHz) 7.2.10
FF-3-A PARAMETRIC AMPLIFIER ASSEMBLY
MONITOR RECEIVER SWITCH 7.2.19
RECEIVER I
RECEIVER 2
SWITCH 7.2.22
SIGNAL GENERATOR 7.2.41
MONITOR RECEIVER-INPUT SELECTOR (TRAVELING WAVE MASER OUT-PARAMETRIC AMPLIFIER OUT)
MIXER/50-Mc PREAMPLIFIER 7.2.30
ATTENUATOR 7.2.32
BANDPASS FILTER 7.2.31
×32 FREQUENCY MULTIPLIER 7.2.30
NOISE FIGURE METER
SPECTRUM ANALYZER
DIRECTIONAL COUPLER 7.2.25
SWITCH 7.2.39
NOISE TEMPERATURE MONITOR DETECTOR 7.2.40
VARIABLE ATTENUATOR 7.2.23
POSTAMPLIFIER 7.2.24
DETECTOR AND BIAS 7.2.26
POWER SUPPLY 7.2.28
POWER SUPPLY 7.2.34
23.4-Mc VCO AND ×3 MULTIPLIER 7.2.29
PRIMARY POWER
RECORDER 7.2.27
TRANSMITTER FINAL AMPLIFIER ASSEMBLY (2.3)
WAVEGUIDE SWITCH
TRANSMITTER ANTENNA SELECTOR 7.4.15 VIA 7.4.3
LOAD 10 kw 2.3.2
TRANSMITTER LOAD SELECTOR 7.4.16 VIA 7.4.3
10 kw
PART OF TRANSMITTER SUBSYSTEM 2
PRESSURE REDUCING VALVE 2.3.6
DRY NITROGEN SUPPLY 2.3.7
HARMONIC FILTER 2.3.8
TEST OUTPUT
FINAL AMPLIFIER 10 kw 2.3.9
HEAT EXCHANGER 2.3.10
TRANSMITTER DRIVE INTERLOCK BEAM VOLTAGE 7.4.3
TRANSMITTER CONTROL 2.3.11
POWER SUPPLY 2.3.12
8.3.1
HYDROMECHANICAL
POWER SUPPLY AND CONTROL
6-ft DEEP
6-ft HIGH
10-ft LONG
OUTSIDE HYDROMECHANICAL
HEAT EXCHANGE
6-ft DEEP
6-ft HIGH
10-ft LONG
CAGE
FINAL AMPLIFIER
3.5-ft DEEP
5-ft HIGH
7-ft LONG
RACKS PICTORIAL
RACK SUBASSEMBLY
RACKS AND MOUNTING FIXTURES
MOUNTING FIXTURES 2.3.14
CABLE SUBASSEMBLY
CABLE
CABLING ASSEMBLY MICROWAVE HARDWARE WAVEGUIDE PRESSURIZED HARDWARE 2.3.13
ACQUISITION COLLIMATION ANTENNA ASSEMBLY (9.3)
S-BAND ACQUISITION AID COLLIMATION ANTENNA 9.3.1
CABLE SUBASSEMBLY 9.3.2
FROM 7.6, 7
HORN
ACQUISITION ANTENNA S-BAND ACQUISITION AID (SAA) 9.3.3
RIGHT-HAND CIRCULAR POLARIZATION SUM
LEFT-HAND CIRCULAR POLARIZATION
RIGHT-HAND CIRCULAR POLARIZATION HOUR ANGLE
LEFT-HAND CIRCULAR POLARIZATION HOUR ANGLE
RIGHT-HAND CIRCULAR POLARIZATION DECLINATION
LEFT-HAND CIRCULAR POLARIZATION DECLINATION
WAVEGUIDE SWITCH
S-BAND ACQUISITION AID SUM CHANNEL POLARIZATION SELECTOR 7.4.10 VIA 7.4.3
S-BAND ACQUISITION AID HOUR ANGLE CHANNEL POLARIZATION SELECTOR 7.4.9 VIA 7.4.3
S-BAND ACQUISITION AID DECLINATION CHANNEL POLARIZATION SELECTOR 7.4.12 VIA 7.4.3
S-BAND TRANSMIT FILTER 9.1.4
S-BAND ACQUISITION DIPLEXER 9.1.3
S-BAND RECEIVER FILTER 9.1.6
S-BAND RECEIVER FILTER 9.1.8
REMOTE CONTROLLED SWITCH ACTUATORS PROVIDED AT PIONEER STATION (GOLDSTONE) ONLY
CABLE SUBASSEMBLY
CABLE
CABLING ASSEMBLY MICROWAVE HARDWARE WAVEGUIDE PRESSURIZED HARDWARE 9.1.9
RACK SUBASSEMBLY
RACKS AND MOUNTING FIXTURES
MOUNTING FIXTURES 9.1.10
ACQUISITION ANTENNA ASSEMBLY (9.1)
PARAMETRIC AMPLIFIER TEST CONTROL (INPUT-OUTPUT)
SWITCH 7.3.3
TEST INPUT
WAVEGUIDE SWITCH
S-BAND ACQUISITION AID SUM CHANNEL SELECTOR 7.4.10 VIA 7.4.3
S-BAND RECEIVER FILTER 7.3.13
DIRECTIONAL COUPLER 40 db 7.3.2
DIRECTIONAL COUPLER 20 db 7.3.5
PARAMETRIC AMPLIFIER 7.3.4
DIRECTIONAL COUPLER 10 db 7.3.6
TO MONITOR RECEIVER SWITCH
POWER SUPPLY
CONSOLE CONTROL 7.3.9
PARAMETRIC AMPLIFIER ASSEMBLY (7.3)
RACK SUBASSEMBLY
RACKS AND MOUNTING FIXTURES
MOUNTING FIXTURES 7.3.8
POWER SUPPLY SUBASSEMBLY
POWER SUPPLY
PARAMETRIC AMPLIFIER POWER SUPPLIES 7.3.11
CONTROL ROOM
ANTENNA MOUNTED
CABLES
RACKS, CABLING AND POWER SUPPLIES PICTORIAL
CABLE SUBASSEMBLY
CABLE
CABLING ASSEMBLY MICROWAVE HARDWARE WAVEGUIDE PRESSURIZED HARDWARE 7.3.10
TEST EQUIPMENT SUBASSEMBLY
TEST EQUIPMENT
NOISE FIGURE METER
CONSOLE CONTROL
JUNCTION PANEL
PARAMETRIC AMPLIFIER TEST CONTROL 7.3.12
ACQUISITION AID SUBSYSTEM (9)
TEST SIGNAL CONTROL ASSEMBLY (7.6)
TEST DIPLEXER 7.6.4
FERRITE ISOLATOR 7.6.7
TO MISSION ORIENTED EQUIPMENT TRANSPONDER (1.1)
TO ACQUISITION AID COLLIMATION TOWER
SWITCH 7.6.3
SWITCH 7.6.5
SWITCH 7.6.6
SWITCH 7.6.1
GSOS TEST TRANSPONDER 1.1.44
TEST SIGNAL INPUT SELECTOR (TRAVELING WAVE MASER-PARAMETRIC AMPLIFIER)
LOCAL REMOTE TRANSPONDER SELECTOR
TRANSPONDER EXCITER TRANSLATOR SELECTOR
10-kw AMPLIFIER EXCITER SELECTOR
SWITCH 7.6.2
TEST OUTPUT FROM EXCITER 2.1.11
2115/2119
7.6.2/7.6.3/7.6.7/7.6.4/7.6.5
TEST SIGNAL CONTROL 7.6.11
RACKS AND MOUNTING FIXTURES 7.6.8
POWER SUPPLY 7.6.9
RACK SUBASSEMBLY
CONTROL ROOM
ANTENNA MOUNT
TEST SIGNAL CONTROL PANEL
USE RACK OF 7.5.3
CABLES
SWITCHES
TEST DIPLEXER ISOLATOR 7.6.10
CABLE SUBASSEMBLY
CABLE ASSEMBLY 7.6.10
RACKS, CABLING AND POWER PICTORIAL
MONITOR-RECEIVER SUBASSEMBLY
REFERENCE MODE SELECTOR
NONSTANDARD MODE SELECTOR
DIRECTIONAL COUPLER 3 db 1.1.1
FERRITE ISOLATOR 1.1.2
FERRITE ISOLATOR 1.1.3
FERRITE ISOLATOR 1.1.5
FERRITE ISOLATOR 1.1.6
DIRECTIONAL COUPLER 3 db 1.1.4
REFERENCE RECEIVER I BYPASS INPUT SELECTOR
REFERENCE RECEIVER 2 BYPASS INPUT SELECTOR
SWITCH 1.1.42
SWITCH 1.1.43
SWITCH 1.1.50
SWITCH 1.1.40
7.4.9 VIA 7.4.3
7.4.10 VIA 7.4.3
7.4.25 VIA 7.4.3
REFERENCE RECEIVER 1 BYPASS INPUT SELECTOR
REFERENCE RECEIVER 2 BYPASS INPUT SELECTOR
POWER SPLITTER 1.1.51
POWER SPLITTER 1.1.52
DIRECTIONAL COUPLER 20 db 2.1.1
ULTRA HIGH FREQUENCY AMPLIFIER 2.1.2
7.62 TEST OUTPUT
ATTENUATOR 3 db 2.1.10
POWER SPLITTER 2.1.11
VARIABLE ATTENUATOR 6 TO 120 db 2.1.5
TEST SIGNAL 2295 Mc
BANDPASS FILTER AND CRYSTAL MIXER 2.1.9
DIRECTIONAL COUPLER 20 db 2.1.7
ATTENUATOR 20 db 2.1.8
45-Mc OSCILLATOR AND ×4 MULTIPLIER 2.1.9
5.2.2†/8.3.1/7.4.3/7.6.1
T-4.9 VIA T-4.3
DIRECTIONAL COUPLER 20 db 1.1.8
PRESELECTOR 1.1.9
MIXER/50-Mc PREAMPLIFIER 1.1.10
VARIABLE ATTENUATOR 1.1.58
FERRITE ISOLATOR 1.1.59
POWER SPLITTER 1.1.57
HOUR ANGLE
DECLINATION
TEST INPUT
DIRECTIONAL COUPLER 20 db 1.2.1
PRESELECTOR 1.2.2
MIXER/50-Mc PREAMPLIFIER 1.2.3
VARIABLE ATTENUATOR 1.2.4
RECEIVER I LOCAL OSCILLATOR
PART I
ANTENNA MOUNTED RECEIVER SUBSYSTEM
REFERENCE CHANNEL MODE SELECTOR
TEST EQUIPMENT POWER SUPPLY
RECEIVER I AND ANGLE RECEIVER 2 AND ANGLE TRANSMITTER EXCITER
LOW-LOSS CABLES
CABLING TO CONTROL ROOM
ANTENNA RECEIVER CONTROL
LOW-LOSS CABLES OR WAVEGUIDE FROM ANTENNA
RACKS, CABLING AND POWER SUPPLIES PICTORIAL
CABLE SUBASSEMBLY
CABLE
EXCITER R-I SUM, HOUR ANGLE, DECLINATION, R-2 SUM, HOUR ANGLE, ACQUISITION, DECLINATION ACQUISITION, TEST MASER, PARAMETRIC AMPLIFIER 1.1.54
POWER SUPPLY SUBASSEMBLY
POWER SUPPLY
RECEIVER AND EXCITER, ULTRA HIGH FREQUENCY AMPLIFIER AND EXCITER, TEST TRANSMITTER AND TEST RECEIVER/TRANSPONDER 1.1.55
TEST EQUIPMENT SUBASSEMBLY
TEST EQUIPMENT
POWER METER
TEST TRANSMITTER
TEST RECEIVER/TRANSPONDER 1.1.56
RACKS
RACK SUBASSEMBLY 1.1.57
DIRECTIONAL COUPLER 20 db 1.8.1
PRESELECTOR 1.8.2
MIXER/50-Mc PREAMPLIFIER 1.8.3
VARIABLE ATTENUATOR 1.8.28
FERRITE ISOLATOR 1.8.34
POWER SPLITTER 1.8.35
POWER SPLITTER 1.1.53
9.2.4 HOUR ANGLE
9.2.5 DECLINATION
DIRECTIONAL COUPLER 20 db 9.2.1
PRESELECTOR 9.2.2
MIXER/50-Mc PREAMPLIFIER 1.8.27
VARIABLE ATTENUATOR 1.8.3
RECEIVER 2 LOCAL OSCILLATOR
DIRECTIONAL COUPLER 20 db 9.2.12
PRESELECTOR 9.2.13
MIXER/50-Mc PREAMPLIFIER 1.8.27
VARIABLE ATTENUATOR 9.2.15
RECEIVER 2 LOCAL OSCILLATOR 1.8.27

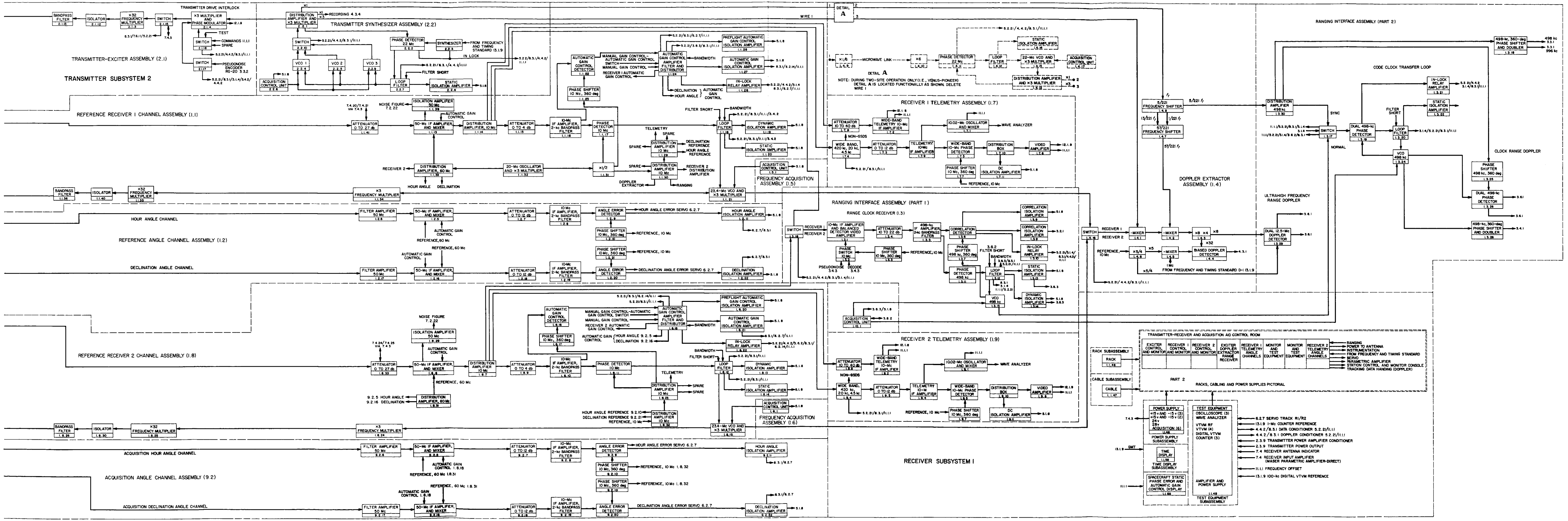

Fig. 1. S-band RF system block diagram

IV. Spacecraft Communication and RF Systems Development

A. GSDS 1964 S-Band RF System

1. Introduction

The S-band RF system (Fig. 1) is comprised of the receiver, transmitter, and antenna microwave subsystems, operating in conjunction with the acquisition aid subsystem in the DSIF tracking and communications system Goldstone duplicate standard (GSDS) 1964 model. The DSIF system is the Earth-based portion of a two-way, phase-coherent, precision tracking and communications system capable of providing command, telemetry, and position tracking for space vehicles. It will measure two angles (local hour angle and declination), radial velocity, and range to the space vehicle as well as provide an efficient and reliable two-way communication capability.

The S-band system provides a dual-channel reception capability and can be operated in various configurations of antennas, low-noise amplifiers, and receivers for acquisition and tracking and/or listening modes. System design is such that state-of-the-art improvement can be incorporated quickly, easily, and economically.

Design of the S-band RF system is complete. The RF system design characteristics are summarized in Table 1. Installation of the first RF system at the Pioneer site was completed during March 1964. Testing and performance evaluation, including compatibility tests with *Mariner* and *Surveyor* equipment, are in process.

This report presents a functional description of the S-band receiver, transmitter, and antenna microwave subsystems. Referring to the block diagram (Fig. 1), it should be noted that the acquisition aid subsystem (which has been described in Ref. 1 and subsequent issues of Vol. III) is closely associated in function and operation with the three subsystems discussed herein. Detailed description of the TWM is also contained in Ref. 1 and subsequent issues. The microwave switch control is described in detail in Refs. 2 and 3.

Table 1. RF systems characteristics preliminary

Item	Characteristics	
Antenna Microwave Subsystem		
Cassegrain feed and microwave circuitry		
(1) Type	Tracking—Transmit	
(2) Gain	*Receive*	*Transmit*
	53 db $^{+1.0}_{-0.5}$	51 db ± 1.0
(3) Losses	0.16 db ± 0.03	0.4 db ± 0.1
(4) Polarization	RHC	RHC
(5) Ellipticity	0.7 db ± 0.3	1 db ± 0.5
(6) Effective noise temperature	27°K ± 3 (including losses)	
(7) Beamwidth	0.36°K ± 0.03	0.45°K ± 0.03
Low-noise amplifier		
(1) Type	*Parametric*	*TWM*
(2) Gain	20 db	30 db
(3) Bandwidth	17 Mc ± 7 (3 db)	11 Mc (1 db) 15 Mc (3 db)
(4) Effective noise temperature	165°K $^{+30}_{-15}$	16°K ± 2
(5) Input signal level range	−70 dbm to threshold	−80 dbm to threshold
Receiver Subsystem		
Type	Phase-coherent double conversion superheterodyne	
Effective noise temperature (antenna at or near zenith)		
(1) SCM and reference receiver	2700°K ± 300	
(2) SCM, TWM, and reference receiver	55°K ± 10	
(3) SCM, parametric amplifier, and reference receiver	270°K ± 50	
Input signal level	−55 dbm to threshold	
Frequency		
(1) Range	2290 to 2300 Mc	
(2) Nominal	2295 Mc	
Noise bandwidth ($2B_L$)	*Threshold BW*	
(1) RF	12 cps $^{+0\%}_{-20\%}$	
	48 cps $^{+0\%}_{-20\%}$	
	152 cps $^{+0\%}_{-20\%}$	
(2) Range receiver	0.8 cps $^{+0\%}_{-20\%}$	
	4.0 cps $^{+0\%}_{-20\%}$	
	12.0 cps $^{+0\%}_{-20\%}$	
Detected telemetry		
(1) Modulation	Phase modulation	
(2) Bandwidth (1 db)	Selectable 2.2 kc, 10 kc, 210 kc, and 0.7 Mc	

Table 1. RF systems characteristics preliminary (cont'd)

Item	Characteristics
(3) Output level	0 dbm (one subcarrier at 1 rad rms modulation index under strong signal conditions)
(4) Output impedance	50 Ω
10-Mc IF output for telemetry	
(1) Modulation	Amplitude, frequency, or phase
(2) Bandwidth (3 db)	6.5 Mc
(3) Output level	0 dbm (non-coherent reception) −22 dbm (coherent reception)
(4) Output impedance	50 Ω
Precision doppler	
(1) Accuracy	0.2-cps rms at carrier frequency (uncorrelated error for one-minute sample spacing)
Angle error detection	
(1) Gain tracking	Differential ±2-db maximum
(2) Phase tracking	Differential ± 15-deg maximum
Transmitter Subsystem	
Frequency control	Phase stable, crystal-controlled oscillator: frequency synthesized from an atomic frequency standard
Stability	
(1) Frequency	$1{:}10^{11}$ for 20 min $5{:}10^{11}$ for 10 hr
(2) Phase	5 deg rms (noise error in BW ($2B_L$) of 12 cps)
Frequency	
(1) Range	2110 to 2120 Mc
(2) Nominal	$2113\frac{5}{16}$ Mc
Power output	10 kw
Modulation	
(1) Type	Phase
(2) Command	
(a) Bandwidth	dc to 100 kc
(b) Sensitivity	3 rad peak/v peak
(c) Input impedance	50 Ω
(3) Range	
(a) Bandwidth	dc to 2 Mc
(b) Sensitivity	5 rad peak/v peak
(c) Input impedance	50 Ω
RF Threshold Signal Levels (antenna at or near zenith)	*Threshold BW* 12 cps $^{+0\%}_{-20\%}$ / 48 cps $^{+0\%}_{-20\%}$ / 152 cps $^{+0\%}_{-20\%}$
SCM and reference receiver	−(154 dbm ± 1.0) / −(148 dbm ± 1.0) / −(143 dbm ± 1.0)
SCM, TWM, and reference receiver	$-\left(170.8 \text{ dbm } ^{+1.4}_{-1.2}\right) - \left(164.8 \text{ dbm } ^{+1.4}_{-1.2}\right) - \left(159.8 \text{ dbm } ^{+1.4}_{-1.2}\right)$
SCM, parametric amplifier, and reference receiver	$-\left(163.9 \text{ dbm } ^{+1.4}_{-1.2}\right) - \left(157.9 \text{ dbm } ^{+1.4}_{-1.2}\right) - \left(152.9 \text{ dbm } ^{+1.4}_{-1.2}\right)$

2. Receiver Subsystem

The receiver subsystem contains eight major functional elements which provide the following functional capabilities:

a. Reference receiver 1. Reference receiver 1 is a narrow-band phase-coherent, double-conversion superheterodyne type which receives signals in the 2290- to 2300-Mc range from the antenna microwave subsystem. It includes the following basic functional capabilities:

(1) Automatically tracks the signal level, frequency, and phase of the received carrier.

(2) Provides gain control and reference signals to the reference angle channel receiver.

(3) Provides outputs for telemetry, doppler extraction, and the range clock receiver.

(4) Provides RF switches, control circuits, and performance monitoring.

(5) Provides a method (open-loop operation) for accurately setting the receiver local oscillator frequency.

b. Receiver 1 telemetry. Receiver 1 telemetry operates in conjunction with reference receiver 1 and provides selectable bandwidth filtering for telemetry demodulation. It provides the telemetry output as demodulated subcarrier(s) or as a modulation spectrum centered at 10 Mc for further information processing.

c. Reference receiver 2. Reference receiver 2 is similar to reference receiver 1 and provides the same basic functional capabilities, except as follows:

(1) It is capable of operating on either the same or a different frequency from reference receiver 1.

(2) It provides (during operation with the acquisition aid subsystem) gain control and reference signals to the acquisition angle channel receiver.

d. Receiver 2 telemetry. Receiver 2 telemetry operates in conjunction with reference receiver 2 and performs the same basic functions as receiver 1 telemetry.

e. Reference angle channel receiver. The reference angle channel receiver is a double-conversion, superheterodyne type which receives two angular error RF signals in the 2290- to 2300-Mc range from the antenna microwave subsystem and accepts gain control and reference signals from reference receiver 1. It detects the angular error RF signals during phase-coherent operation to provide dc error signals in local hour angle and declination angle to the antenna servo in the antenna mechanical subsystem.

f. Acquisition angle channel receiver. The acquisition angle channel receiver is a double-conversion, superheterodyne type which receives two angular error RF signals in the 2290- to 2300-Mc range from the acquisition aid antenna and accepts gain control and reference signals from reference receiver 2. It detects the angular error RF signals during phase-coherent operation to provide dc error signals in local hour angle and declination angle to the antenna servo in the antenna mechanical subsystem.

g. Doppler extractor. The doppler extractor operates in conjunction with either reference receiver 1 or 2 by selection. It includes the following basic functional capabilities:

(1) Accepts reference frequencies from the transmitter subsystem which are coherently related to the transmitted carrier frequency.

(2) Accepts the 10-Mc reference and a frequency coherently related to the receiver voltage-controlled local oscillator (VCO) from either reference receiver 1 or 2.

(3) Accepts a stable 1-Mc bias signal from the frequency and timing standard subsystem.

(4) Processes the signals in (1), (2), and (3) in order to provide continuously the two-way doppler frequency at the received carrier frequency. Adds the 1-Mc bias signal to this two-way doppler frequency to provide biased UHF doppler to the tracking data handling subsystem.

(5) Provides signals to the range clock receiver which contains unbiased two-way RF doppler frequency information at one-fourth the received carrier frequency.

(6) Provides a transmitter-derived clock frequency to the range clock receiver. The clock frequency is coherently related to the transmitter carrier frequency.

h. Range clock receiver. The range clock receiver operates in conjunction with either reference receiver 1 or

2, the doppler extractor, and the ranging subsystem. It includes the following basic functional capabilities:

(1) Accepts the received range code modulation spectrum centered at 10 Mc from either reference receiver 1 or 2 by selection.

(2) Accepts the range decoding signal (from the ranging subsystem) which, during closed-loop ranging, is correlated with the received range code modulation to provide continuously the doppler-shifted clock frequency to the receiver clock phase-coherent tracking loop.

(3) Provides the clock frequency (coherently related to the transmitter frequency) to the range encoder in the ranging subsystem.

(4) Provides the clock frequency to the range decoder (in the ranging subsystem) via a phase-coherent clock transfer tracking loop. The input to the clock transfer loop can be switched between the transmitter-derived clock frequency and the doppler-shifted received clock frequency.

(5) Processes the transmitter-derived clock frequency and the doppler-shifted received clock frequency continuously to provide two-way clock doppler shift to the ranging subsystem.

(6) Processes the RF signals from the doppler extractor continuously to provide two-way RF doppler shift to the ranging subsystem.

3. Transmitter Subsystem

The transmitter subsystem contains three major functional elements which provide the following functional capabilities:

a. Transmitter synthesizer. The transmitter synthesizer includes the following basic functional capabilities:

(1) Accepts a stable reference signal (1 Mc from the frequency and timing standard subsystem) supplied from an atomic frequency standard.

(2) Synthesizes RF frequencies (at $\frac{1}{96}$ transmitter carrier frequency) selectable in 0.01-cps increments which are phase coherent with the 1-Mc reference signal [in (1) above].

(3) Provides a voltage-controlled oscillator (at $\frac{1}{96}$ transmitter carrier frequency) which generates an RF signal of high spectral purity. When operating in conjunction with a phase-coherent tracking loop and the signal in (2) above, the VCO provides a frequency stability, related directly to the atomic frequency standard.

(4) Provides the RF drive signal to the transmitter exciter.

(5) Provides the transmitter reference signals for doppler extraction (receiver subsystem).

(6) Provides a method (open-loop operation) for precisely setting the transmitter frequency.

(7) Provides RF switches, control circuits, and performance monitoring.

b. Transmitter–exciter. The transmitter–exciter includes the following basic functional capabilities:

(1) Provides frequency multiplication of the RF signal to the desired S-band transmit frequency.

(2) Accepts the range code and/or command modulation signals and provides the required modulation spectrum at the S-band transmit frequency.

(3) Provides the RF drive signal to the 10-kw klystron amplifier.

(4) Provides an RF signal at the S-band receiver frequency (2295 Mc nominal), which is derived from the S-band transmit frequency.

(5) Provides RF switches, control circuits, and performance monitoring.

c. Transmitter final amplifier. The transmitter final amplifier includes the following basic functional capabilities:

(1) Provides amplification of the S-band transmit signal to a 10-kw output level over the 2110- to 2120-Mc range.

(2) Provides waveguide filtering at the 10-kw output level to effectively eliminate harmonics of the transmitted RF carrier and interference in the 2290- to 2300-Mc receiver frequency range.

(3) Provides waveguide switching at the 10-kw output level to select transmission between the Cassegrain feed (antenna microwave subsystem) and the acquisition antenna (acquisition aid subsystem).

(4) Provides a 10-kw RF load and the required waveguide switching for 10-kw load tests.

(5) Provides switches, control circuits, and performance monitoring.

4. Antenna Microwave Subsystem

The antenna microwave subsystem contains six major functional elements which provide the following functional capabilities:

a. Cassegrain feed. The Cassegrain (SCM) feed is a single-horn monopulse amplitude comparison feedhorn, bridge, and diplexing filter assembly which, operating in conjunction with the hyperboloidal subreflector assembly on the 85-ft-diameter equatorial-mounted paraboloidal antenna, provides diplexed transmit–track capability. It includes the following basic functional capabilities:

(1) Provides a received sum RF signal (2290- to 2300-Mc range) to the low-noise preamplifier. Polarization of the received signal incident on the 85-ft-diameter paraboloidal reflector is normally right-hand circularly polarized (RCP)[1]. The Cassegrain tracking feed is capable of simultaneous reception and transmission of RCP and left-hand circularly polarized (LCP) with a sum and two orthogonal error channels for each polarization. At the Pioneer site (Goldstone, California) only, remote control is provided by the microwave switch control to select polarization. System design is such that, for special situations, reception and transmission with LCP can be obtained at other stations.

(2) Provides two RF error signals to the receiver subsystem, whose amplitude and phase in two orthogonal planes (local hour angle and declination angle) within the main antenna beam are a direct measure of the angular error between the angle of arrival of the received signal and the RF axis of the DSIF antenna.

(3) Provides the transmission of an RF signal (2110- to 2120-Mc range), supplied by the transmitter subsystem at 10 kw, to the spacecraft. Polarization of the transmitted signal radiated from the 85-ft-diameter paraboloid reflector is normally RCP[1].

b. Traveling wave maser (TWM). The TWM includes the following basic functional capabilities:

(1) Provides ultra low-noise amplification for the SCM reference channel received signal in the 2290- to 2300-Mc frequency range.

(2) Provides waveguide switching to permit selection of an alternate signal path for the SCM sum channel received signal. The normal alternate signal path is provided by amplification through the parametric amplifier.

(3) Provides waveguide switching to permit selection of reference temperature loads at the input to the low-noise amplifier(s) which are used in conjunction with measurement of the effective noise temperature in the receiving system SCM sum channel.

(4) Provides the closed-cycle refrigeration (CCR) required for operation of the TWM at the specified cryogenic temperature to provide the specified RF performance.

(5) Provides the instrumentation required for measurement and calibration of the over-all receiving system SCM sum channel noise temperature, low-noise amplifier gain, and signal spectrum display.

(6) Provides RF switches, control circuits, and performance monitoring.

c. Parametric amplifier. The parametric amplifier includes the following basic functional capabilities:

(1) Provides low-noise amplification for either the S-band acquisition aid (SAA) reference channel received signal in the 2290- to 2300-Mc frequency range or as an alternate signal path for the TWM.

(2) Provides waveguide switching to permit selection of an alternate signal path for the SAA reference channel received signal, while simultaneously providing an alternate signal path for the SCM reference channel.

(3) Provides noise instrumentation (which is partially common to the TWM instrumentation) for measurement of SAA sum channel noise temperature or the alternate SCM sum channel parametric amplifier signal-path noise temperature.

(4) Provides RF switches, control circuits, and performance monitoring.

d. Microwave switch control. The microwave switch control provides the control and mode display for all microwave and RF switches which select the various configurations of antennas (transmission and reception), low-noise amplifiers, and receivers for acquisition and

[1]Normal polarization for reception and transmission is RCP.

tracking and/or listening modes. It includes the following basic functional capabilities:

(1) Provides selection as to which antenna feed (SCM or SAA) the transmitter output is connected.

(2) Provides selection as to which antenna feed (SCM or SAA) each receiver reference channel (Channel 1 or 2) is connected. In addition, provides selection as to which low-noise amplifier (TWM or parametric amplifier) is utilized with each reference channel and provides simultaneous attenuator switching at the 50-Mc IF frequency in each reference receiver (in the receiver subsystem) to permit angle tracking.

(3) Provides indication as to the polarization (RCP or LCP) of the SCM and SAA antenna feeds. (See Footnote 1, p. 38.)

(4) Provides selection of reference temperature loads at the input to the low-noise amplifiers during receiver calibration.

(5) Provides selection of a high-power RF water load at the output of the transmitter subsystem during transmitter calibration.

(6) Provides a key switch which permits the controls to be locked in any desired configuration.

(7) Provides a manual mode which permits individual control of each switch from its associated switch controller.

(8) Provides interlocks to the transmitter subsystem which turn off exciter RF drive to the high power amplifier and interrupts beam voltage during periods of switching in the waveguide circuitry fed by the high power amplifier.

(9) Provides switch control circuits, mode display, and control panels.

e. Collimation microwave. The collimation microwave provides a calibrated signal source (GSDS S-band test transmitter/transponder) and antenna for calibration and performance evaluation of signal sensitivity and angle tracking (antenna boresight) of the complete RF system from a distant collimation tower.

f. Test signal control. The test signal control provides the switches, test diplexer, control, and display required to accomplish closed signal path testing of the complete RF system in conjunction with a GSDS S-band test transmitter/transponder, a non-GSDS (program peculiar) S-band test transponder, or an S-band, transmitter-derived test signal. It also provides an S-band test signal to the acquisition aid subsystem.

References

1. "S-Band Acquisition Aid for the DSIF," *SPS 37-23*, Vol. III, pp. 60–61, Jet Propulsion Laboratory, Pasadena, California, September 30, 1963.

2. "DSIF Microwave Switch Control Assembly," *SPS 37-25*, Vol. III, pp. 53–57, Jet Propulsion Laboratory, Pasadena, California, January 31, 1964.

3. "Microwave Switch Control Assembly," *SPS 37-27*, Vol. III, p. 49, Jet Propulsion Laboratory, Pasadena, California, May 31, 1964.

V. Communications Engineering Developments

A. S-Band Implementation for DSIF

1. TWM for DSIF

a. Summary. The plan to install traveling wave masers (TWM) in closed-cycle refrigerators (CCR) in the DSIF S-band system is in progress. These subsystems have arrived at the Woomera and Johannesburg Stations and are currently being installed and checked out. The installation at the Pioneer site has been in satisfactory operation for several weeks.

The prototype gearless-drive crosshead in the Goldstone Venus site radar receiver TWM/CCR installation has been in continuous operation 24 hr/day, 7 day/wk for 1700 hr and appears to fulfill all expectations. We plan to retrofit the standard DSIF units with this simpler drive system.

b. Recent work. The only significant design change in the subsystem since the inception of the program has been in the choice of noise tube for the instrumentation. It was found that the gas tubes originally planned for use in the system displayed a rather high rate of failure, apparently as a result of thermal stresses in the glass. The complex replacement problem and concomitant high repair costs have necessitated the use of an alternate design gas tube. Fortunately, the original power supply can be used with the new gas tube and no further system changes are expected to be required.

The Canberra TWM/CCR is currently being tested at Goldstone. The Madrid equipment will be assembled soon.

2. Acquisition Aid for DSIF

a. Summary. As a part of the DSIF S-Band Implementation Project, an S-band acquisition aid (SAA) has been developed for the 85-ft antennas. The first system, to be ultimately installed at Canberra, Australia, has been installed and evaluated at the Goldstone Pioneer site; the second and third systems have been shipped overseas for installation at the Woomera, Australia, and Johannesburg, South Africa, Stations.

b. Recent work. The VSWR performance of the SAA system was described in Ref. 1. Since that time transmission line losses between the SAA and the electronics cage interface have been measured. These losses are given in Table 1, together with the calibrated antenna gains of the SAA and the SAA collimation tower antenna. The probable error in these values is felt to be 0.1 db.

Table 1. Insertion loss and gain parameters of SAA subsystem

Item	Frequency, Mc	Loss or gain, db	Remarks
Reference channel	2295	−0.25	Includes diplexer
Declination channel	2295	−1.8	Includes filter
Hour angle channel	2295	−1.6	Includes filter
Transmitter channel	2115	−0.85	Includes diplexer, WG in electronics room
Collimation tower test line	2295	−9.0	–
SAA gain, reference channel	2295	+22.3	At electronics cage interface
Collimation tower antenna gain	2295	+18.4	–

On May 22, a carefully calibrated helicopter track with full recording was performed at the Goldstone Pioneer site. Because servo switchover tests had already been performed and had demonstrated successful rapid switchover, this test was run with tracking entirely on the SAA in an attempt to quantitatively evaluate the tracking accuracy of the SAA system. Particular attention was paid to the boresight alignment of the system. Since the receiver angle detector output slope is approximately 70 mv/deg and boresight stability of better than 0.1 deg is desired, the receiver angle detector balance and reference-to-error-channel crosstalk are exceedingly critical performance parameters. For this test the receiver was aligned and balanced to a level of 1 to 2 mv. In terms of reference-to-error-channel crosstalk, this balance level corresponds to a suppression of approximately 50 db. Sufficient data are not yet available to determine the practicality of maintaining this high level of performance in the field over an extended period.

Table 2 shows the boresight alignment of SAA and SCM systems prior to, and during, track; the difference between the pre-track calibrations and the flight data is presumably due to a combination of small misalignments between the SAA and SCM optical systems, drift in the receiver and servo systems, and structural distortions in the antenna during track. Unfortunately, schedule time did not permit any post-track calibrations. It should be pointed out, however, that since the SAA error peak separation is 19 deg, the boresight discrepancy shown in Table 2 is a small effect.

The tracking performance of the SAA system as a function of elevation angle is shown in Fig. 1. In plotting this figure, tracking data were sampled at 2-sec intervals, and the angular coordinate with the largest error at each time was chosen for the plot. Parallax between the SAA and SCM, which varied from 0.01 to 0.07 deg during the track, was also corrected. For elevation angles less than 9 deg, servo switchover from SAA to SCM appears hopeless. From 9 to 12 deg, switchover is possible by activation of the switchover control at a time when both declination and hour angle errors are less than 0.2 deg. This procedure involves little risk, since an unsuccessful switchover is immediately obvious by diverging SAA error voltages, and an immediate return to SAA tracking can be effected. For elevation angles greater than 12 deg, switchover can be successfully effected at any time. In the event that a large boresight misalignment were to exist between SAA and SCM, it would be necessary to wait until the 12-deg elevation angle had been reached and then utilize the SAA offset bias adjustment prior to switchover.

The relative signal level between SCM and SAA is shown in Fig. 2. It can be seen that above approximately 9-deg elevation, the SAA tracking accuracy and SCM sidelobe distributions are such as to ensure a stronger signal on the SCM channel. These data imply that the same would be true of the 2115-Mc Earth-to-space link; hence, the two-way acquisition could be successfully achieved (above 9-deg elevation) with the transmitter on SCM rather than SAA. Such procedure would eliminate transmitter switchover with its attendant interlock and time delay problem. This mode of two-way acquisition has, however, not yet been evaluated in detail.

It is felt that the S-band acquisition system has been successfully demonstrated, with adequate performance levels. Present effort is being directed toward completion of the documentation and installation of the Woomera and Johannesburg L- and S-band systems.

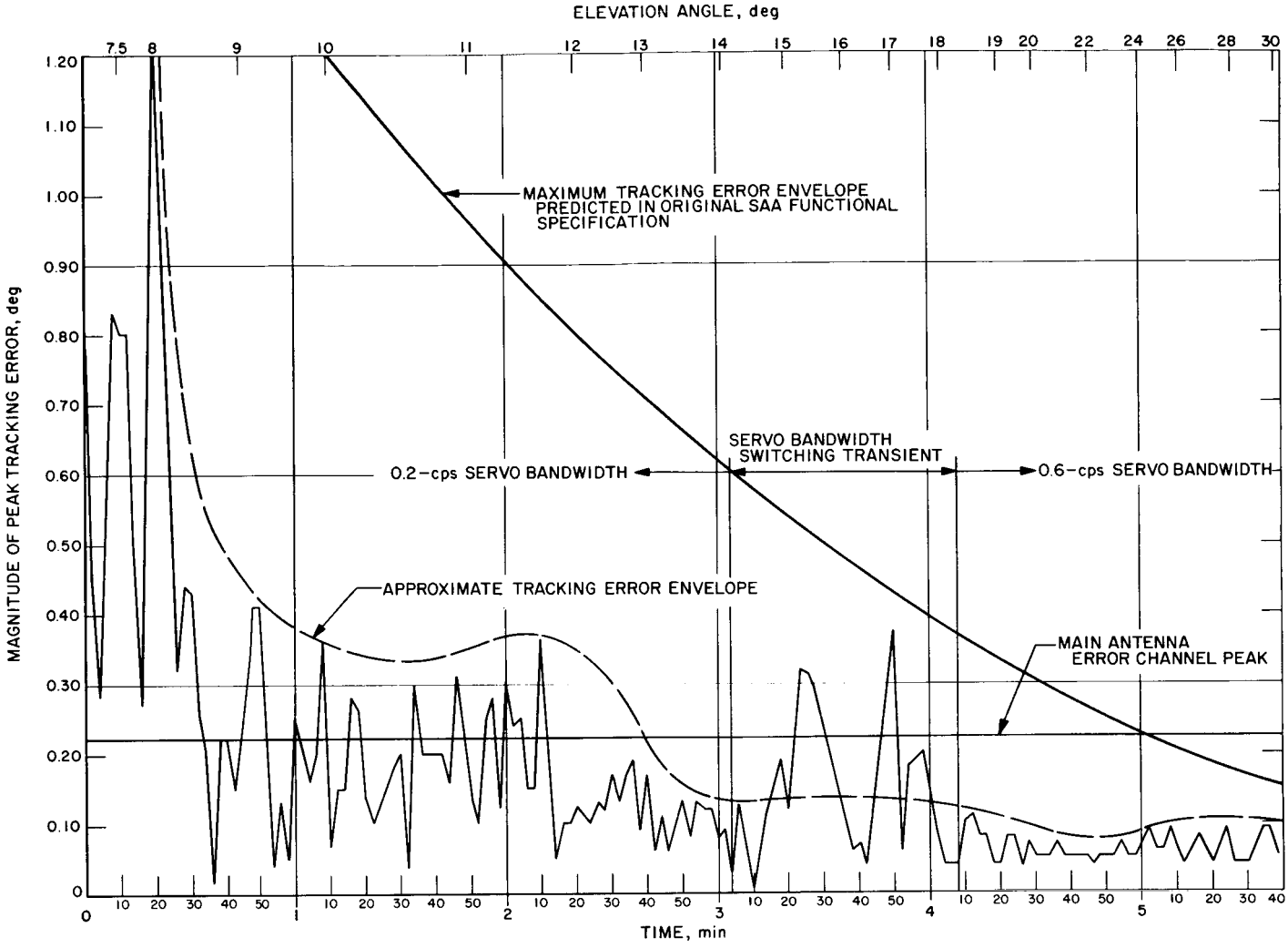

Fig. 1. SAA tracking performance

Table 2. S-Band system boresight data, helicopter track (May 22, 1964)

Coordinate	SCM (RF), deg	SCM (optical), deg	SCM (boresight), deg	SAA (RF), deg	SAA (optical), deg	SAA (boresight), deg	SCM—SAA (boresight), deg	Average SCM—SAA (boresight)[a], deg
Declination	325.980	325.984	−0.004	324.572	324.570	+0.002	−0.006	−0.05
Hour Angle	311.150	311.152	−0.002	300.260	300.286	−0.026	+0.024	+0.05

[a]20- to 30-deg elevation during track.

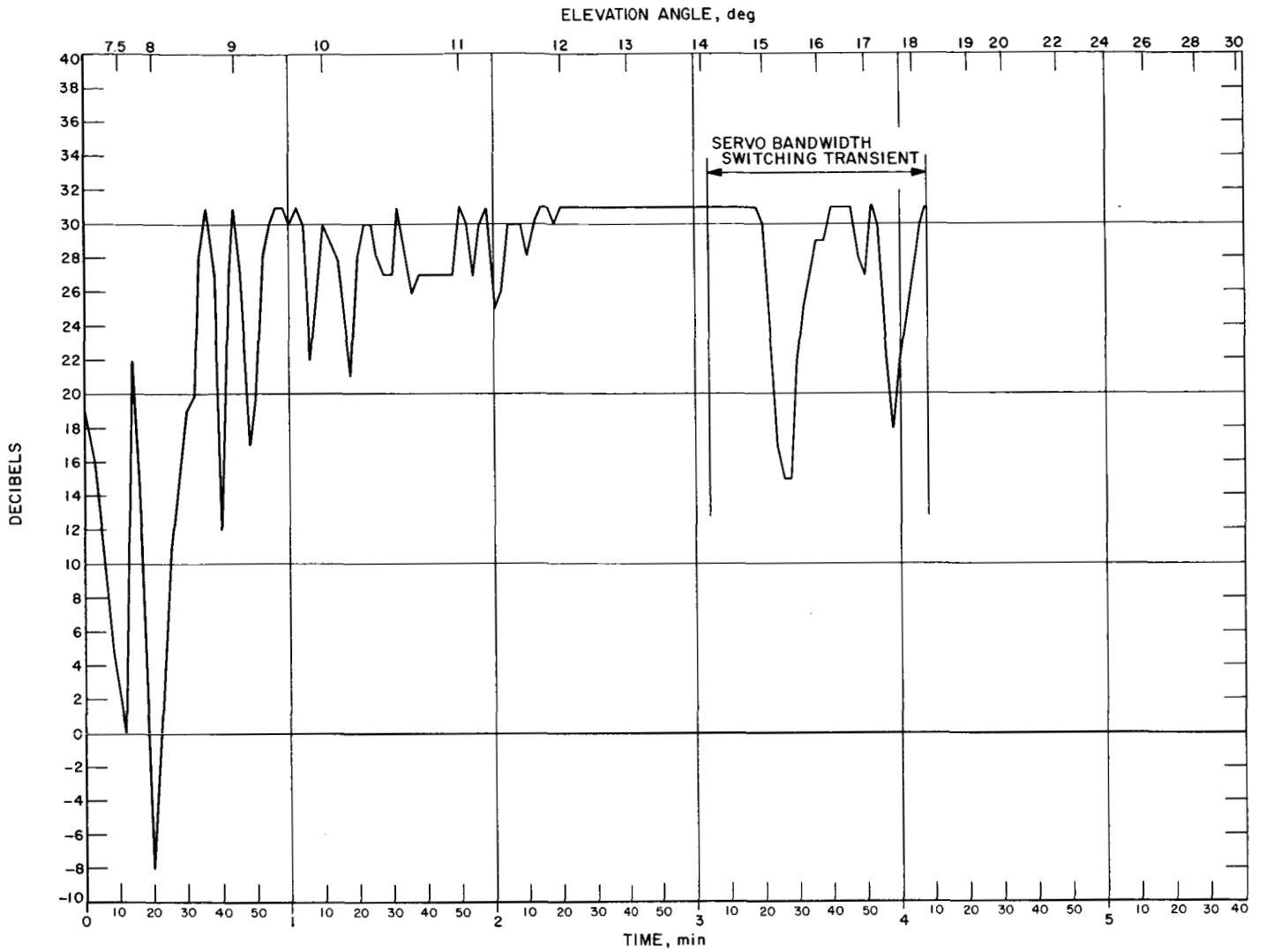

Fig. 2. Relative signal level between SCM and SAA

B. *Mariner C* Transmitter Development

3. *Mariner C 100-kw Transmitter*

a. Introduction. A ground transmitter power of 100-kw continuous wave (CW) will be required for the *Mariner C* Project under certain operating conditions. The complete transmitter system to meet this requirement consists of a 100-kw klystron amplifier subassembly, a ground test and checkout facility, and specialized controls for this installation.

b. Klystron amplifier subassembly. The amplifier subassembly was delivered to the Goldstone Venus site on June 2, 1964, and installed in the Cassegrain feed cone (Fig. 3). The interior of the feed cone with the amplifiers installed is shown in Fig. 4. Fig. 5 shows the complete installation up to the input to the turnstile junction. The original plans were to have the contractor install the JPL furnished feed; however, schedule difficulties dictated that the feed be installed by JPL.

c. Ground test and checkout facility. The facility for testing the klystron amplifiers on the ground is being completed in the power supply building at the Goldstone Venus site. It will be first used for testing the 100-kw amplifiers for *Mariner C*. Fig. 6 is the monitor cabinet

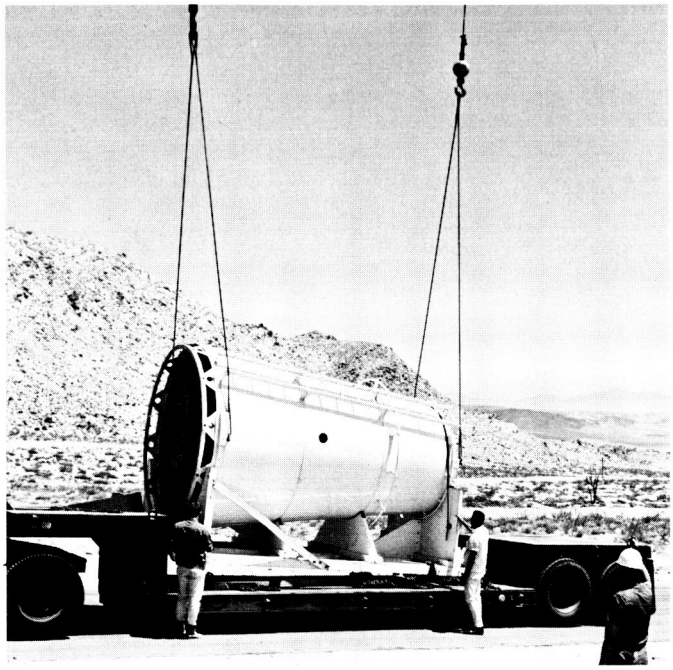

Fig. 3. Cassegrain feed cone in transportation cradle

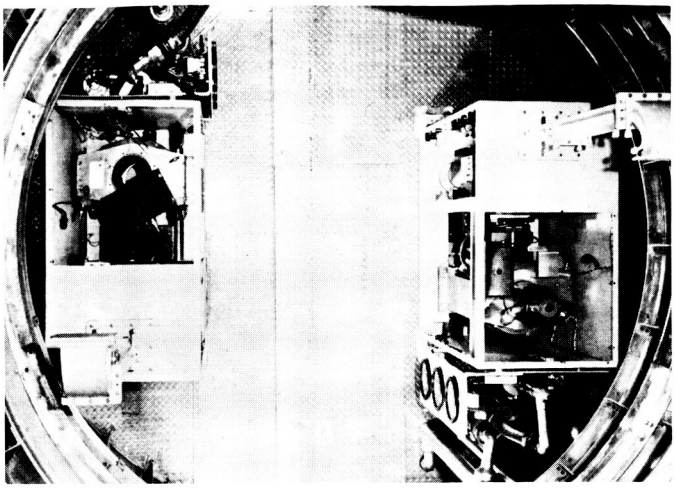

Fig. 4. Interior of cone before installation of waveguide and RF switch

Fig. 5. Interior of cone before installation of feedhorn and associated components

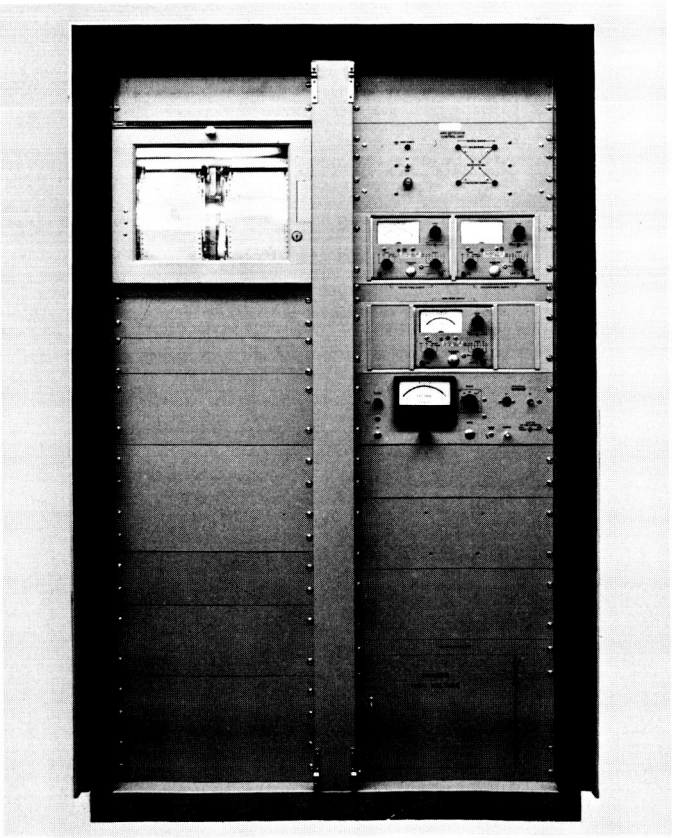

Fig. 6. Monitor cabinet for test area

for use with this test facility. In addition to the power meters, arc detector controls, and klystron body current meters, the monitor cabinet contains a 40-channel event recorder to monitor the system interlocks. This will provide a permanent record of outages and probable causes.

d. Work in progress. During the next reporting period, the amplifier subsystem will be tested on the ground; simultaneously, the 85-ft Az–El antenna will be made ready to accept the Cassegrain cone with the two amplifiers for final test on the antenna.

Reference

1. "Acquisition Aid for DSIF," *SPS 37-27*, Vol. III, p. 49, Jet Propulsion Laboratory, Pasadena, California, May 31, 1964.

VI. Communications Research and Development

A. Ground Antennas

1. Precision Drive System for 30-ft Antenna

A precision servo drive system has been designed, fabricated, assembled, and is presently being installed on the 30-ft antenna located at the Goldstone Venus site. The principal objective of the new drive system is to provide very precise steering over a large speed range. If the objective is satisfied, we will have versatile performance for satellite-to-astronomical-target tracking over a range of frequencies from S-band to 20 to 30 Gc to support several deep space communications related experimental programs. A description of the project plan was given in Ref. 1. The design, assembly, and installation have been done by JPL based on the use of commercially available components.

The project has followed the schedule shown in Fig. 1. The installation on the 30-ft antenna is now complete, and testing has been started.

ITEM	1963			1964						
	OCT	NOV	DEC	JAN	FEB	MAR	APRIL	MAY	JUNE	JULY
PROPOSAL AND PRELIMINARY DESIGN										
DETAIL DESIGN										
PROCUREMENT										
ASSEMBLY									13	
INSTALLATION									15–22	
CHECKOUT AND PRELIMINARY TESTING									22–24	
USE ON VENUS MILLIMETER WAVE EXPERIMENT									24	–20
CONTINUING SYSTEM TESTING, ADJUSTMENTS, AND INTEGRATION									25	–15

Fig. 1. Project schedule for 30-ft antenna precision drive system

2. Antenna Instrumentation

A transportable instrumentation system is being developed for use in research and development testing of the structural and mechanical properties of large ground antennas. It has been used in a measurement program on the 85-ft antenna at the Goldstone Venus site; it will be used extensively during the alignment and testing of the 210-ft-diameter Advanced Antenna System (AAS). There is a detailed description of the instrumentation system in Ref. 2, and progress reports have been made in subsequent issues. The latest block diagram of this system is in Ref. 3.

A second simplified transportable instrumentation facility is being prepared to provide recording of some data required continuously from the early stages of the on-site construction in the AAS project. It will be used initially for measurements of the concrete pedestal structure related to the hydrostatic azimuth bearing installation, and subsequently for the initial performance testing of the bearing. This facility will be built in a 10-ft trailer van and provided with air conditioning. It will contain a standard 50-channel, low-speed data scanner; a data conditioning and digital measurement system; and paper and magnetic tape recording, including an IBM typewriter for essentially on-line print-out of measured data. The tapes obtained will be suitable for data processing using standard JPL computer facilities. The trailer wiring is approximately 75% completed, and the data system is undergoing laboratory tests. A simplified block diagram of the system is shown in Fig. 2.

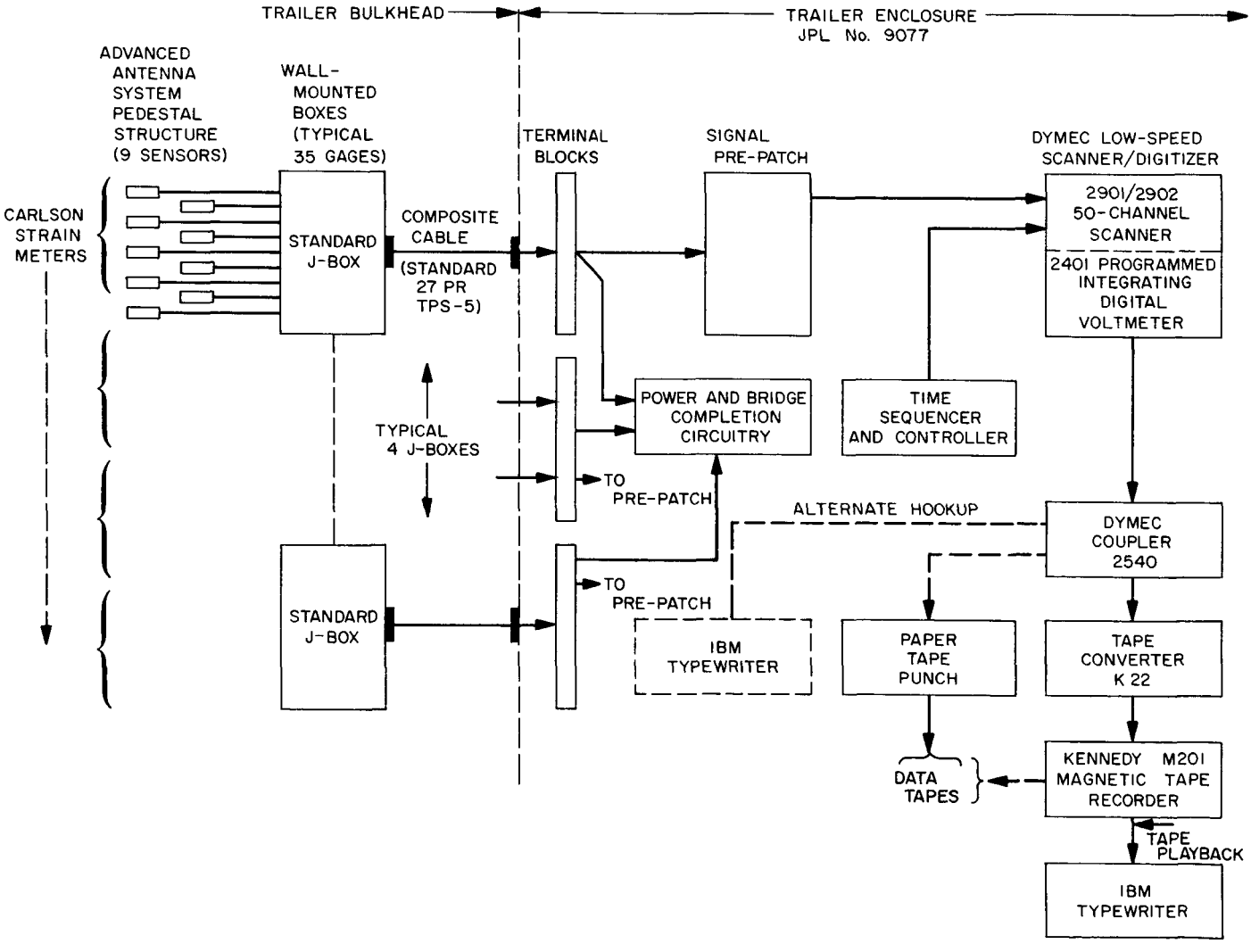

Fig. 2. Simplified instrumentation system for AAS erection phase continuous measurements

A data reduction program is being developed for reducing data recently obtained with the transportable instrumentation system on the 85-ft Az–El antenna. The reduced data will give the detailed surface waviness of the reflector panels. Approximately 20 points were measured on each of one-half of the total number of panels. The measurements were made at zenith only because the surface test fixture is not adaptable to operation at other angles. The results will be checked against data obtained using a theodolite.

3. Radio Calibration Techniques

a. Simultaneous lobing radiometric tracking system.

Summary. The S-band systems for the DSIF 85-ft and future 210-ft antennas will use simultaneous lobing angle tracking feed systems. A radiometer which could be used with the tracking feed would be a useful device for angle pointing and gain calibrations of the antenna system using radio star sources.

An X-band laboratory demonstration model of a simultaneous lobing radiometer receiver channel has been constructed. A noise tube is used to simulate the signal from a radio source. Preliminary experiments have been performed to examine the angle detector output versus reference/error channel differential phase shift and error channel noise-to-signal ratio. This work was described in Ref. 4.

The intermediate frequency and direct current components of the demonstration system were recently operated at the Echo site of the Goldstone Tracking Station using the 85-ft antenna and the L-band receiver system. It was possible with an effective system temperature of approximately 500°K to automatically track a radio star which produced an antenna temperature in the reference channel of 5°K; a source which produced a 59°K antenna temperature provided good automatic tracking. Data were taken to evaluate the tracking accuracy and are presented.

Recent work. On the night of April 30/May 1, 1964, the experimental simultaneous lobing radiometer was installed and tested on the Echo site 85-ft antenna to perform automatic RF angle tracking at 960 Mc of the Crab Nebula, Virgo A, and Hercules A. A discussion of the work and reproductions of the strip chart data taken can be found in Ref. 5. The data obtained during the experiment from the datex angle encoders on the antenna axes have been reduced with the aid of an IBM 1620 computer.

The method of reduction of the digital angle data consists of computing a nominal ephemeris and finding the standard deviation of the experimental data points. This method was used because an absolute boresight of the antenna to the required accuracy was not available.

For comparison purposes, the 85-ft antenna was subsequently driven at sidereal rate by slaving to computer control. During the slave mode drive experiment, the antenna was moved through the same angle coordinates as during the auto-track of Crab Nebula made on the night of April 30/May 1, 1964. The outputs of the datex encoders were recorded during the slave track, and the standard deviations of these data points were found. Because of time limitations during the April 30/May 1 test, insufficient data were taken on Virgo A (approximately 17°K antenna temperature) to make a meaningful statistical analysis of tracking errors.

Figs. 3, 4, and 5 show the pointing error of the antenna as both a function of time and of antenna hour angle for slave drive, Crab Nebula auto-track, and Hercules A auto-track, respectively. The graph of the Crab Nebula pointing error data points indicates what appears to be a cyclical systematic error in the system of a few thousandths of a degree. This systematic error is probably in the datex encoders. The graph of slave drive pointing error does not show this cyclical systematic error in absolute antenna pointing because of the feedback between the datex encoders and the control computer. The cyclical error does not show up in the auto-track of Hercules A due to the masking effect of the larger random errors.

R. Manasse (Ref. 6) has shown that, for a receiver configuration and a noise-like signal as used in these experiments, the best rms angle tracking error (standard deviation) one can obtain is given by:

$$\delta_\theta = \frac{2}{\pi}\,\frac{\lambda}{D}\,\frac{(1 + P_s/P_n)^{1/2}}{(P_s/P_n)\,(2\tau W)^{1/2}}\,(57.3)$$

where

δ_θ = rms tracking error in degrees

λ = wavelength

D = (circular) aperture diameter in consistent units of length

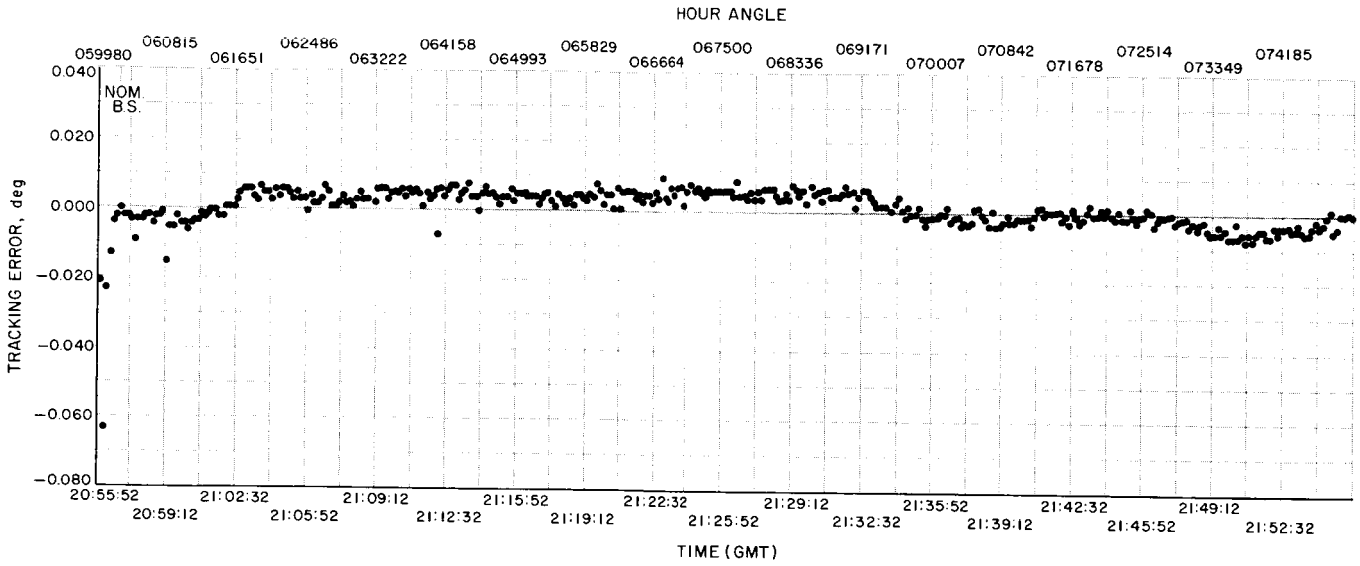

Fig. 3. Slave drive antenna pointing error

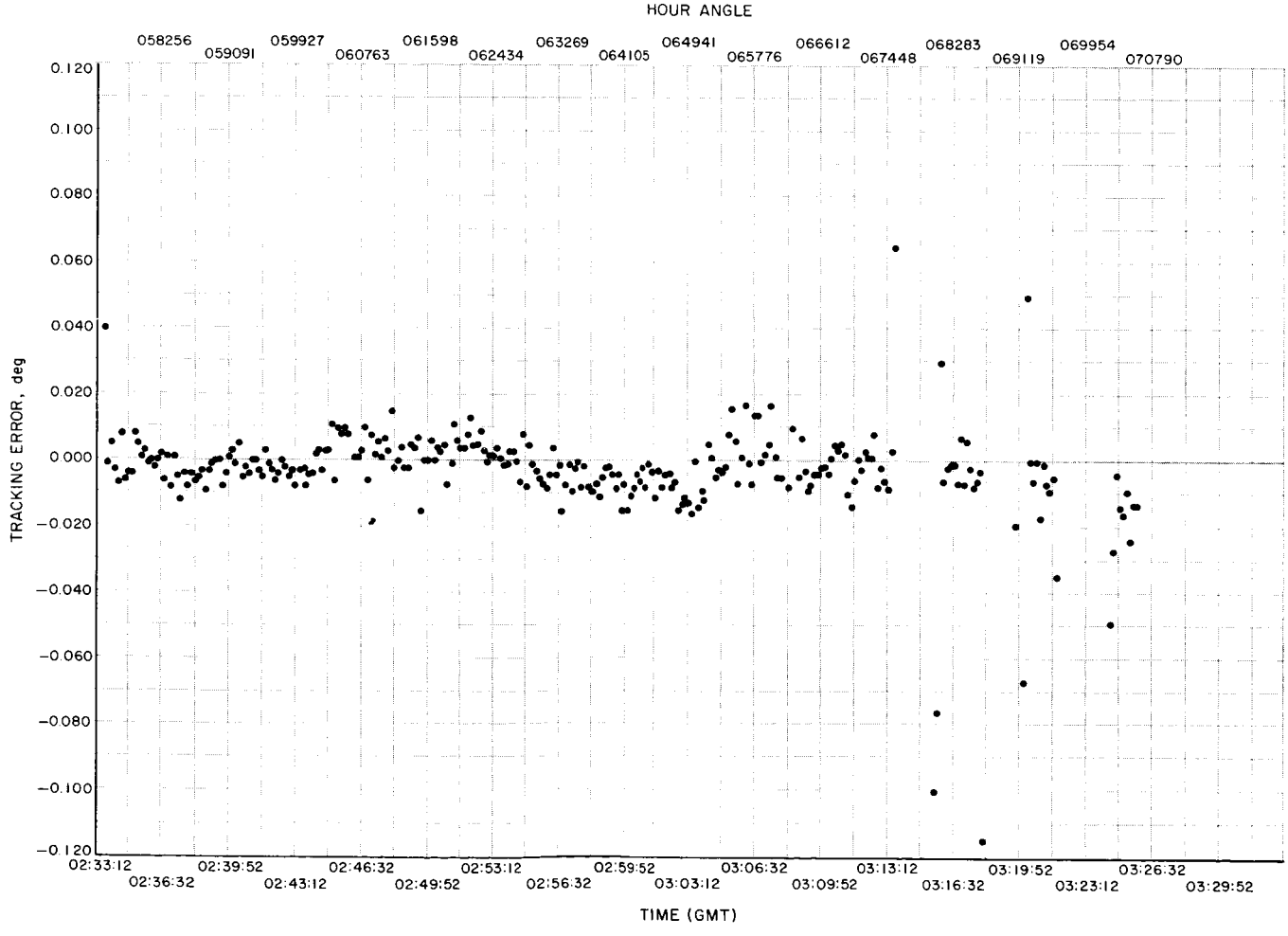

Fig. 4. Crab Nebula antenna pointing error

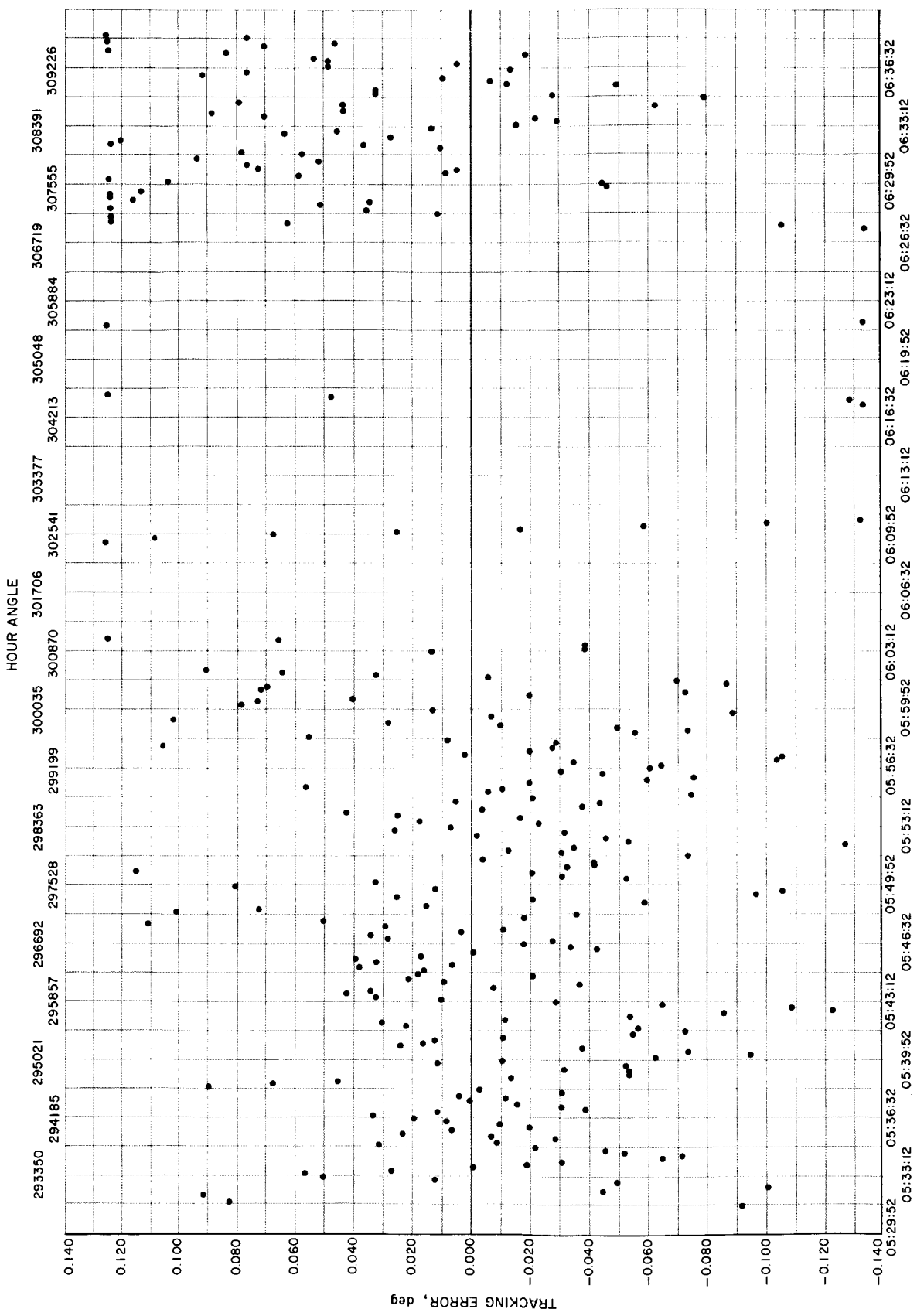

Fig. 5. Hercules A antenna pointing error

P_s = source noise power

P_n = system noise power

τ = system time constant

W = predetection bandwidth

Since P_s and P_n appear only as ratios, we may substitute the temperatures, T_{source} and T_{noise}. The effective T_{noise} of the system used during the experiments is approximately 500°K. This figure is the geometric mean of the two front-end temperatures (165°K for the reference channel parametric amplifier and 1500°K for the error channel mixer).

$$D = 85 \text{ ft}$$

$$\lambda \cong 1 \text{ ft}$$

$$\frac{P_s}{P_n} = \frac{T_s}{T_n} = \frac{T_s}{500°\text{K}}$$

$$W \cong 2 \times 10^6 \text{ cps}$$

$$\tau = 10 \text{ sec (estimated)}$$

Table 1 compares the standard deviations of the various tracks to the theoretical best standard deviation that one could expect on the basis of Manasse's formulation.

The tracking experiment discussed above demonstrates the feasibility of auto-tracking radio noise sources to aid in the calibration of the DSIF antennas. A prototype version of a system that could be developed for installation in the DSIF S-band system is currently being built and bench tested.

Table 1. Comparison of experimental tracking standard deviation and theoretical best tracking standard deviation for Crab Nebula and Hercules A

Track	Standard deviation, deg	
	Experimental	Theoretical best
Crab Nebula (59°K source)	0.006	0.0006
Hercules A (5°K source)	0.050	0.007
Slave	0.004	—

B. Venus Site Experimental Activities

1. Summary

Experimental operations activity at the Goldstone Venus site for the period February 20 to April 20 was reported in Ref. 7. The 100-kw S-band klystron amplifier tube in the radar transmitter was shut down on April 16 as a result of a cathode structure failure; it was returned to the manufacturer on April 19 for repair. The repair period on the tube consumed 10 days of planetary radar experiment operating time; however, it provided time for extensive maintenance, modification, and testing work. Also, during the radar experiment downtime, radio star tracking data and Venus blackbody measurements were made. A repaired klystron amplifier tube was installed on April 29, and the planetary/lunar radar experiments were restarted.

Venus radar experiments were conducted with the AM receiver, and the continuous wave (CW) receiver. Signal strength, spectrum analysis, and doppler frequency data were obtained from the planet. Also, radar signal strength and spectrum data were obtained from the planet Mercury during this period.

Table 2. Summary of Venus site radar experimental activity (April 20 to June 16)

Activity	Total hours (approx)
Primary experiments	
Planetary radar	580
Lunar radar	0
Secondary experiments	
Venus thermal radiation	32[a]
Radio star track	124[a]
Testing, calibration, construction, maintenance (scheduled)	402
Downtime (due to equipment failure; includes unscheduled maintenance)	298[a]
Holidays	32
	1468
24 × 58 = 1392	− 76[b]
Total hours during this report period:	1392

[a]During the 10 days that no klystron was available, the 240 hr were used as follows:
Venus thermal radiation: 22.5
Radio star track: 53.5
Unscheduled maintenance: 164.0
Total: 240.0

[b]Venus thermal radiation and radio star track data time during the non-scheduled downtime.

In addition to the radar data from Venus and Mercury, radio star track data for antenna boresight evaluation were obtained from the radio sources Cygnus A, Cassiopeia, Crab Nebula, Virgo, and Hercules.

In order to evaluate relatively broad-band deep space communications, a preliminary Venus voice bounce experiment was performed using the radar transmitter in either a frequency modulated or single sideband modulated mode. The speech was compressed by a factor of 32 times because of limited bandwidth due to low signal-to-noise ratio. Intelligible recordings of voice messages were obtained on the following dates: June 3, 4, 5, 11, 12, 15, 16, and 23. Table 2 shows a summary of the operating time of the various activities with the planetary/lunar radar at the Venus site. The table includes the entire 10 days of downtime when the klystron was being repaired as nonscheduled downtime; during the 10-day period, maintenance and experiments not requiring the transmitter were performed with the system. Exclusive of the 10-day period, there were approximately 58 hr of nonscheduled downtime resulting from system failures.

2. Subsystem Performance

a. Transmitter. The 100-kw klystron amplifier failed on April 16, 1964; a replacement could not be made available for installation until April 29, 1964. During the period April 29 to June 16 inclusive, the replacement klystron had been operated a total of 1069.8 hr with filament voltage applied and 752.1 hr with beam voltage applied. Approximately 90%, or 677 hr, of the beam-on time has been at a nominal power output of 100 kw. The efficiency, at 100-kw power output, of the tube immediately after installation was 34.5%; the efficiency at the present time is 33.2%. This change is considered too small to be significant; it can be accounted for by measurement tolerances.

During the period April 29 to June 16, the transmitter subsystem has accumulated approximately 36.5 hr of nonscheduled downtime because of various failures. Some major contributors were: (1) 28-v power supply failure in the Mod IV exciter control panel on May 3: 3 hr, (2) waveguide arc detector module failure on May 12: 3½ hr, (3) 28-v power supply in the Mod IV exciter control panel on June 10: 25 min. (Thermal circuit breakers tripped repeatedly, the trouble was remedied by installing "muffin" fans behind the panel to provide forced air cooling.) The remainder of the nonscheduled downtime is attributable to various protective devices removing the beam power during fault condition, e.g., high back power, waveguide arc, body over-current, etc.

The 100-kw power amplifier klystron is normally operated in either a continuous wave or phase modulated mode. In these modes, the ability of the klystron to operate as a linear power amplifier is not important. However, for certain space communications experimental work (e.g., the recent preliminary Venus voice bounce experiments), amplitude modulation or single sideband modulation is desirable. In order to investigate the system capability for this type of use, a series of tests was conducted on the klystron to measure the range of linear power amplification at various beam voltages. It was found that higher beam voltages result in linear amplification over a greater range of input radio frequency power; the limiting factor is the maximum beam voltage rating for the klystron.

The previous power amplifier klystron filament power supply has been replaced with one designed and built by Energy Systems, Inc. Slight physical modification of the klystron enclosure was necessary before the new power supply could be fitted into place. Additional turns were also required on the associated current transformer in order to obtain sufficient output to drive monitoring instruments. No difficulty has been experienced with the filament supply since installation and checkout.

b. Receiver/maser. During the present reporting period, the Mod IV receiver has had uninterrupted operation as the central data conditioning device for the planetary and lunar radar experiments; it has been used in the following modes of operation: AM receiver signal strength, spectrum analysis and mapping, CW receiver signal strength and spectrum analysis, Venus ranging measurement, synchronous receiver doppler frequency measurement, and radio star track for RF boresight data.

Minor modifications and additions have been made to the receiver for use in the Venus voice bounce experiment. For the voice experiment, the receiver was operated as a single sideband (SSB) or as a frequency modulation (FM) receiver. A block diagram of the SSB receiver configuration is shown in Fig. 6. The upper sideband 455-kc output from the existing synchronous receiver channel is amplified in a narrow-band (75-cps bandwidth) IF amplifier, mixed with 455 kc, filtered in a bandpass filter, and recorded on an Ampex recorder. The FM receiver block diagram is shown in Fig. 7. The modulated signal is taken from the output of the existing synchronous receiver channels balanced, mixed, and fed

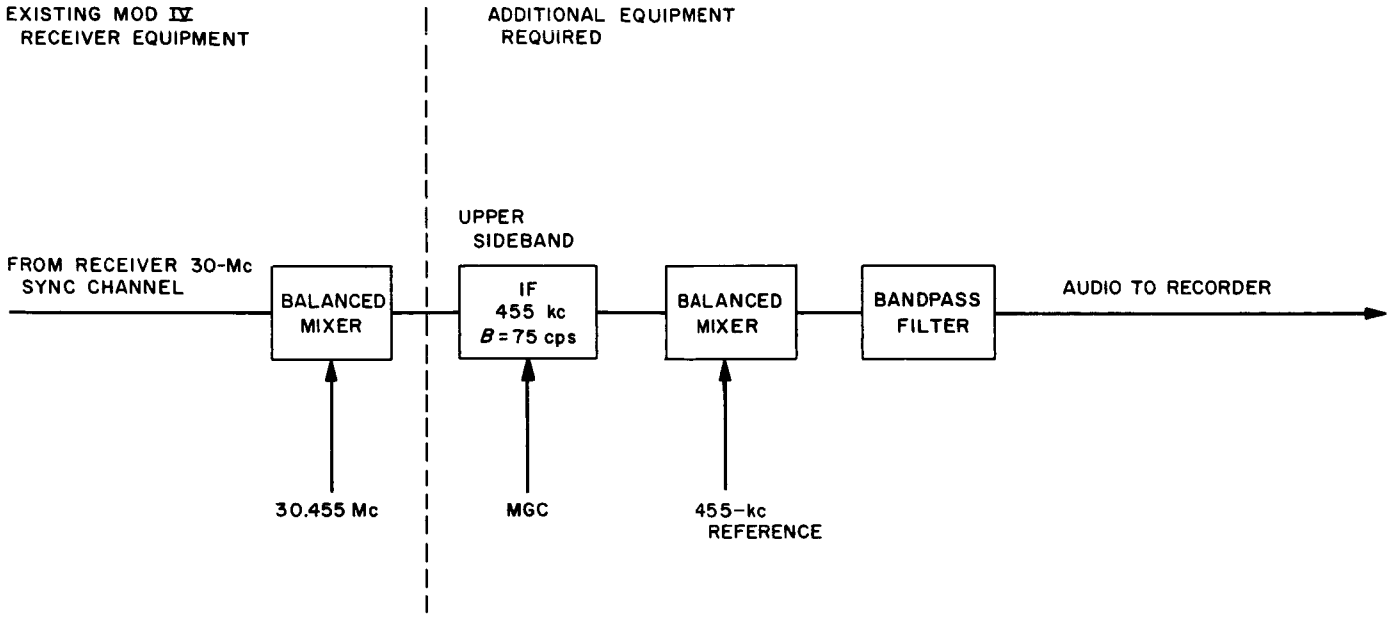

Fig. 6. Single sideband receiver block diagram

into the frequency discriminator circuits and finally into the same audio recording equipment. These two modes of receiver operation are being experimentally investigated to determine the most satisfactory means of modulating the 100-kw S-band transmitter.

The programmed local oscillator (LO) has operated almost continually with but minor errors. The machine has, on occasion, read the tape incorrectly; this causes it to search for the correct tape time after the tape is ahead of the station time. A minor pulse symmetry adjustment was made to eliminate this error with the result that fewer tape reading errors are occurring. In the RF portion of the LO, only one operation difficulty occurred when one UP-loop 475-kc crystal would not work and had to be replaced by the next crystal closest in frequency. All the required adjustments and replacements were made without loss of planetary radar data time.

The operation of the traveling wave maser/closed cycle refrigerator has been continuous except for a 2-hr downtime as a result of failure of the pump klystron.

As mentioned, the cause is not yet known for the small changes in the system temperature of the radar receiver. A thorough investigation is not planned until the system is shut down for modification in late July. On April 18, the maser was shut down for a 6-hr period due to a power switchover at a power substation. As soon as power was restored, the maser was cooled down. After cool-down was completed on April 20, the system temperature on the antenna (T_{SA}) had dropped from about 35°K prior to warm-up to about 28°K (Fig. 8).

Starting May 20 the system temperature T_{SA} increased from 28 to 30°K to 36°K. System checks indicated that the maser/CCR and its instrumentation apparently were operating correctly. Fig. 8 shows the system temperature on the antenna at zenith, on the nitrogen load, and on the helium load. It may be noted that, on May 20, all system temperatures went up approximately the same absolute amount.

On June 4, the system temperatures all decreased by about 5°K (Fig. 8), within about 2 to 3°K of what is considered to be normal system temperatures.

On May 30, the maser became somewhat unstable during radio star measurements. Investigation revealed that the valves in the CCR crosshead were sticking; the valves were adjusted and the maser stability returned to normal.

c. Antenna system. The servo electronics system was modified to enable the new Scientific Data Systems (SDS) 910 computer to drive the antenna in the slave mode. During May and June, approximately 60 hr of data were taken to evaluate the computer in preparation for its use with the 30-ft antenna operations.

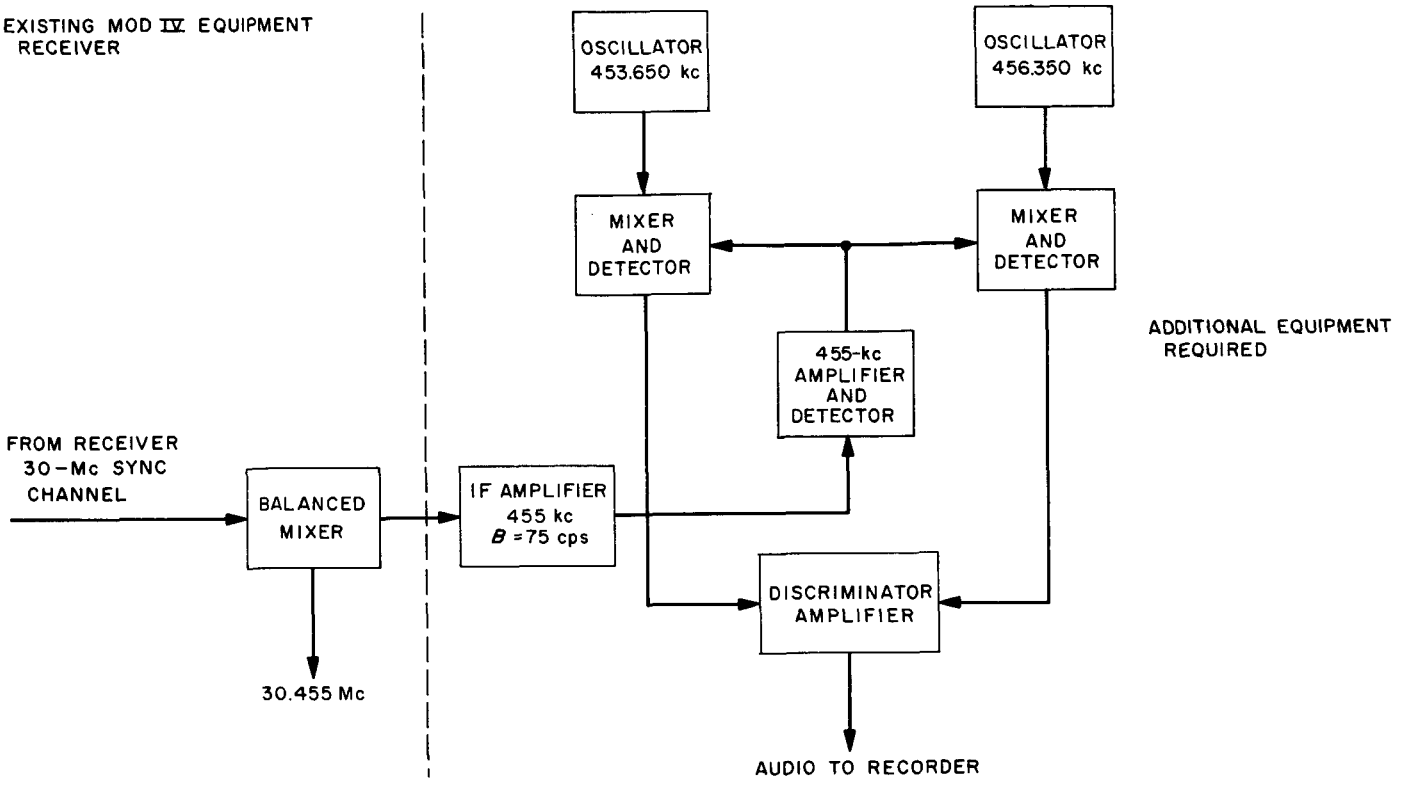

Fig. 7. Frequency modulated receiver block diagram

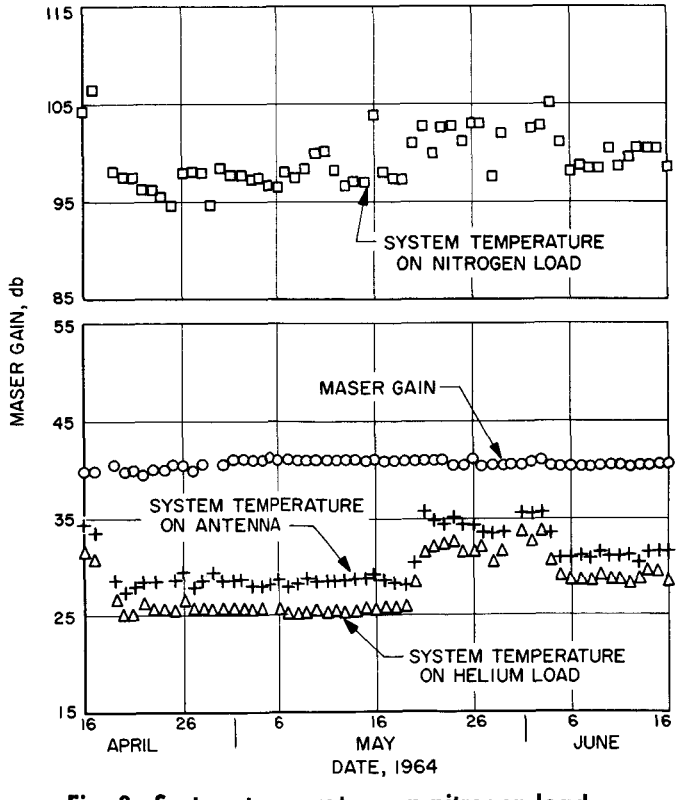

Fig. 8. System temperature on nitrogen load

A unique failure in the hydraulic system occurred on April 22. A check valve in the hydraulic return line stuck open after the system was shut down. This allowed the oil in the lines to the antenna to drain back into the reservoir tank causing it to overflow. The faulty valve was replaced. The hydraulic system was changed to the alternate pumping skid at this time. On June 17, the azimuth followup unit in the servo console was replaced because of intermittent operation. No electronic failures occurred, and no time was lost to mechanical malfunctions during the tracking period, April 20 to June 16 1964.

d. Digital equipment. No new digital equipment has been installed at the Venus site since the last reporting. Two new operational programs have been written and are in use: Planetary Ranging Program for the Mod III stored program controller (SPC) and an Antenna Pointing Program for the Scientific Data System (SDS) 910 computer.

The Planetary Ranging Program for the Mod III SPC is used to control the 511 length planetary coders and the transmitter–receiver cycle times. The 511 coders are used to bi-phase modulate the transmitter exciter and

the receiver local oscillator. During the receive cycle, the program shifts the receiver coder left and right one digit period every second, and a measurement is made of the signal strength in two adjacent range gates. The program can be used to produce ranging S-curve printout, or the derived S-curve can be used for a closed loop range tracking mode. In the ranging S-curve printout mode, the receiver coder is shifted at a constant rate to obtain information on the scattering law of the planet and to validate over-all system operation. In the tracking mode, the receiver coder shifting signal is obtained by differencing the signals in the two adjacent range gates. A point on the planet is tracked which results in the average signal strengths in the two adjacent range gates being equal.

The Planetary Ranging Program outputs information on a line printer, paper tape punch, strip chart recorder, and *X-Y* plotter. The clock number, integration time, station time, range, offset from the ephemeris, signal strength, and error signal are put out on the line printer and punched paper tape as nine octal words. The punched paper tape is converted to IBM cards and sent to the Pasadena Laboratory for analysis. The signal strength in the left and right gate, error signal, and ephemeris offset are displayed on the strip chart recorder for use by operating personnel. The S-curve is drawn on the *X-Y* plotter. A typical ranging S-curve derived (on site) from Venus measurements is shown in Sect. VI-C-1, Fig. 15 of this report.

The Antenna Pointing Program has been used with the SDS 910 computer for several nights of radio and optical star tracks with results comparable to those obtained with the punched paper tape ephemeris system. This program has also been used to track the planet Venus with rate offsets. All of the antenna pointing work thus far has been done on the 85-ft Az–El antenna. The SDS 910 will be used for pointing the 30-ft Az–El antenna at the Venus site as soon as that antenna is available for use. Sidereal clock drive with rate offsets will be used with the 30-ft antenna for the Venus millimeter (20 to 24 Gc) radiometer experiment planned for early July.

e. Preliminary experiment results. Since the last reporting, the following radar measurements of Venus have been started: ranging, cross-polarized total spectrum, cross-polarized CW spectrum, and linearly polarized CW spectrum. Previously used Venus radar experiments still in operation are: mapping, CW spectrum, and synchronous receiver. Also, measurements of the 2.4-Gc thermal radiation of Mars have been continued.

The ranging experiment was conducted 2 hr a day for 20 days before Venus conjunction. A digit period of 125 uses has been chosen for giving the best results. A preliminary analysis of the data shows the ephemeris offsets to fall on a smooth curve with an rms jitter of about 1.5 mi. The ranging S-curve has been used in conjunction with the tracking data to attempt to establish the location of the surface of Venus with respect to the tracking point.

In the cross-polarized total spectrum experiment, both transmit and receive cycles are made with the same polarization, either right or left circular polarization. In this mode, the transmitter is run on CW and reception is made in one channel of the nine-channel correlator. Two prominent features and several minor features have been visible in the output spectrum. None of these features corresponds to the front cap of the planet. Presumably, because of the slow relative rotation of the planet near conjunction and the narrowing of the spectrum, no movement of these features has been observed.

The cross-circular-polarized CW spectrum experiment uses the same system configuration as the total spectrum except that the signal is recorded on magnetic tape and sent to the Pasadena Laboratory for spectrum analysis on the IBM 7094 instead of being done in real time on site. The results of this experiment are not yet available.

Linearly polarized CW spectra have been taken with runs made every 30 deg of polarization rotation. The purpose of this experiment is to obtain the axis of rotation of Venus since vertical and horizontal polarized waves have different scattering characteristics from a rough surface. The results of this experiment are not yet available.

C. S-Band Lunar/Planetary Radar Project

1. A Precision Long-Range Tracking Radar System for Planetary Ranging

a. Introduction. Deep-space radar has previously been used in many ways to measure interplanetary ranges,

and many of these have not only drastically reduced the uncertainty in such ranges, but have indicated the true value of certain astronomical constants. A much improved method for precision planetary range tracking has recently been implemented at the Venus site—a method capable of distinguishing the sub-earth point of the planet Venus to about 2 or 3 mi. This article describes this system, its analysis, calibration, and preliminary results.

b. System concept. The precision planetary tracking radar uses much the same physical equipment as the range-gated lunar radar (Ref. 8). The only differences lie in that the 85-ft antenna is used for both transmission and reception (the lunar experiment used a 6-ft antenna to receive), different methods are used to isolate transmitter and receiver, a different set of variable digit-period coders is required, and the Mod III stored program controller operates under a different set of instructions. Detection, modulation, transmission, and reception are identical to the lunar radar. The significant difference in system concept embodied in this radar over previous *planetary* schemes is one of extreme flexibility, high accuracy, and high precision. Flexibility is achieved by use of the Mod III as the over-all system monitor, signal processor, and data handling unit. High accuracy and precision are obtained by the methods of modulation, detection, and signal processing used.

A system diagram is shown in Fig. 9. During the transmit portion of the duty cycle, the carrier is biphase-modulated ±90 deg by a pseudonoise sequence whose period is 511 digits (a nine-stage linear shift register sequence), and whose digit length is variable in multiples of 125 μsec. This modulated carrier is reflected from the planet back into the receiver some minutes later, with a time delay proportional to the range.

During the receive portion of the cycle, the incoming return is mixed with a local signal biphase-modulated by the receiver code. This mixing, which takes place at the output of the preamplifier in the Cassegrain cone on the antenna, essentially multiplies the return signal by the local code. The output of this mixer has three components:

(1) Narrow-band, 30-Mc signal proportional in strength to the correlation between the received waveform and the receiver code.

(2) Wide-band signal corresponding to signal echoes from points at distances whose time delays do not correspond to the inserted delay between transmitter and receiver coders.

(3) Noise.

The transmitter and receiver codes are pseudonoise codes; thus, Term (1) above is negligible whenever the

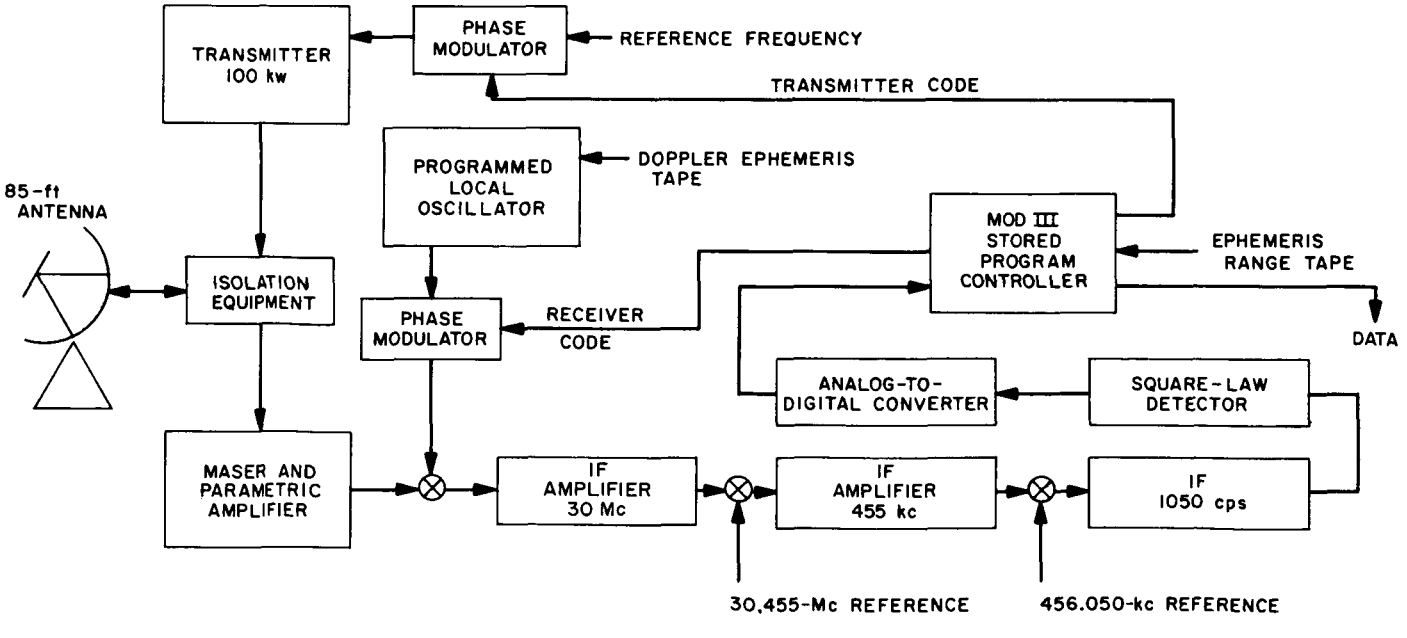

Fig. 9. Precision planetary tracking radar

phases of the received signal and that of the receiver code differ by more than one digit period. This means, for a fixed delay between transmitter and receiver coders, that the strength of Term (1) is only significant if the distance to a target is such that the round-trip time, transmitter–target–receiver, is equal to this fixed delay, plus or minus one code-digit period.

The distance over which a target may vary, but yet contribute energy to Term (1) is called a *range gate*. The output of the power detector for a point target appears as in Fig. 10(a).

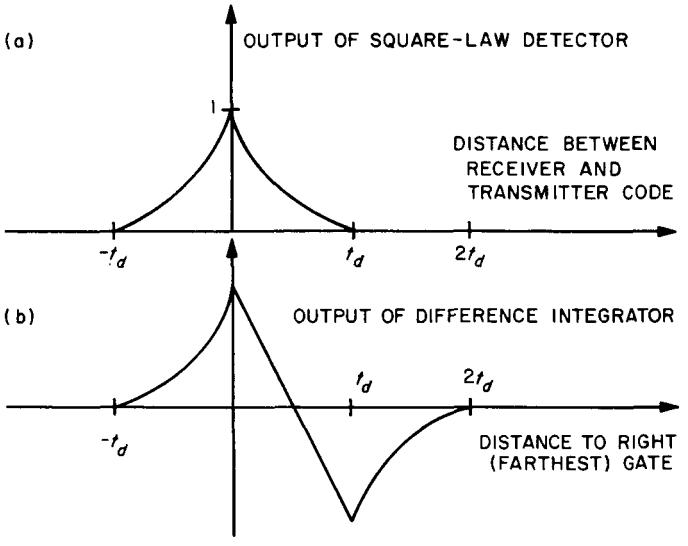

Fig. 10. The correlation function as seen at the output of square-law detector, and error curve for tracking loop, point target

For a target extending in depth, such as a planet (and for a planet we must also either assume a slow rotation rate, or a "shiny" front face), Term (1) is proportional to that part of the transmitted signal reflected from points on the planet inside a range gate.

The second term (2) is made negligible by suitable narrow-band filtering in the third IF amplifier. The output of the square-law device is thus proportional to the received signal power coming from a particular planetary range gate, plus the instantaneous noise power. (A square-law device is used in the receiver because planetary echoes are noncoherent, at random phase.) Converted to a digital series, this output is sampled and integrated (summed) by the Mod III stored program controller.

The tracking, or "S"-curve is made by first integrating the signal for 3 sec at a fixed receiver code phase, then integrating the signal for 3 sec but with the receiver coder offset one digit period less in range, and at the end of these 6 sec, differencing the two results. This difference, in the absence of noise, indicates the relative strengths of signals emanating from two adjacent range gates. This difference, scaled by some constant, directs a phase shift in the receiver coder, to decrease the integrated difference above. This continues until the difference becomes zero, indicating that both gates are receiving equal energies. Fig. 10(b) shows the error curve if the echo were noiseless and from a point target, and Fig. 11 shows a simplified equivalent diagram of the receiver. When noise is present, the differencing operation removes bias due to noise, much in the same fashion that a Dicke radiometer does.

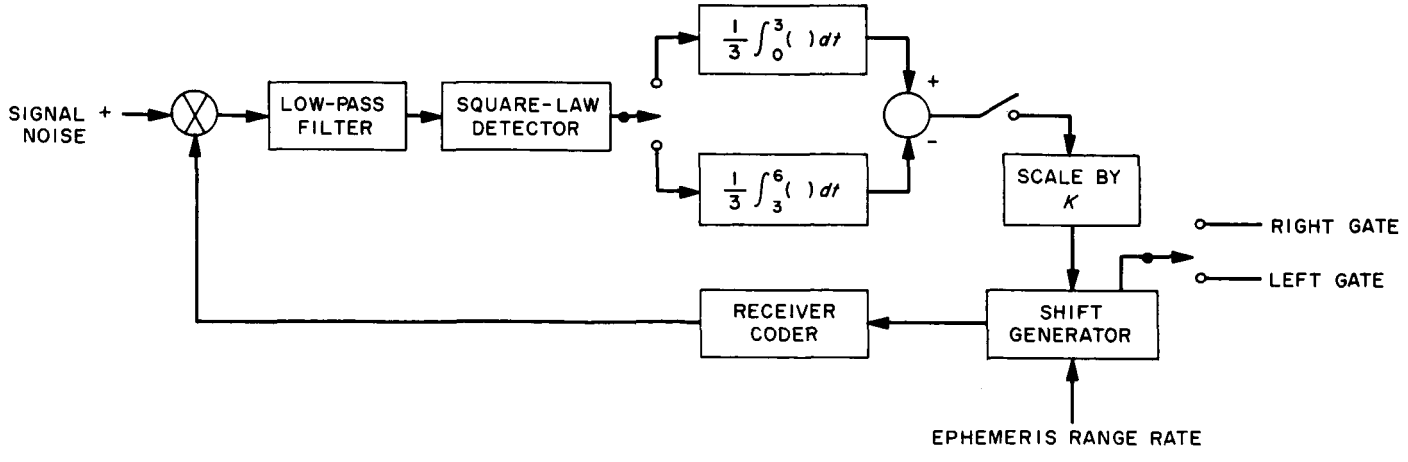

Fig. 11. Tracking loop for the planetary radar

A programmed local oscillator is used to remove the continuously changing doppler shift in the return due to the motion of the planet, so that the return is centered in the bandpass of the third IF amplifier. A range tape containing ephemeris values is also used to take out major variations in range; the loop then need only track the offset from this ephemeris.

c. Analysis of the tracking loop. Since ephemeris range is removed from the tracking, then so far as the loop is concerned, there is only a (relatively) constant range difference (measured in units of time delay) between that of the incoming signal and that given by the ephemeris.

We shall, for the present, assume a single specular return (point target) at range D.

Let time be divided into intervals T sec long, and let $y(t)$ denote the waveform at the output of the square-law device. We shall denote the time delay between the transmitted signal and the farthest gate, which we shall call the *right gate*, by r; the near gate, or *left gate* delay, as l; and the point half-way between these two, or *mid-gate*, as m. Then if the bandwidth B of the filter preceding the square law is less than the period of the code,

$$y(t) = \begin{cases} PR^2(r-D) + N(t) & (n-1)T < t < \left(n - \frac{1}{2}\right)T \\ PR^2(l-D) + N(t) & \left(n - \frac{1}{2}\right)T < t < nT \end{cases}$$

Here P is proportional to the received signal power; $R(\tau)$ is the (voltage) autocorrelation function of the code; t_d is the time per digit for the code; and $n(t)$ is the noise output of the detector.

$$R(\tau) = \begin{cases} 1 - \frac{|\tau|}{t_d} & |\tau| < t_d \\ 0 & \text{otherwise} \end{cases}$$

At the end of the nth interval, the accumulated error voltage is

$$e_n = P\left[R^2(r-D) - R^2(l-D)\right] + \frac{2}{T}\int_0^T \left[N(t+(n-1)T) - N\left(t + \left(n - \frac{1}{2}\right)T\right)\right] dt$$

Let us assume that $0 < r - D < t_d$; then $-t_d < l - D < 0$, so we have

$$R^2(r-d) - R^2(l-D) = -2\left(\frac{m-D}{t_d}\right)$$

There is then a linear portion to the S-curve as shown in Fig. 11. And since this S-curve is linear about the lock-in point (null), we can use linear methods to analyze the range-tracking loop.

Restricting $-\frac{1}{2}t_d < m - D < \frac{1}{2}t_d$, the error curve is the same as if a step function of magnitude D were put into an equivalent loop, shown in Fig. 12, with the multiplier (serving as a phase detector) replaced by a differencing junction. This is now a linear sampled-data system. In the nth interval, m_n is given by

$$m_n = m_{n-1} + Ke_{n-1} = \frac{2KPD}{t_d} + m_{n-1}\left(1 - \frac{2KP}{t_d}\right) + KN_{n-1}$$

and N_n is a zero-mean random variable

$$N_n = \frac{2}{T}\int_0^{T/2}\left[N(t + (n-1)T) - N\left(t + \left(n - \frac{1}{2}\right)T\right)\right] dt$$

whose variance is approximately, for a single-sided spectral density N_0 and for $P << N_0$,

$$\sigma_N^2 = \frac{N_0^2 B}{T}$$

We set $2KP = K'$ so

$$m_n = \frac{K'D}{t_d} + m_{n-1}\left(1 + \frac{K'}{t_d}\right) + K'\left(\frac{N_{n-1}}{2P}\right)$$

If we let $\nu_n = N_n/2P$, then ν_n is a zero-mean random variable with variance

$$\sigma_\nu^2 = \frac{N_0^2 B}{4TP^2} = \frac{1}{2\lambda_i^2 BT}$$

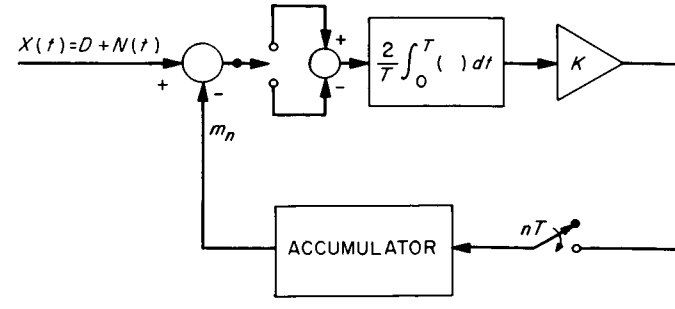

Fig. 12. Equivalent model for the tracking loop

in which λ_i is the input signal-to-noise ratio. Taking z-transforms, and solving for the transforms $M(z)$ of m_n gives

$$M(z) = \frac{K'D}{t_d}\left[\frac{1}{(1-z)\,(1-z(1-k'/t_d))}\right] + \frac{K'v(z)}{\left(1-z\left(\frac{1-K'}{t_d}\right)\right)}$$

The inverse transform then provides the solution for m_n:

$$m_n = D(1-e^{-\alpha n}) + V_n$$

Here V_n is a zero-mean random variable with variance

$$\sigma_V^2 = \frac{K'}{t_d(4\lambda_i^2 BT)\,(2-K'/t_d)}\,(1-e^{-2\alpha n})$$

and α is given by

$$\alpha = \ln\left(\frac{1}{1-K'/t_d}\right) = \ln\left(\frac{1}{1-\frac{2KP}{t_d}}\right)$$

As a special case, if α is small (i.e., a long response time with respect to the sample rate)

$$\alpha \approx \frac{2KP}{t_d}$$

$$\sigma_V^2 \approx \frac{KP}{4Tt_d\lambda_i^2 B}$$

and since at time $t_n = nT$, the value of m_n is

$$m(t_n) = D(1-e^{-\alpha t_n/T}) + V_n$$

the system time constant τ, for small α is

$$\tau = \frac{Tt_d}{2KP}$$

$$\sigma_V^2 = \frac{1}{8\tau B\lambda_i^2}$$

The quantities in the loop are all specified, except that P may be unknown. However $2P/t_d = s$ is the slope of the S-curve, so if this is at hand,

$$\tau = \frac{T}{Ks}$$

d. Calibration of the system for target extending in depth. The analysis above shows that for point targets, the loop behaves linearly with a prescribed time constant. A planet, however, does not behave as a point source, and it is therefore necessary to determine the position of the front face, as distinguished from the tracking point. As an approximation, let us assume that the scattering law, over the front portions of the planet, has the form as shown in Fig. 13(a)

$$l(r) = 1 - a\left(\frac{r-D}{t_d}\right) \qquad \text{for } 0 < a < \frac{1}{2}$$

This law is not observable, as such, but is convolved with the gate function

$$w(r) = \begin{cases} \left(1-\left|\frac{r-D}{t_d}\right|\right)^2 & |r| < t_d \\ 0 & \text{otherwise} \end{cases}$$

giving the observed scattering law $L(r)$ shown in Fig. 13(b). The difference between this convolved law as seen by right and left gates produces the tracking curve $L(r) - L(r-t_d)$ shown in Fig. 13(c). The point b, at

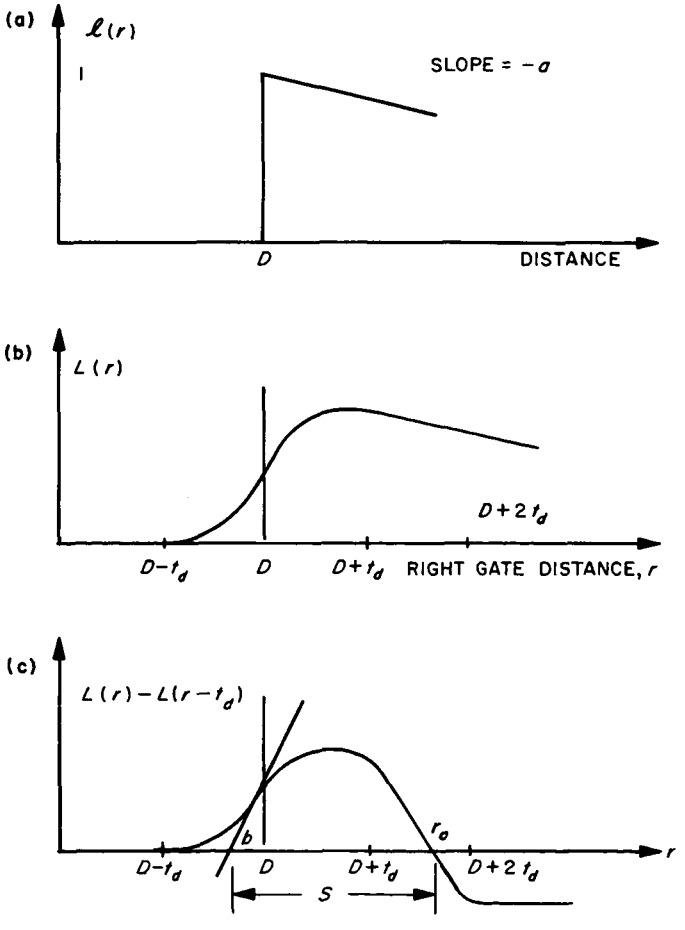

Fig. 13. Model of planetary scattering law, convolved law, and tracking curve

which a slope line through the S-curve at D intersects the r-axis,

$$b = D - \frac{1}{3} t_d \left(\frac{1 - a/4}{1 - a/3} \right)$$

is very insensitive to changes in a, and for all assumed values of a, the approximation

$$b \approx D - \frac{1}{3} t_d$$

is valid to 1.67% of t_d.

The loop tracks at some position r_0 of the right gate, at the null of the S-curve; this is some distance S past the point b as shown in Fig. 13(c). Both S and b are easily found, given the S-curve. Thus, the distance to the front face is

$$D = r_0 - S + \frac{1}{3} t_d,$$

or in terms of the distance l_0 to the left-gate

$$D = l_0 - S + 4/3\, t_d,$$

and in terms of mid-gate distance, m_0

$$D = m_0 - S + 5/6\, t_d.$$

e. System performance. Using the 100-kw transmitter, maser receiver, and 85-ft Venus site antenna as part of the precision planetary tracking radar described above, the planet Venus has been tracked recently with great success. Except for a few days for system checkout and parameter specification, the radar has provided measurements of range to the planetary mean-tracking-point with peak variations less than 15 to 20 μsec of round-trip delay (2.25 to 3 km in range). The mean-tracking-point can thus be determined, over a 1-hr period, to better than 4-μsec accuracy. Calibration of the internal system delay has been previously measured to be only about 0.55 μsec. Fig. 14 shows typical plots of this tracking data as a function of time. It must be remembered that part of the time is allotted for transmission, and tracking only occurs on the receive portion. The first parts of Fig. 14(a) and (b) show the loop pulling in from a deliberately induced error. Fig. 15 shows plots of S-curves, along with calibration numbers, and Fig. 16 indicates the day-to-day trend of the front-face range offset. Calibrations of the S-curve are estimated to about ±20-μsec accuracy, for the most part, and this represents the essential accuracy of the system for the day-to-day analysis.

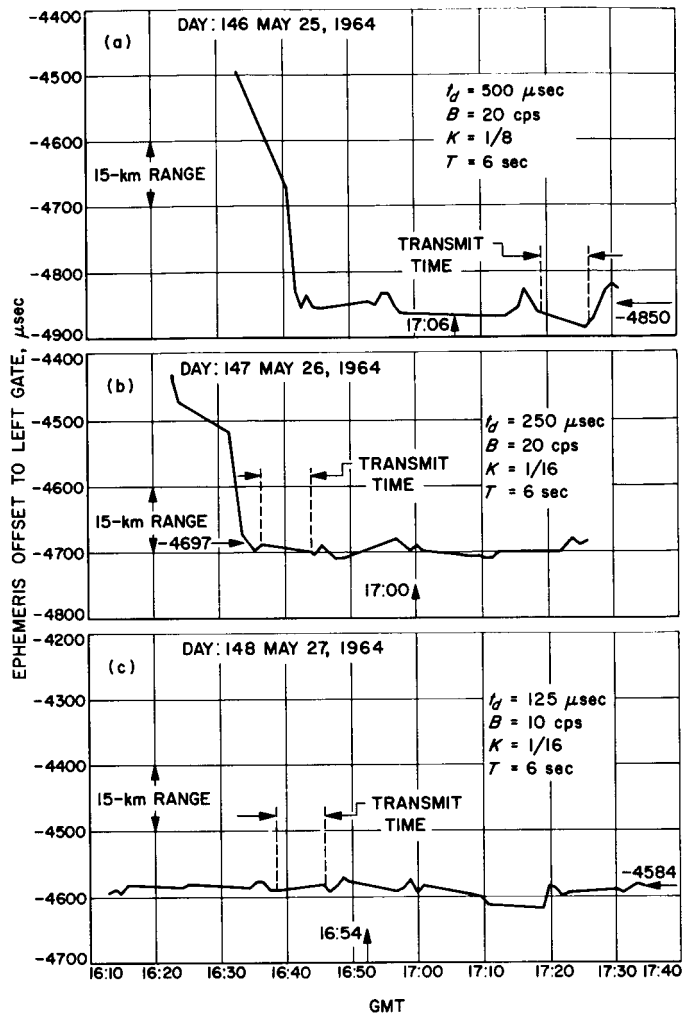

Fig. 14. Lock-in and tracking data for Venus (May 25, 26, 27, 1964)

As shown in the figure, during the days that these data were taken, the ephemeris was not only in error, but this error was changing by about 120 μsec per day (5 μsec/hr). Deviations larger than ±20 μsec are probably due to surface features.

Parameter values ranging from t_d = 1000 μsec to 125 μsec, K = 1 to 1/32 μsec/v, B = 20 to 10 cps, with T = 6 sec have been tested. The best performance has been obtained, as it should according to the analysis, at K = 1/32, t_d = 125 μsec, and B = 10 cps. A representative value of $s = 2P/t_d$ from an S-curve is about 5/3 units/μsec. A typical value of input SNR is $\lambda_i = 1$ for the early runs. Data in Fig. 14 (c) were taken with

$$t_d = 125\ \mu\text{sec}, B = 10\ \text{cps}, T = 6\ \text{sec}, K = 1/16.$$

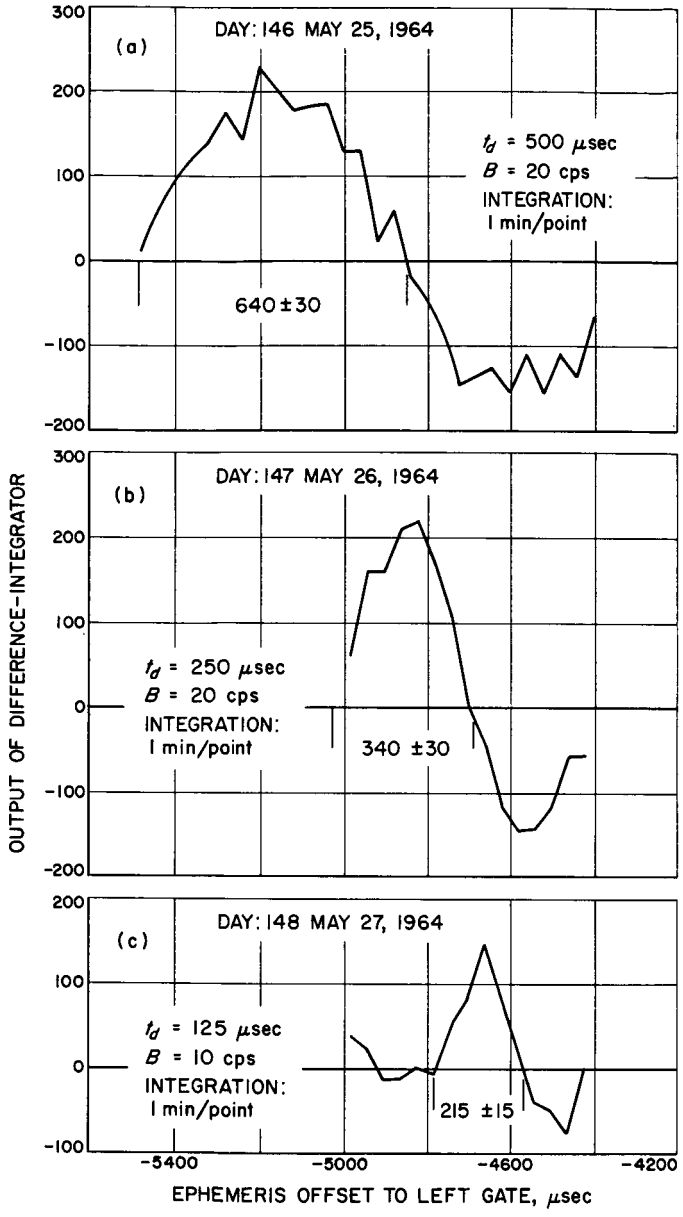

Fig. 15. Error curves for calibration, Venus (May 25, 26, 27, 1964)

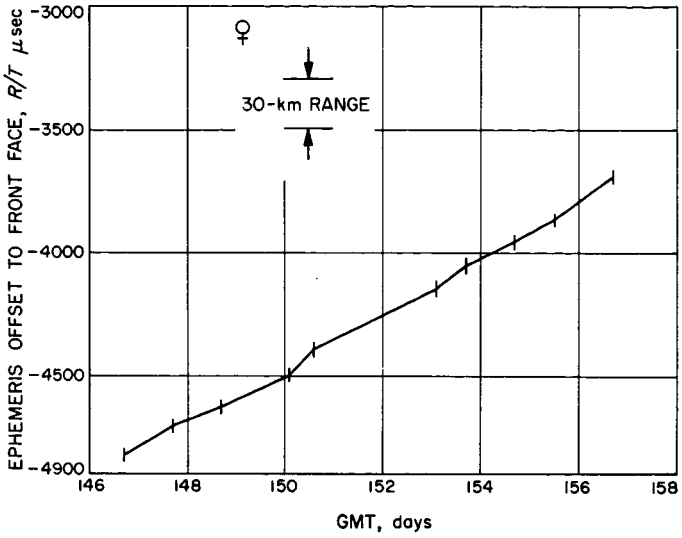

Fig. 16. Day-to-day tracking data, Venus (May 25, 26, 27, 1964)

These parameters give the system a time constant of about

$$\tau = 63 \text{ sec}$$

and an rms range deviation of

$$\sigma_V = 15 \ \mu\text{sec}$$

both of which are verified by the data. Later data with $K = 1/32$ give

$$\tau = 135 \text{ sec}$$

$$\sigma_V = 10 \ \mu\text{sec}.$$

2. *100-kw S-Band Transmitter*

a. Introduction. The period covered by this report was primarily devoted to radar tracking of Venus and Mercury. The transmitter was temporarily equipped with a linear exciter for an experiment in single sideband (SSB) modulation of the klystron for a planetary "voice-bounce." The site was in operation from 16 to 20 hr/day; during the remainder of the day, some developmental testing was done; an improvement in the instrumentation was made by the installation of an event recorder to provide a permanent record of 35 functions, which occur intermittently during the operation of the transmitter.

The characteristics of the linear modulator are treated herein. The developmental testing, also described in this report, was a study of improvement in the linearity of klystron amplifiers and some measurements on a high-voltage switching system intended to reduce the receiver system noise by turning off the klystron during receiving cycles when the radar is used on the Moon.

Two devices are being designed and constructed: the high-voltage switching system and a surge resistor assembly to limit peak currents in the klystron. They will be installed on the transmitter in the future.

b. Linear exciter. A linear 2388-Mc power amplifier (exciter) used to drive the 100-kw S-band transmitter during the Venus radar voice-bounce experiment has been installed in the 85-ft antenna at the Venus site, GTS.

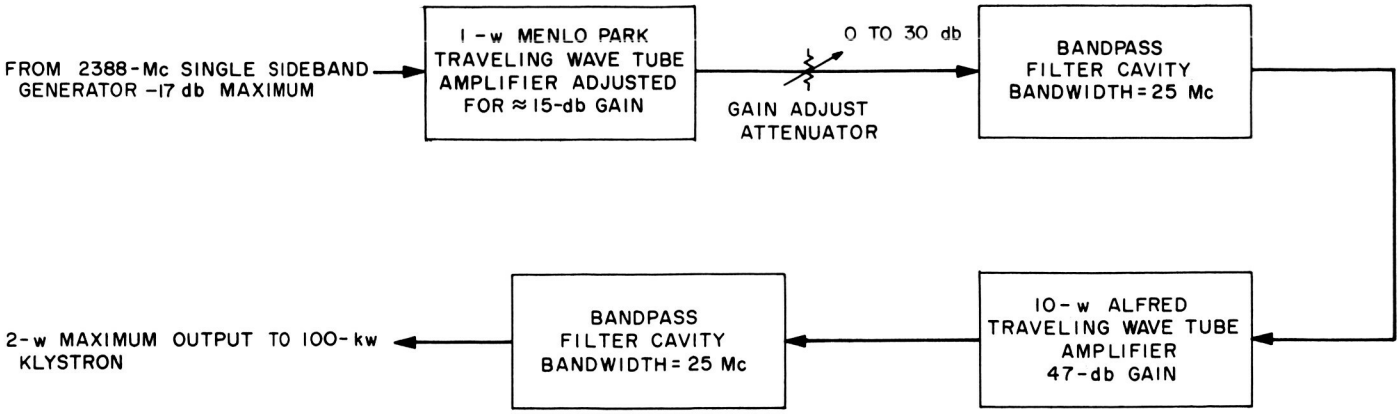

Fig. 17. SSB linear power amplifier block diagram

Its function is to provide linear, high-gain, power amplification of low-level, voice-modulated, 2388-Mc SSB signals; power outputs of 2 w (36 dbm) with gains approaching 60 db are required. The power amplifier consists of two cascaded traveling wave tube amplifiers (TWTA). Fig. 17 is a block diagram of the exciter and Fig. 18 shows the rack-mounted TWTAs installed in a cabinet in the antenna cage.

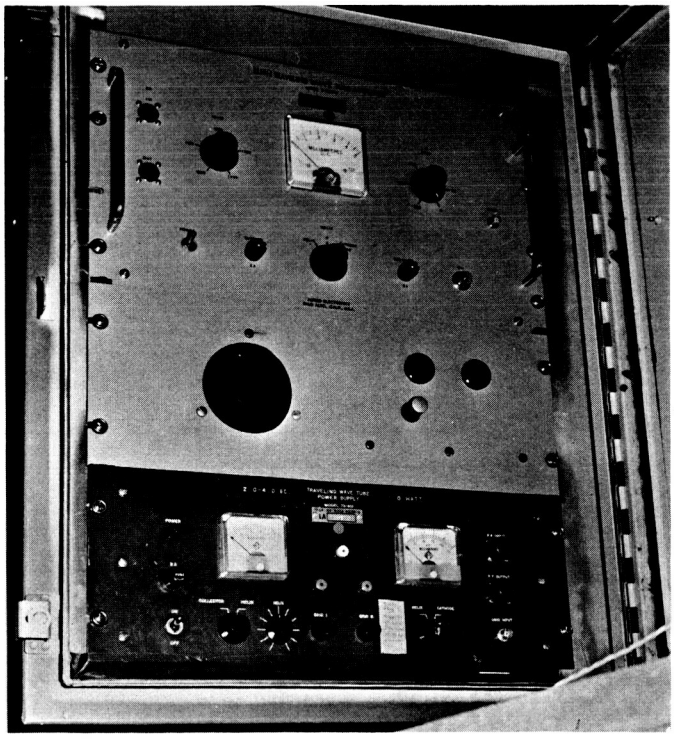

Fig. 18. Photograph of TWTAs installed in 85-ft antenna

Linear amplification is a requirement of a SSB exciter. A nonlinear system not only distorts the modulated signal but also spreads the output frequency spectrum over a wide-band, thereby reducing the effective radiated power that lies within the bandpass of the receiver.

The 3-w, 2388-Mc grounded-grid triode amplifiers that are normally used in the planetary radar experiments (Ref. 9), were tested for linearity and power output. The linearity curve for a typical amplifier tested is shown in Fig. 19. Since the maximum power output in the linear range (32 dbm or less) was marginal at best and the total gain was some 30 db less than required, the 3-w amplifiers were considered unsuitable for SSB use.

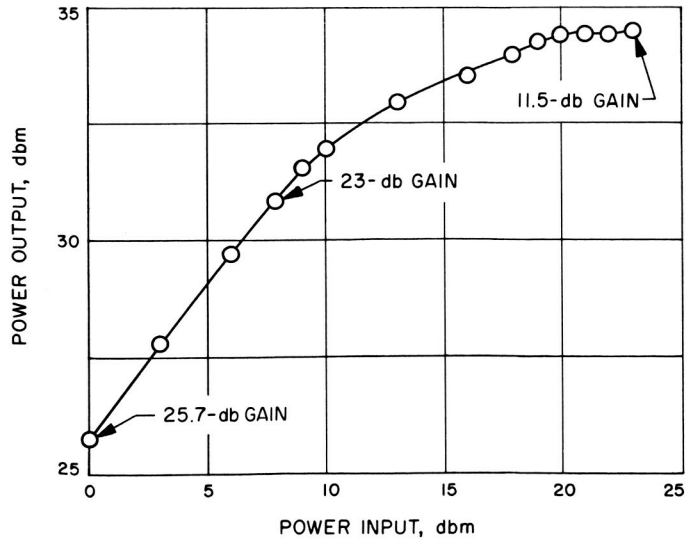

Fig. 19. 3-w, 2388-Mc amplifier power output versus power input

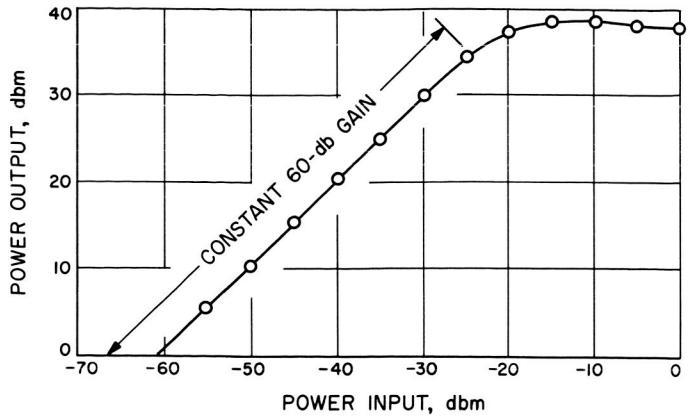

Fig. 20. Cascaded TWTAs power output versus power input

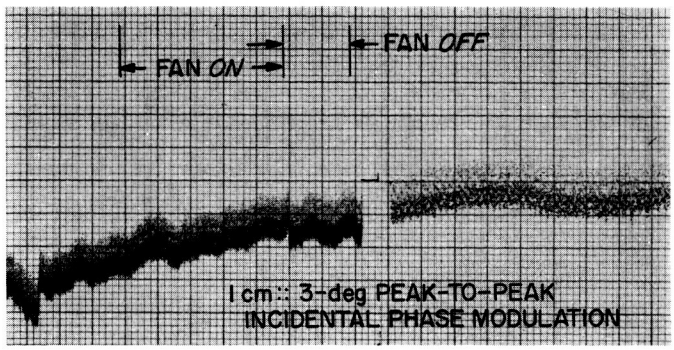

Fig. 21. Incidental phase modulation of cascaded TWTAs

Fig. 20 shows the very linear gain characteristics of a 10-w Alfred Model 5-6868V TWTA cascaded with a 1-w Menlo Park Model TA-401 TWTA. The gain of the 10-w TWTA is about 47 db, and the gain of the 1-w TWTA is approximately 15 db. The 1-w TWTA nominal gain of 40 db was decreased to the 15-db figure by reducing the helix and grid voltages of the TWTA.

The TWTAs used had typical noise figures of 30 db or more. This noise is distributed over a very wide band of hundreds of megacycles. With both TWTAs cascaded, noise powers of 11.5 dbm were measured at the output with a power meter. In the initial linearity checks, this noise masked the 2388-Mc injected signal and made the gain characteristics appear nonlinear at low input power levels. This noise masking effect was made negligible after bandpass filters were installed in the outputs of each TWTA; the noise power was reduced to −8.6 dbm allowing accurate gain measurements.

TWTAs are inherently susceptible to phase noise due to both helix voltage variations and helix mechanical vibrations. The incidental phase modulation (IPM) of the cascaded TWTAs was measured using the same IPM test unit as described in Ref. 9. Fig. 21 shows the measured 2.25-deg peak-to-peak IPM of the cascaded TWTA with and without the external fan running. It was feared that the fan vibration might introduce IPM. The cooling fan is necessary to help dissipate the 1500 w consumed by the units.

Amplitude variations in the TWTA output as high as 6 db were noted after the unit was first installed in the antenna. These variations were due to the RF feedback from the output of the 100-kw klystron to the TWTAs; both TWTAs are nonshielded, rack-mounted units and the door of the cabinet housing the TWTAs was left open. It was originally intended to leave the door open to provide fan forced air cooling of the units. With the door closed, the variations in power were relatively minor. Subsequently, vent holes were drilled in the door and covered with screen for the forced air cooling; the rubber gasket around the door was replaced with RF gasket material. After the above was done, the amplitude variations caused by klystron RF feedback ceased to be a problem.

c. Improvement in the linearity of high-power klystron amplifying tubes. High-power klystron amplifying tubes are operated in a saturated condition and "high-efficiency" tuned when maximum power output at maximum efficiency is desired. In this mode, the input amplitude versus output amplitude response is very nonlinear. High-efficiency tuning requires 10 db more drive power; but the output power is increased about 10% over synchronous tuning.

Klystrons are more linear with lower drive levels; at 70% of rated output, the deviation from linearity is about 10%. Below this output level the deviation is even less. In voice communication experiments, using passive reflectors in space (i.e., Echo and Venus), it has been necessary to sacrifice power output to achieve linearity. This reduces the signal-to-noise ratio and degrades the intelligibility.

The linearity can be improved at rated power output by increasing the dc beam voltage above that at which the tube is nominally operated. Fig. 22 illustrates this point. The VA-858 klystron is usually operated at 32.5-kv beam voltage, and delivers 100 kw when saturated and only 70-kw average when used for linear transmission.

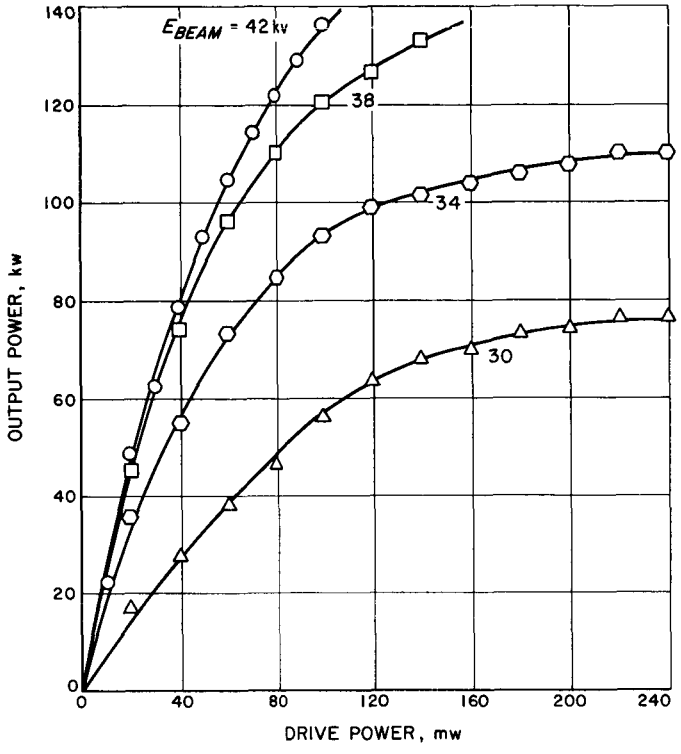

Fig. 22. Drive power, mw klystron linearity; VA-858, No. 1

For 42-kv beam voltage, the improvement in linearity is significant. Data for these curves were obtained by CW operation. In an actual experiment, the average power level would be set to 100 kw and the peak power would be about 150 kw.

By synchronously tuning the tube, the linearity can be improved slightly, as shown in Fig. 23.

d. 100-kw transmitter event recorder. The 100-kw transmitter is a complicated system with numerous events, signals, and interlocks which are constantly changing during the course of operations. Failures and unusual behavior are often difficult to analyze due to this multiplicity of functions occurring intermittently and often quite rapidly. Two 20-channel event recorders have been installed to record these transitory indications and provide a permanent record.

The data are recorded on paper tape which will then be stored at the site where it will be available for trouble-shooting and future system analysis.

The two 20-channel recorders are shown in Fig. 24. They are mounted in the auxiliary control cabinet used

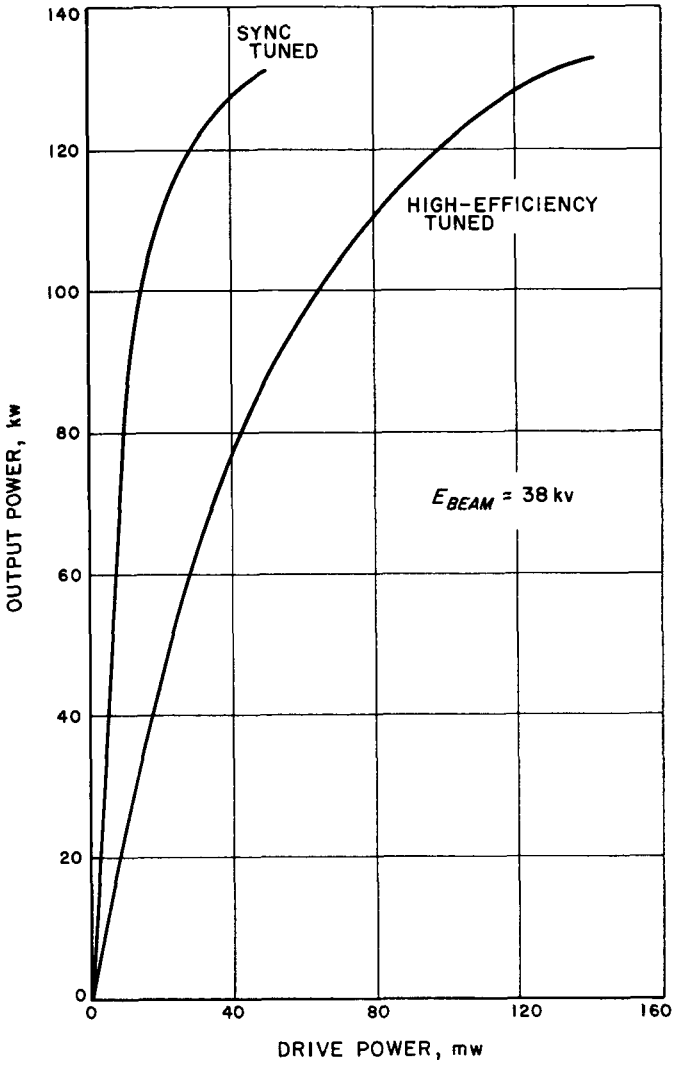

Fig. 23. Comparison of linearity sync tuned versus high-efficiency tuned

for testing *Mariner C* and Venus transmitters in the cone storage area. The control panel, immediately below the recorders, permits the control and indication of recorder power, paper drive, pen heaters and paper drive speed-shift. Thermal recording pens eliminate pen servicing and thereby leave only the changing of chart paper as the single daily maintenance requirement. The tape speeds available are ¾, 1½, 3, 6, 12 in./hr and ¾, 1½, 3, 6, 12 in./min. The fast speed, obtained by operating the speed-shift panel switch, is useful for system turn-on, special tests and recording malfunctions.

The following interlocks and functions concerned with the klystron will be recorded:

(1) Interlock reset energized.
(2) RF output unterminated.

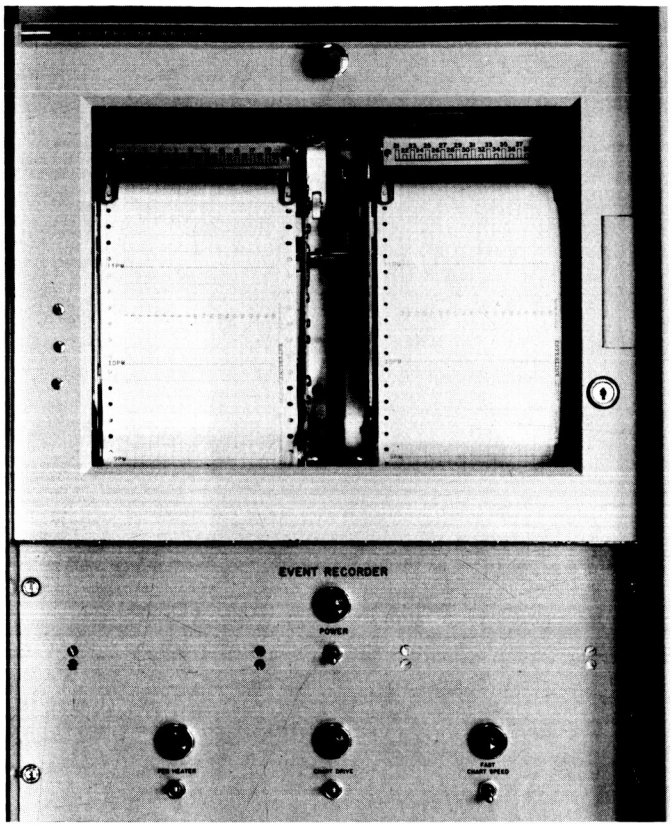

Fig. 24. 100-kw transmitter event recorder

(3) Waveguide low-pressure.
(4) Collector water low-flow.
(5) Body water low-flow.
(6) Magnet water low-flow.
(7) RF load water low-flow.
(8) Vac-ion switch nonoperating position.
(9) Filament air failure.
(10) Filament time delay incomplete.
(11) Filament under-current.
(12) Vac-ion over-current.
(13) Collector over-current.
(14) Body over-current.
(15) Reflected power over-power.
(16) Klystron window arc.

The following interlocks and functions concerned with the system will be recorded:

(1) Door interlocks open, ground units.
(2) Door interlocks open, antenna units.
(3) Cable-connections interlock open.
(4) Heat exchanger failure.
(5) Main generator over-current lockout.
(6) Main motor-generator starting incomplete.
(7) High-voltage rectifier filament time delay incomplete.
(8) High-voltage control off zero.
(9) Crowbar logic energized.
(10) Crowbar arc-gap fired.
(11) High-voltage dc over-current.
(12) High-voltage dc over-voltage.
(13) Coolant over-temperature.
(14) External system interlocks open.
(15) Series limiter interlock open.
(16) High-voltage rectifier current unbalance.
(17) Low system power factor.
(18) High-voltage transformer oil over-pressure.
(19) RF drive on.

Five spare channels will provide the needed flexibility for instrumenting special tests. These data will become a part of the daily maintenance log. When the paper event recorder tapes and the maintenance and operation logs are assembled together, a permanent record in detail will be available for future analysis.

e. Klystron surge resistor assembly. The power klystron is sometimes subjected to momentary overloads and surge currents when internal arcing and outgassing occur. The klystron surge resistor assembly is being built to limit these occasional peak currents, thereby protecting the klystron and prolonging its life.

The klystron is now protected from overloads by two separate devices: the crowbar system and the series limiter tube. The crowbar is a spark-gap which, when triggered by external equipment, causes a gap to break down, thereby rapidly removing voltage from the klystron. The series limiter is an emission-limited diode tube which limits the peak surge-currents that the klystron can draw from the power supply.

In spite of the double protection offered by these devices, there are still situations which may occur, such as klystron cathode-to-body arcs and waveguide arcs, which could damage the tube or reduce its life. This is due to the finite time required for the crowbar system to sense a fault and discharge the power supply. In addition, the capacity in the cable between the series limiter and the klystron has considerable stored energy and the series limiter cannot limit the discharge of this energy. This cable capacity was measured and found to be 17,600 $\mu\mu$f. The energy that would be stored in this cable, at an operating voltage of 32,000 v, is 8.7 joules.

Assuming a klystron cathode-to-body arc resistance of 4 Ω, the instantaneous peak current would be 8,000 amp.

The proposed solution is a power resistor assembly installed in the antenna as close to the klystron as possible. The incoming klystron high-voltage lead is connected to the series resistor, and the other end of the series resistor assembly is connected to the klystron. A 10-Ω surge resistor would limit the instantaneous peak current to about 2,200 amp and the energy of the tube arc would be reduced to 2.3 joules. Thus, the energy dissipated in the klystron tube arc as a result of the charged power supply cable capacity would be reduced to 30% of the non-limited case. The energy of the power supply would be removed in the conventional manner by the crowbar and arc-gap system. A weatherproof housing is being procured to protect the equipment from the climatic elements and to protect the personnel from accidental electrical shock. A water manifold assembly is being designed to remove the heat from the assembly.

An additional advantage to be gained by limiting the klystron current at the klystron is the elimination of the series limiter. This device, a diode which uses a temperature limited tungsten filament, is very inefficient. The power lost due to the voltage drop across the tube is about 90,000 w. An additional 21,600 w are expended to heat the series limiter tube filaments from the 400-cycle auxiliary generator. The elimination of the series limiter will also permit the realization of the full 1-Mw output power from the high-voltage dc power supply.

f. 100-kw transmitter beam-voltage switch. A lunar mapping program has been proposed wherein radar signals reflected from the Moon will indicate its surface irregularities and contours. By using narrow range gates, accurate and useful data may be obtained which will be of value to any lunar program. To obtain maximum resolution, the minimum possible range-gate width should be used. However, the system signal-to-noise ratio sets a lower limit on range-gate width.

A method to make possible an increase in range resolution by decreasing the system noise is to remove the transmitter klystron beam voltage during the receive cycle. The klystron produces noise in the absence of RF drive due to the perturbations in the electron beam. This is a problem inherent in klystrons since a monochromatic klystron generator or amplifier is not available. The velocity cross-section of the klystron beam is not constant and gas and impurities constantly change the effective work function at the cathode.

The signal-to-noise ratio was previously shown (Ref. 10) to be:

$$\frac{S}{N} = \frac{H}{B} \frac{P}{kT + a\alpha P^x} \tag{1}$$

where

$$H = \eta \frac{G_{trans} \; A_{target} \; A_{rec}}{(4\pi R^2)^2} \tag{2}$$

When based upon the 85-ft transmitting dish, the following parameters apply:

$\eta = 0.01$ (target cap and system loss)

$G = 53$ db (85-ft antenna gain)

$A_{target} = 1.64 \times 10^9$ m² (effective area of 300 m deep front cap resulting from a range-gate width of 150 m.)

$A_{rec} = 1.25$ m² (effective area of 6-ft antenna)

$R = 4.66 \times 10^8$ m (at apogee)

Therefore, from formula (2)

$$H = 0.01 \frac{2 \times 10^5 \times 1.64 \times 10^9 \times 1.25}{[4\pi(4.66 \times 10^8)^2]^2} = 5.5 \times 10^{-25}$$

The receiver bandwidth B is 20 cps, and the system temperature T is assumed to be 100°K, and $k = 1.38 \times 10^{-23}$ w/cps (Boltzmann's constant). The klystron noise was expressed as:

$$\alpha P^x$$

where

$\alpha = 5 \times 10^{-25}$

P = transmitted power when RF drive is applied

$X = 2.85$

The isolation between the transmitter antenna and the "tunneled" 6-ft receiving antenna is taken as −90 db, and designated as "a." Therefore, the signal-to-noise

ratio at the optimum power of 18.5 kw is, from formula (1):

$$\frac{S}{N} = \frac{5.5 \times 10^{-25}}{20} \frac{1.85 \times 10^{4}}{1.38 \times 10^{-23} \times 100 + 10^{-9} \times 5 \times 10^{-25} \times (1.85 \times 10^{4}) 2.85}$$

$$\frac{S}{N_{db}} = -6.62 \text{ db}$$

The effect of keying the klystron beam voltage off during receiving is mathematically equivalent to removing the $a\alpha P^x$ term in the denominator of formula (1). In addition, there is no longer a restriction on the value of power output P for optimum signal to noise.

Therefore, using the full 100-kw capability of the transmitter and eliminating the receiver-transmitter isolation problem, we have in the beam-keyed case:

$$\frac{S}{N} = \frac{H}{B} \frac{P}{kT}$$

$$\frac{S}{N} = \frac{5.5 \times 10^{-25}}{20} \quad \frac{10^{5}}{(1.23 \times 10^{-23})\ 100} \qquad (3)$$

$$\frac{S}{N_{db}} = +3.5 \text{ db}$$

The advantage of the beam-keying method is plainly evident by the demonstrated 10.1-db gain in signal-to-noise ratio. In addition, there is no limitation on future transmitter expansion programs and the concomitant increases in transmitted power and decreases in receiver–transmitter isolation.

In order to fully utilize the mission time, the transmitter must be turned on and off at approximately 2-sec intervals to allow the receiver to function when the reflections return. A pair of vacuum switches has been selected for this purpose (Fig. 25). One vacuum switch connects the power supply to the klystron and the other connects to the dc water load. These switches operate at 180 deg to each other, so that the load on the power supply is maintained and serious voltage transients are avoided.

These switches were tested manually at the Venus site transmitter. No klystron was employed in these preliminary tests as the experiment was designed to evaluate the vacuum switches. The high-voltage dc power supply was alternately connected and removed from the dc water load. A 2000:1 capacity divider was used to view the voltage across the load, and a system current-shunt was used to view the current passing through the load (Fig. 26).

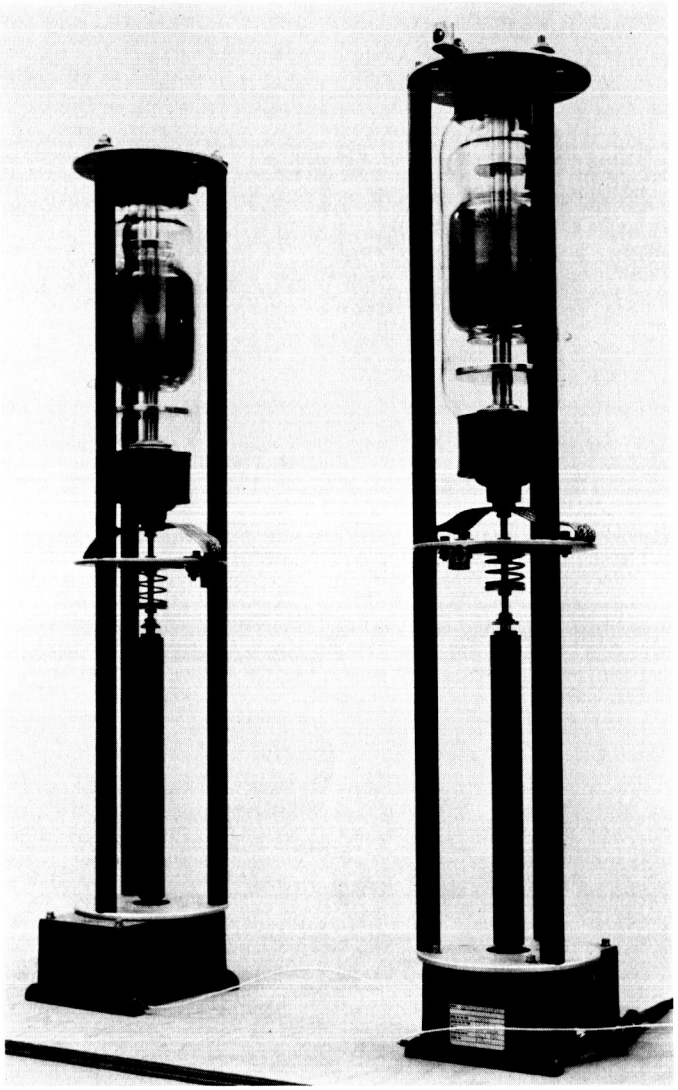

Fig. 25. Klystron beam-voltage vacuum switches

Fig. 27 shows a typical voltage waveform across the water load as the power supply was interrupted by the vacuum switch. Since the high-voltage power supply is negative, the waveform deflects to the top of the oscilloscope screen. The exponential decay after the waveform rises to zero potential is due to the nature of the capacity-divider test instrument and may be disregarded in analyzing results. Arcing can be observed as vertical spikes 2 msec before the switch breaks the connection to the load. Note: the turn-off time from the removal of solenoid current to switch-opening is 18 msec.

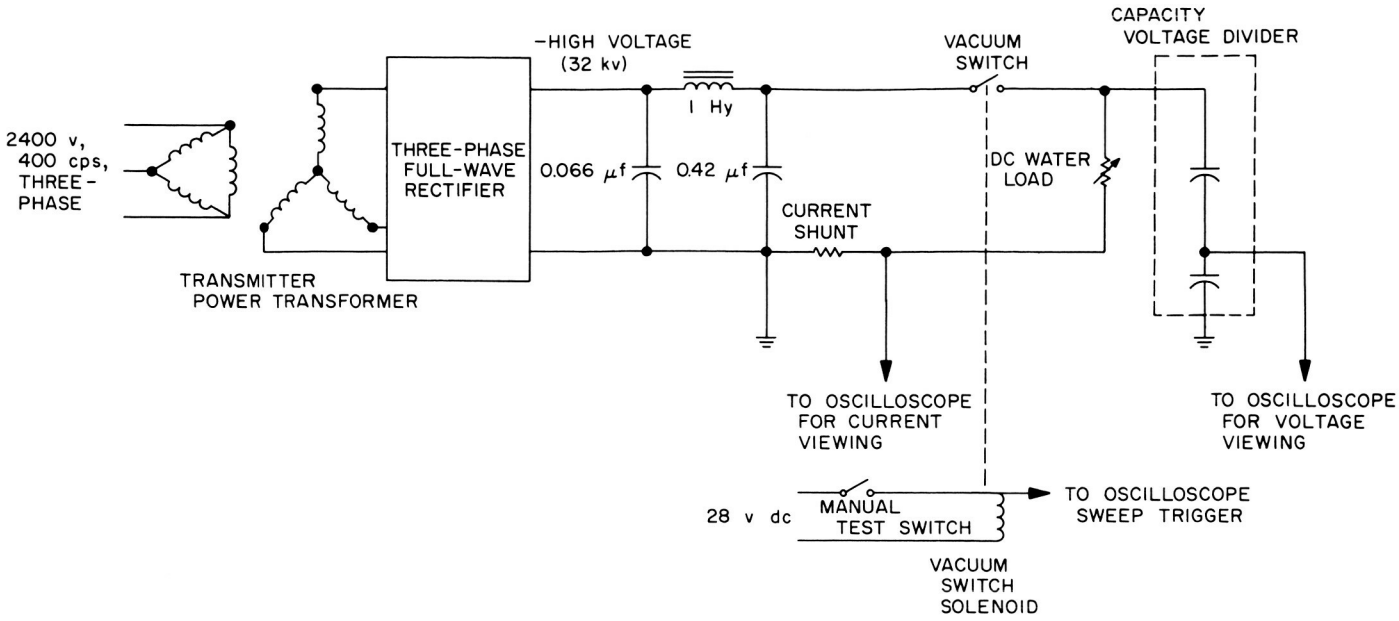

Fig. 26. Transmitter power supply and beam-switch test circuit

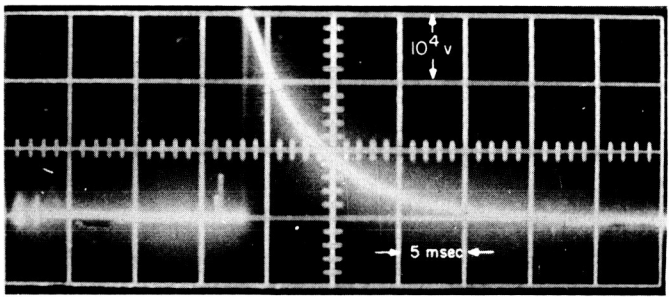

Fig. 27. Vacuum switch operation showing opening voltage transient at load

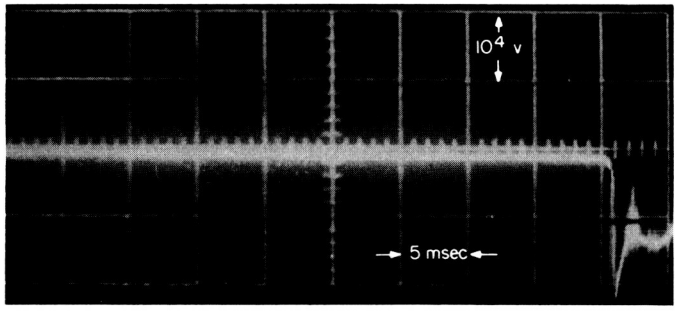

Fig. 28. Vacuum switch operation showing closing voltage transient at load

Fig. 28 shows a typical voltage waveform across the water load as the power supply is applied to the load via the vacuum switch. Here the voltage waveform drops from zero to a negative value. Note the arcing due to switch contact "bounce" in the first 3½ msec. The closing time is shown to be 46 msec after energizing the switch solenoid.

Fig. 29 shows the current waveform when the vacuum switch interrupts the power supply connections to the water load. Arcing appears for 2 to 3 msec.

Fig. 30 shows the current waveform when the vacuum switch connects the power supply to the water load. Arcing appears for 4 msec. (The small periodic negative and positive spikes on the last two current waveforms are residual rectification spikes and may be ignored.)

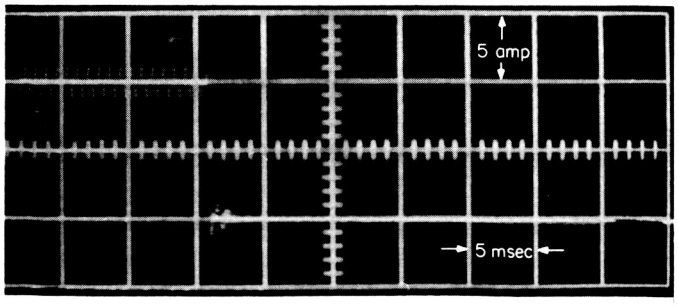

Fig. 29. Vacuum switch operation showing opening current transient at load

These tests have shown that the vacuum switch can successfully switch the required voltage and interrupt the required current. The short periods of arcing were expected and will not affect the system performance. The

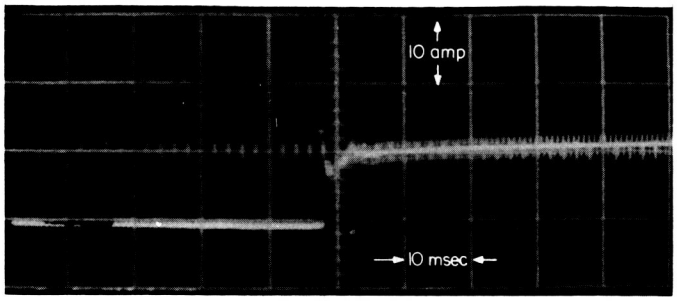

Fig. 30. Vacuum switch operation showing closing current transient at load

arcing will, however, heat the switch contacts. The manufacturer has stated that this arc duration is tolerable for this particular application.

Since the closing time for the vacuum switch is much longer than the opening time, an electronic speed-up circuit is being designed. In addition to providing a faster switch closure, the completely solid-state circuitry will accept the computer pulses from the digital control equipment and translate them into vacuum switch operations without the use of electro-mechanical relays or other such mechanical devices. Special adjustable delay circuits will be provided to control the initiation of the switching function at each vacuum switch. This will insure a minimum transient in the high-voltage power supply whenever the klystron is turned on or off.

The manufacturer has given assurances that the switch life, when operating at 35,000 v and 10 amp, would exceed 1,000,000 operations. When used in the lunar mapping program, this would provide over 3 mo of operation based upon a 12-hr-operating day, before replacement of the vacuum switch contacts became mandatory. The result is a system which reduces the receiver noise threshold while maintaining an adequate useful life and a nominal operating cost.

D. X-Band Lunar/Planetary Radar Project

1. Maser and Instrumentation

a. Introduction. An 8448-Mc maser was purchased from Hughes Research Laboratories, Malibu, California. The maser will be used in a low-noise radiometer/radar-astronomy receiver for advanced communications systems and components experiments on the 30-ft antenna at the Goldstone Venus site. The maser capabilities were evaluated at JPL; measurements of bandwidth, gain and gain stability, input match, and noise-temperature were made. A detailed report of the maser performance is given in Ref. 11.

b. Maser description. The complete Dewar-mounted maser assembly is shown in Fig. 31. The maser has an RG-51/U (H-band) waveguide at the input and output and consists of nine cavity amplifiers, separated by isolators that are cooled to liquid helium temperature; it does not require an external circulator. The ruby *c*-axis is positioned 54.7 deg with respect to the applied magnetic field. The magnet, located inside the Dewar, is equipped with a trim coil for magnet tuning. The magnetic field strength can be permanently set by applying pulses of the correct polarity to the trim coil, thereby eliminating gain instability normally caused by instability in the trim coil current. The complete lower end of

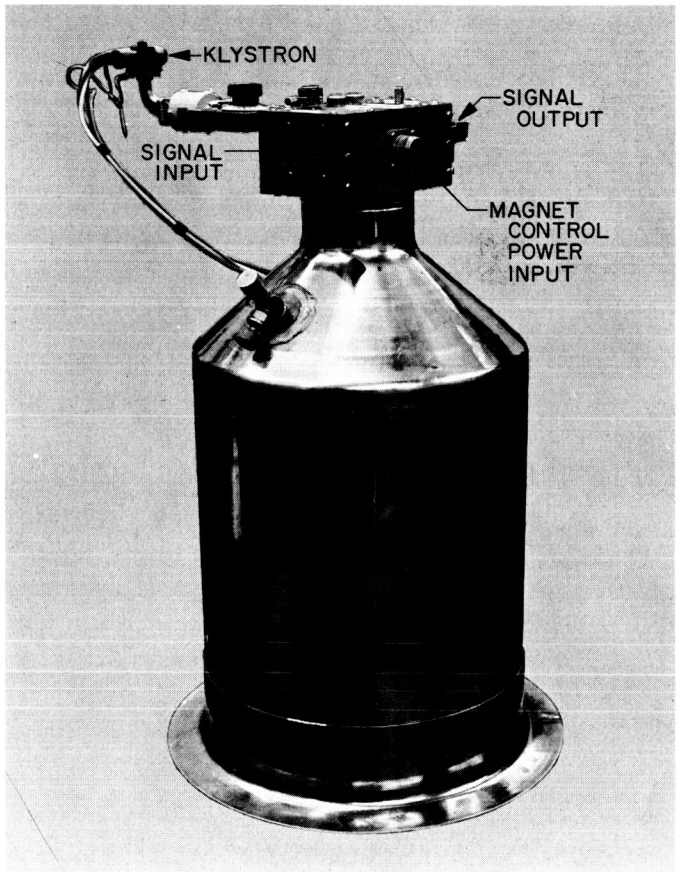

Fig. 31. 8448-Mc, nine-cavity maser amplifier mounted in a 6-liter Dewar

the maser assembly (cavity amplifiers, magnet, and trim coils) is encased in a copper jacket, which is lead-plated to provide a superconducting magnetic shield. The orientation of the maser assembly in the Earth's magnetic field does not appreciably affect maser gain. Thermal radiation shielding is achieved by placing a copper jacket around the 6-liter helium Dewar, which is cooled by escaping helium gas rather than by the usual method of liquid nitrogen cooling. Removal of the microwave pump power increases the liquid helium life slightly.

c. Dewar performance. A maser operating life of 24 hr is provided by the 6-liter helium Dewar, which is equipped with a single fill hole for liquid helium transfer. The diameter of the liquid helium fill hole is constricted, so that a standard fill tube cannot project to the bottom of the Dewar. Since filling difficulty was experienced (10 liters to refill the Dewar), a small $\frac{7}{32}$-in.-diameter flexible fill tube was constructed (Fig. 32) that would enable penetration to the bottom of the Dewar.

d. Maser amplifier performance. The measured 1- and 3-db bandwidths at 33-db nominal net gain are approximately 9 and 15 Mc, respectively. The 3-db tuning range is approximately 15 Mc. The maser has a pump on/off gain of 55 db. When no pump power is supplied, the maser has an insertion loss of 22 db, of which 12 db are caused by ruby absorption. The maser gain starts to saturate at an input signal level of approximately −76 dbm.

The equivalent noise temperature of the maser amplifier was measured using calibrated liquid helium and liquid nitrogen cooled terminations matched to VSWR less than 1.03 at the operating frequency. The insertion loss measurements of the RG-51/U waveguide assemblies have been made accurate to about 0.001 db. Noise temperature measurements of T'_R (defined at the input to the directional coupler) for various combinations of cooled input terminations are given below:

Input termination temperature combinations	T'_R, °K
Liquid helium to ambient	23.0
Liquid nitrogen to ambient	25.0
Liquid helium to liquid nitrogen	22.5

The average of these measurements results in $T'_R = 23.5°K$. T'_R may be related to the maser input temperature T_R defined at the input to the waveguide tuning section, including the 0.12-db loss waveguide window. The relation between T_R and T'_R separated by a loss L at a temperature T_0 is,

$$T_R = \frac{1}{L}\left[T'_R - T_0(L-1)\right] \qquad (1)$$

With a measured loss of 0.075 db for the directional coupler at 298°K, the maser input temperature is approximately 18°K. The contribution of the postamplifier

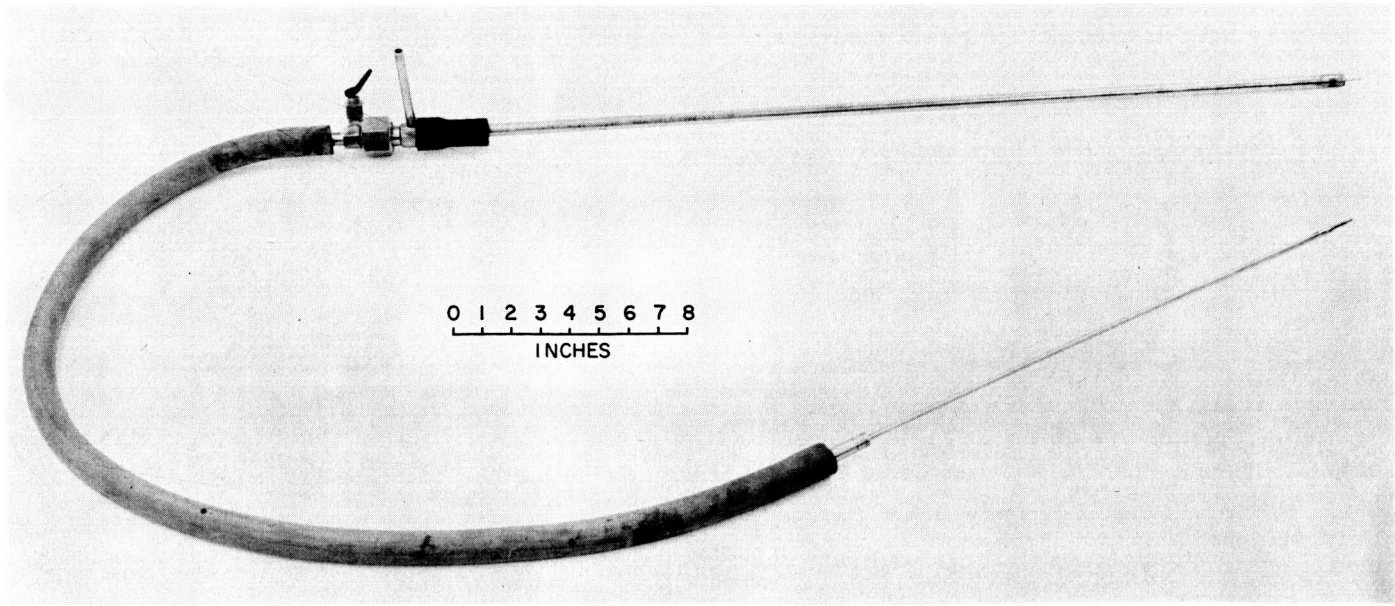

Fig. 32. Small-diameter, flexible liquid helium fill tube

was measured to be 0.3°K. The equivalent noise temperature of the maser amplifier is, therefore, 18°K, measured to better than 2°K accuracy.

e. Maser installation. The maser assembly will be mounted in the electronics cage of the 30-ft antenna below the antenna surface. The input of the maser can be switched between the antenna, liquid nitrogen, or liquid helium cooled terminations (Fig. 33) allowing accurate noise temperature measurements to be made. The output of the maser can be fed to the X-band radar receiver or the monitor receiver. The monitor receiver, mounted in the electronics cage, will have high-gain stability and will be used for maser evaluation and radio-astronomy measurements. The maser gain will be measured by setting the signal generator attenuator for equal output when the CW signal from the signal generator in the control room is switched between the maser input and output (Fig. 33, NOISE BOX).

2. Diplexer, Cassegrain Cone Installation, Noise Calibration Sources

a. Summary. The waveguide and calibration system to be used for the 30-ft antenna X-band lunar and planetary radar system is similar to the 85-ft S-band radar system. This article describes the diplexing, switching, and calibration systems involved in the waveguide and maser network. The major differences in the X- and S-band waveguide systems are due to the greater flexibility available in waveguide design due to the smaller dimensions of the X-band guide. The smaller mass of the waveguide switch rotors permits us to switch rapidly enough to diplex for lunar radar. This was not possible at S-band.

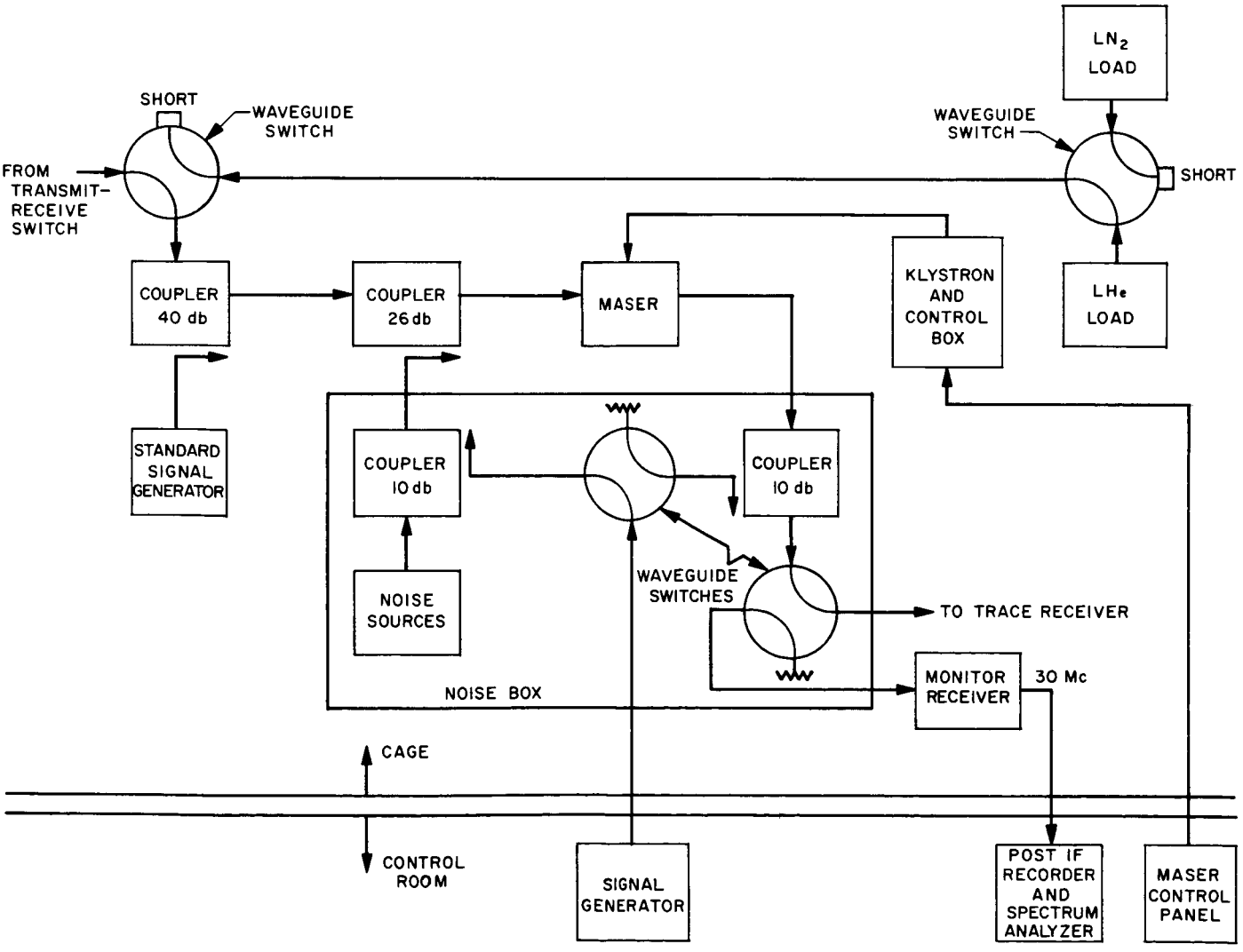

Fig. 33. Block diagram of X-band maser instrumentation

The smaller dimensions of the 30-ft dish, however, make it impossible for the Cassegrain cone to contain as much instrumentation as at S-band.

b. Diplexer and noise calibration systems. Modified WR 112 waveguide will be used in the X-band 30-ft antenna system. The waveguide is made of oxygen free high conductivity (OFHC) copper with a wall thickness of 0.125 in. The flange is a CPR 112 type which has been modified by making it thicker and adding two guide pin holes (Fig. 34). This type flange is to be used throughout the complete system wherever practical. It is estimated that the OFHC waveguide to be used in the system will have from 0.02-to 0.03-db loss per foot, which represents from 0.46 to 0.69% loss. At the anticipated future power capability of 25 kw the dissipation is from 115 to 173 w/ft. Therefore, it was decided to water cool the waveguide using conventional methods, such as soldering ¼-in. copper tubing to the waveguide walls on the transmitter run. Water from the transmitter cooling system will be used.

The switches used for all the waveguide switching including the noise and calibration box are identical. The switch body and rotor are to be built of OFHC copper. A unit similar, but not identical, to the proposed switch design was loaned to JPL for evaluation. The measured insertion loss of this switch was less than 0.02 db and the VSWR was less than 1.02. If the final switches are as good or better than the evaluation unit, the performance should be satisfactory.

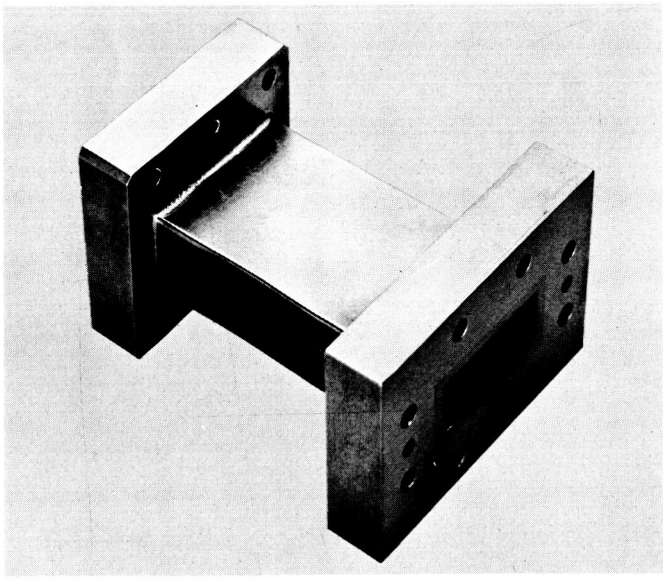

Fig. 34. Modified CPR 112 flange

The proposed Cassegrain cone layout is shown in Fig. 35. The diplexing switch is in the cone to minimize the common waveguide shared between the transmitter and maser, keeping to a minimum the problems from internal

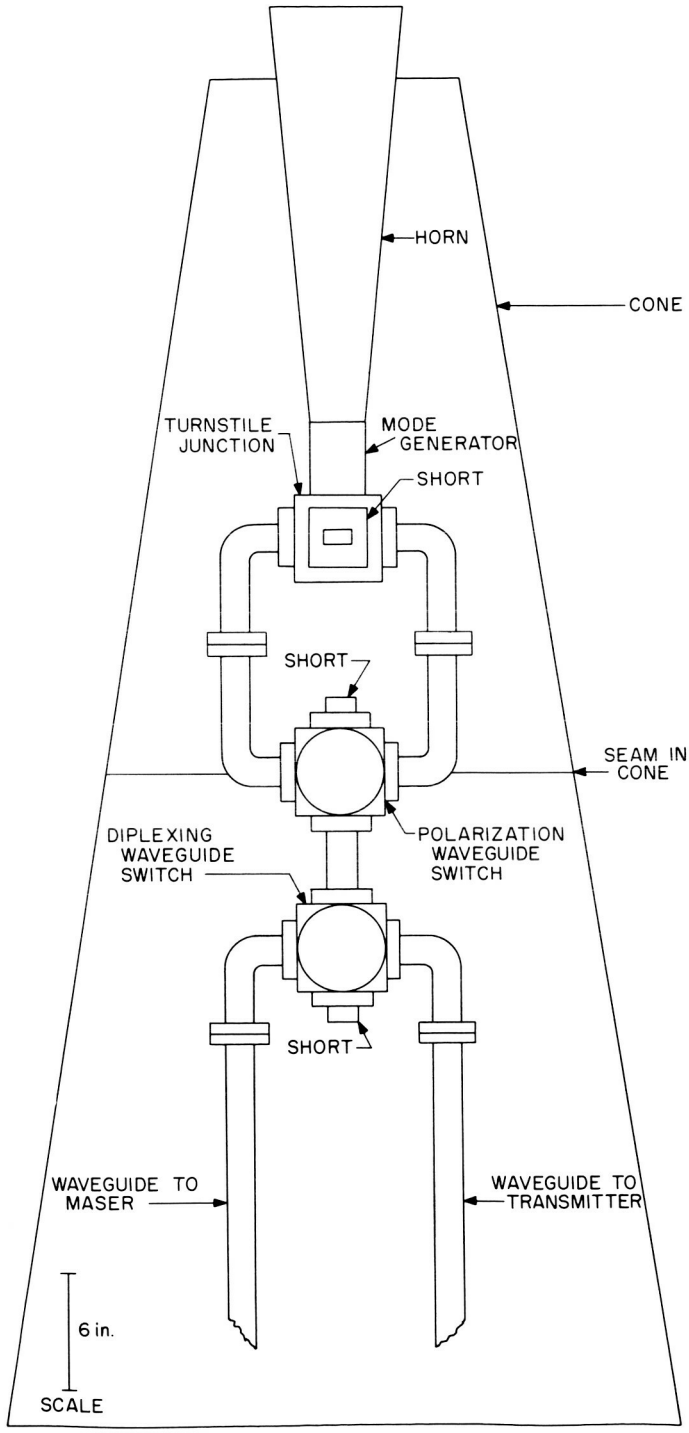

Fig. 35. Waveguide layout for 30-ft antenna Cassegrain cone

waveguide surface heating during the transmit cycle. The complete switching and diplexing system is shown in Fig. 36.

The dual mode horn (Ref. 12) is fed by a turnstile junction which can be used to generate either linear or circular polarization. The polarization switch permits the remote selection of orthogonal modes of polarization. The choice of circular or linear polarization is determined by the lengths of a pair of waveguide shorts on the turnstile junction; the shorts must be changed manually.

The diplexing function is accomplished by a waveguide switch which selects a path from the polarization switch to either the transmitter or receiver systems. The specification for isolation of the waveguide switches is greater than 60 db. One switch will not be enough to isolate the receiver from the transmitter; therefore, the calibration switch (Fig. 36) is actuated simultaneously with the diplexing switch and is used for additional isolation. The calibration switch permits connection of the maser to either the cryogenic load switch or the antenna. The cryogenic load switch will allow an accurate temperature scale to be set up on an absolute basis. The helium load will not be used continuously in the system. It will be installed on the antenna only for periodic calibration of the gas tubes. The transmitter can normally radiate either into the antenna or into the water load. The water load is used to calibrate the transmitter output as well as serving as a full power output termination.

Two cross guide couplers will be used for calibration purposes (Fig. 36). The 40-db coupler will be used in conjunction with the precision signal generator for cali-

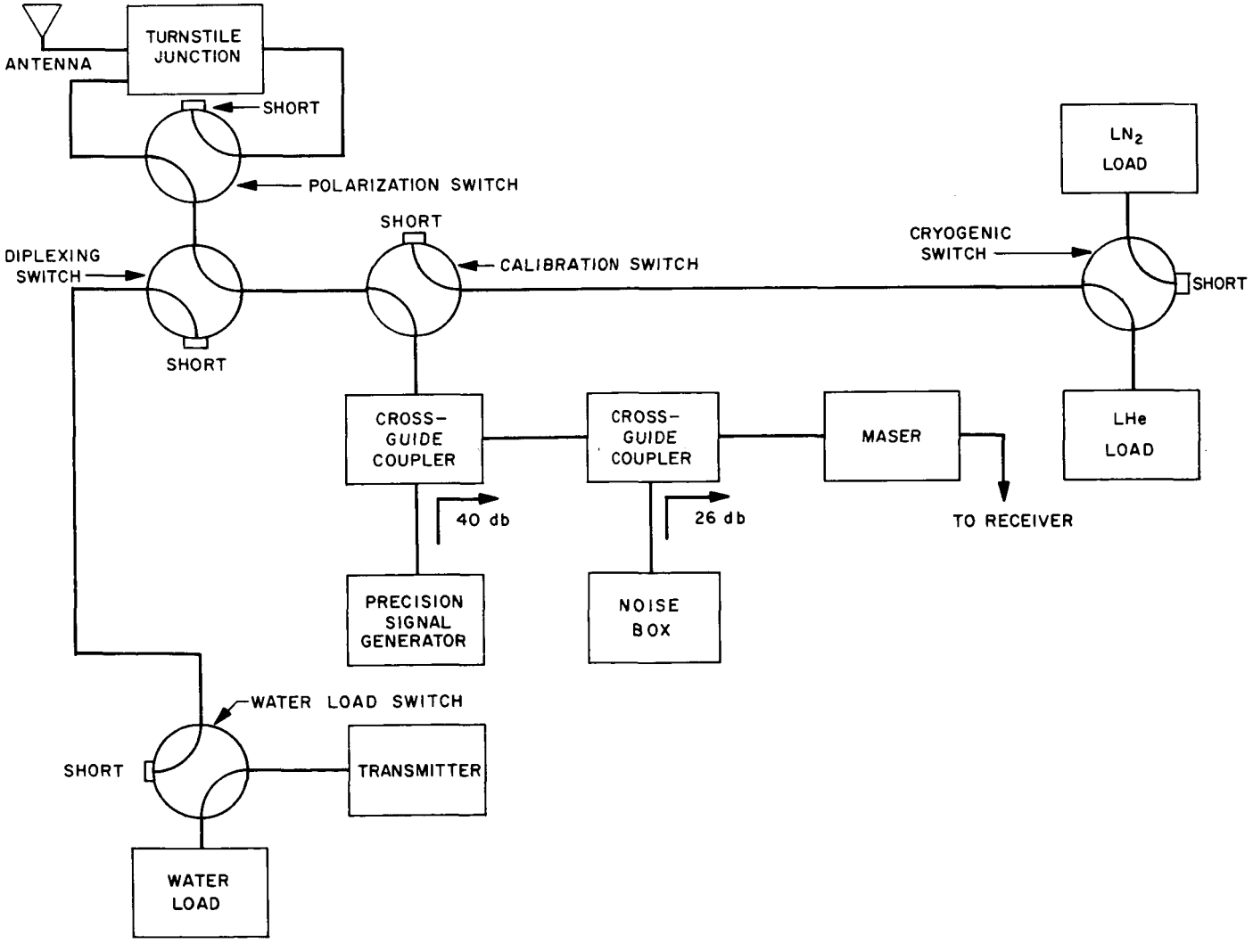

Fig. 36. X-band waveguide diplexer/calibrate system

brating the receiver gain and for calibrating the range measurement system. The noise box (Fig. 37) will be used in conjunction with the 26-db coupler to calibrate the receiver in terms of noise temperature. By coupling a test signal in before and after the maser, the maser gain can be measured. The calibration system for the maser will largely be dependent upon noise tubes; the system will be enclosed in an RF tight box as indicated in Fig. 37. The noise tubes planned for use in the circuit are TD-23 neon gas tubes which have an approximate 20,000°K output noise temperature. The circuits shown will permit the insertion of either 5 or 50°K of excess noise into the main transmission line to the maser.

The noise tubes will be left on continuously, and a waveguide switch will be used to couple the noise into the system. The reason for this configuration is based on results of tests made with two TD-11 argon gas tubes. One TD-11 was turned on and off and another was switched in and out of the circuit with a waveguide switch. It was found that the gas tube which was turned on and off had a peak-to-peak noise output variation of about 3%, over a period of 1 wk, whereas the tube which was switched with the waveguide switch had no detectable output variations.

3. Feed

a. Summary. The feed for the 8448-Mc X-band experimental radar will provide switchable circular and orthogonal linear polarization through the use of a turnstile junction polarizer. Components used in previous X-band projects are being modified for high-power use; fabrication of the feed subassembly is expected to begin shortly.

b. Recent work. Components to be used in the feed subassembly include:

(1) Hyperboloid, 34-in. diameter, $M = 4.89$ (AAS scale model).

(2) Dual mode horn and mode generator.

(3) Turnstile junction.

Both the mode generator and the turnstile junction will be constructed of OFHC copper and will be drilled for coolant passages. The dual mode horn will be made from a single piece of 6061-T6 aluminum and will have a window of 3 mil (0.003 in.) weatherable Mylar. It is expected that the horn window and clamp will operate with 10-psig internal dry gas pressure.

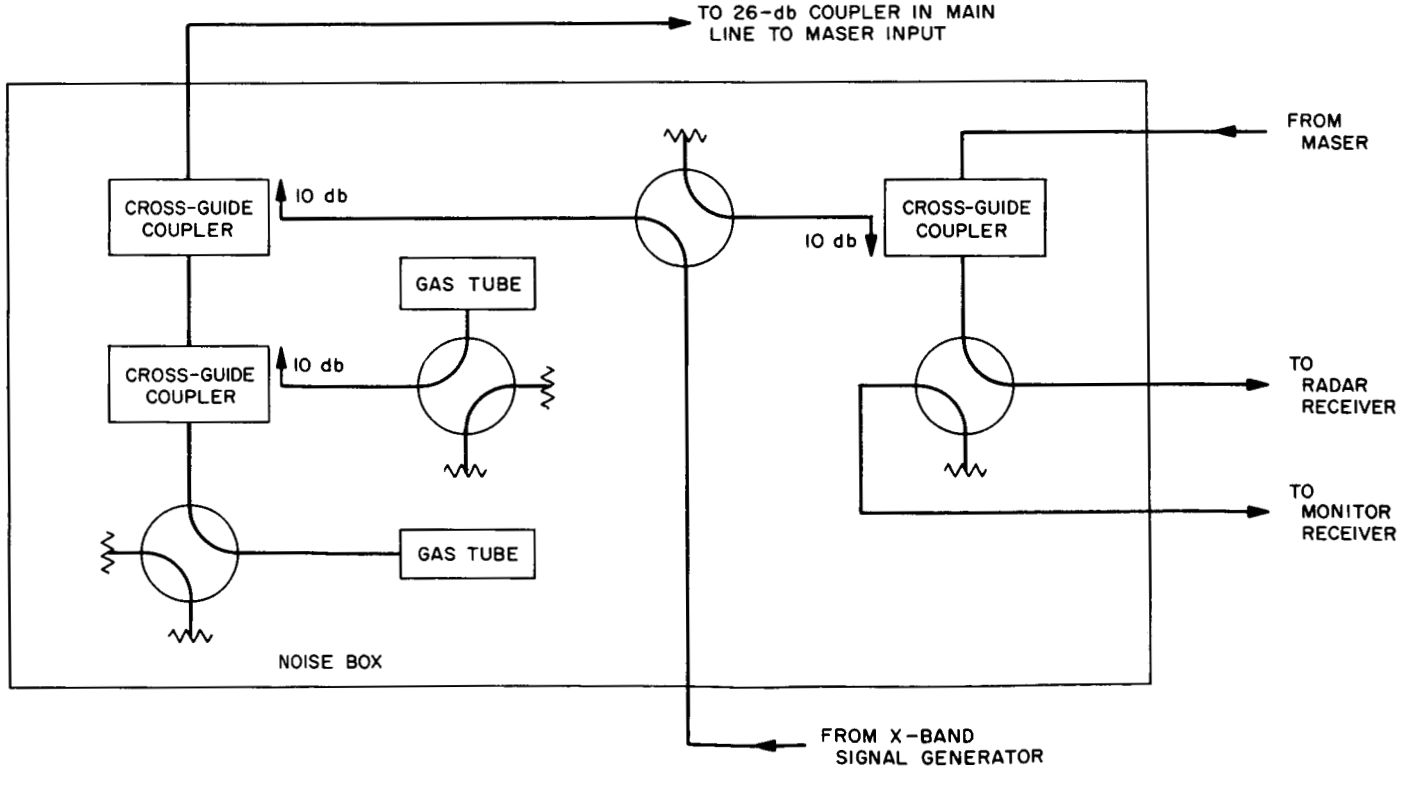

Fig. 37. Noise pulse and maser calibration system

4. S- and X-band Interim Frequency Synthesizer

a. Summary. The S- and X-band interim frequency synthesizer is currently being constructed. Original plans for the system were presented in Ref. 13. Since that time, two new modules have been added to the system.

b. New additions. One of the additional modules will be a $\times 8$ frequency multiplier to synthesize 8 Mc from the 1-Mc rubidium standard. The coherent 8-Mc signal will be used as a clock frequency for the 8-Mc precision coder subsystem.

The second module will be a data condition unit (DCU) which will receive the outputs of the in-lock detectors. The DCU will provide output voltages for the synthesizer in-lock and out-of-lock panel indicators. A relay closure is also provided in the DCU for the data recording equipment. If any one of the six reference frequency loops in the synthesizer is out-of-lock, the relay closure will indicate "bad" data at the data recording equipment.

c. Recent work. The synthesizer now requires 18 new modules to be built or to be purchased. Eleven of these modules are now completed. Two distribution amplifiers are being fabricated at the Industrial Products Division of ITT with delivery commensurate with overall system scheduling. Three more modules are nearing completion, and the two modules discussed above are in the design stages.

The 1-Mc crystal filter (Fig. 34 in Ref. 13) immediately following the rubidium standard produced a 5-cps bandwidth in the breadboard stage. A bandwidth approaching 1 cps is expected in modular form with oven temperature control.

The 35.075- and 3.635-Mc balanced mixer designs discussed in Ref. 14 are proving satisfactory in practice. The rejection of all spurious frequencies not harmonically related to the output signal is better than -120 db at the output terminal.

Two attached racks have been taken from storage and modified to house the interim frequency synthesizer. The cold plates are drilled and tapped for the mounting of modules. The rubidium standard is mounted on slides for ease of service and repair. The dc power supplies have been delivered and power distribution boxes have been constructed. The indicator and switch panels are ready to be installed in the racks.

Preliminary laboratory tests of a Montronics, Inc. 30.455-Mc synthesizer (Ref. 13) have shown the unit to be no better than the existing synthesis loop. Modifications are being considered to improve the phase noise of the unit for possible use in the synthesizer.

The S- and X-band interim frequency synthesizer is due to be shipped to the Venus site at Goldstone in midsummer of 1964.

5. Multiplier Chains

a. Introduction. Three complete frequency multiplier chains are required for conversion of the existing S-band equipment to X-band for the Lunar Radar Project. One each of these chains is used for the transmitter exciter, signal generator, and receiver local oscillator (LO) and all are capable of digital phase modulation and keying. All sub-units comprising these multiplier chains with the exception of the final $\times 4$ multiplier, have been engineered at JPL, and are being fabricated by outside sources for equipment integration in time for installation at Goldstone by mid-August. A modified stock item will be used for the final $\times 4$ multiplier.

Transitionally coupled bandpass filters are used as coupling elements, and heavy resistive loading is used to minimize mismatch due to changes in load conditions. In order to accommodate drift in center frequency, bandwidths in excess of those required for the present modulation and keying conditions are used.

The digital phase modulator utilizes passive elements throughout, in a configuration that calls for attenuation and phase stabilities of certain elements not to exceed ± 0.012 db and ± 2.8 deg, respectively.

b. Initial $\times 4$ frequency multiplier. Two active solid-state doublers are cascaded for multiplying the input frequency to approximately 140 Mc. Transitionally coupled bandpass filters having 3-db bandwidths of 9.5% are used as coupling elements and provide an over-all bandwidth of 7.5%. The over-all gain is reduced to -5 db by means of heavy resistive loading which effectively swamps changes in load conditions.

c. VHF amplitude limiting amplifiers. Two solid-state amplifying stages provide a gain of 15 db at a nominal input of 8 dbm. The over-all input/output characteristic is such that, for inputs between 4 and 12 dbm, the output lies between 22 and 24 dbm.

The 3-db bandwidth of the bandpass filters used as coupling elements is set at 35 Mc, which provides an over-all bandwidth of 25 Mc for one amplifier or 20 Mc for two amplifiers in cascade.

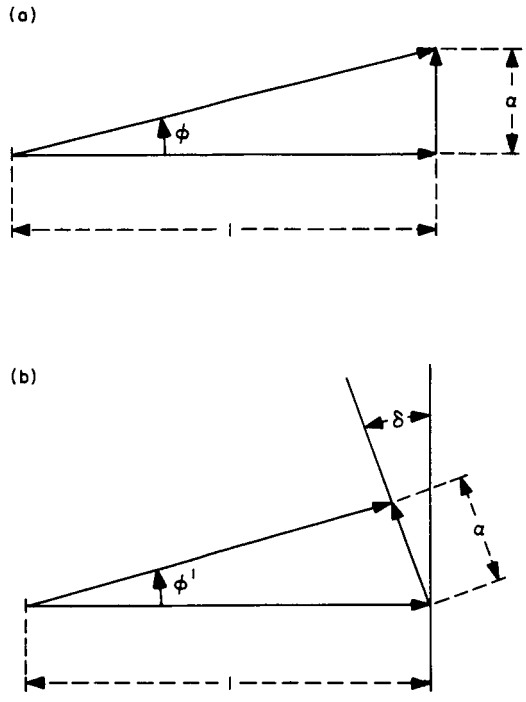

Fig. 38. Vector diagrams

d. × 15 frequency multiplier. The ×15 multiplier provides a nominal output of 21 dbm ± 1 db for a nominal input of 23 dbm. Two passive solid-state multiplier stages, a ×5 followed by ×3, are used. The first multiplier has two idlers, tuned to twice and three times the input frequency; the second, one idler at twice its own input frequency. In order to obtain a sufficiently wide and stable bandwidth, low Q idlers are used in the ×5 multiplier and to some extent in the ×3 multiplier also. Under these conditions the over-all insertion loss is about 12 db, so that a VHF amplifier having a nominal gain of 10 db precedes the passive multipliers. This amplifier is of the amplitude limiting type so that for inputs between 21 and 25 dbm the variation in output does not exceed 1 db.

e. Digital phase modulator. Digital phase modulation is obtained by the selection of either of two modulation states by means of a solid-state switch. Deviation of the main carrier is obtained by the addition of a suitably attenuated quadrature component as shown in Fig. 38(a) where the phase modulation

$$\phi = \tan^{-1} \alpha$$

Fig. 39 shows a block diagram of the complete modulator. The variable directional coupler provides the preset attenuation of the quadrature component; the variable

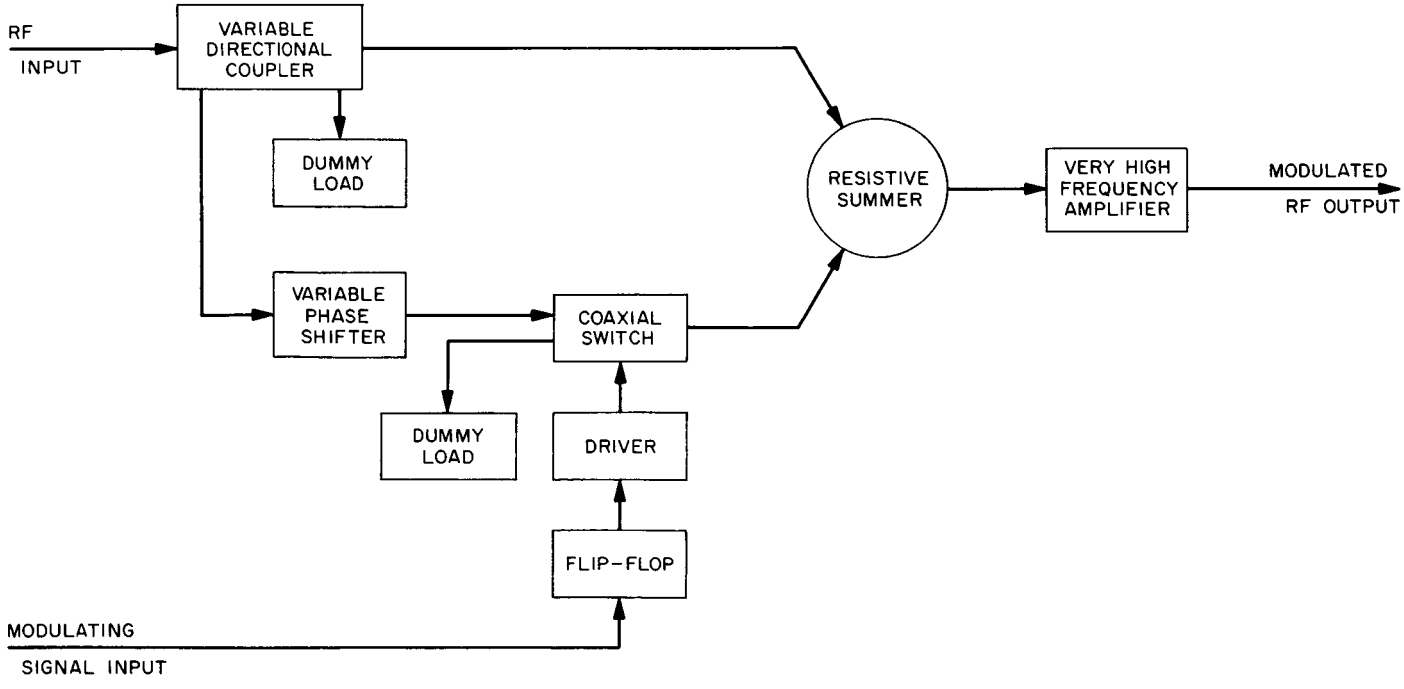

Fig. 39. Phase modulator

phase shifter provides compensation of external connection delays; switching and summing of the signals is provided by the solid-state coaxial switch and resistive summing junction, respectively. A single-stage VHF amplifier with a 3-db bandwidth of 30 Mc is included to make up for the losses in the passive elements.

The modulator operates from a push-pull square wave modulating signal having peak-to-peak voltage amplitudes of -0.5 ± 0.2 v and -1.5 ± 0.2 v. The dc flip-flop shapes and amplifies this signal so as to provide an output of 7 v peak-to-peak for the driver of the coaxial switch which, under these conditions, will have a delay of 10 nsec and a rise time not exceeding 20 nsec.

Phase modulation is performed at 1/60 of the output frequency and may be preset to any angle between 18 and 180 deg peak-to-peak at the output frequency by means of a continuously variable control which covers the range in approximately 3½ complete turns.

As explained in *SPS* 37-27, Vol. III, a deviation stability of 0.13% is required to meet a target carrier suppression of 50 db.

For small values of ϕ, required attenuation $1/\alpha = 20 \log 180/\pi\phi$ db, so that the gain stability must equal 0.012 db. The estimated stability of the system, based on supplier's figures on the variable directional coupler (0.01%/17°C), coaxial switch (0.0015%/°C) and resistive summer (0.001%/°C) amounts to 0.01% for a ±3°C cold plate tolerance.

Referring to Fig. 38(b), if δ is the phase error of the quadrature component, then the phase modulation will be ϕ^1 where

$$\tan\phi^1 = \frac{\alpha \cos \delta}{1 - \alpha \sin}$$

and phase stability

$$\frac{\tan \phi^1}{\tan \phi} = \frac{\alpha \cos \delta}{1 - \alpha \sin} \times \frac{1}{\alpha}$$

$$= \frac{\cos \delta}{1 - \alpha \sin \delta}$$

so that phase stability can equal 2.8 deg, which is three orders higher than the 0.002 deg required by the direct method indicated in Fig. 39(a) and (b). (See Ref. 15.)

f. Keyer. Keying takes place immediately after phase modulation, and is performed by a switching unit using the same components as those used in the digital phase modulator. However, since the resistive summer is not required, the single-stage amplifier is deleted, and the output is taken directly from the coaxial switch.

6. 8.448-Gc Standard Signal Generator

a. Introduction. The 8.448-Gc standard signal generator, alternately referred to as the X-band signal generator, was discussed in a previous report (Ref. 16) which described the circuit arrangement and performance characteristics.

This article deals with some circuit design changes and the current status of the project to provide this equipment.

b. Requirement change. As previously stated, the required output level was a range of −80 to −180 dbm, at the generator. The present arrangement in the X-band lunar system is such that the signal generator is coupled to the maser input through the 40-db arm of a directional coupler. Thus, the required output of the generator is a range of −40 to −140 dbm. However, since the maser (located nearby) operates at −180 dbm, the generator leakage must be kept well below the −180 level.

The 40-db isolation is required to avoid degrading the system noise temperature. The present arrangement using a directional coupler in the main signal line is shown in Sect. VI-D-1, Fig. 33 in the article entitled "Maser and Instrumentation." This arrangement is an improvement over the earlier one used in the S-band planetary radar in that the standard signal generator ties into the main signal line from the antenna via a directional coupler. This permits calibration of the signal generator independent of changes in other components of the system, as was previously the case when the noise tube and associated circuitry were switched in and out of the generator line. Also, this latest arrangement enhances accuracy, since signal substitution is accomplished under unchanged loading and matching conditions.

The effect of the 40-db insertion loss external to the generator results in a more severe leakage problem. The calibrated output attenuator operates at 40-db higher levels than previously anticipated, and hence radiation around its protruding shaft is increased.

c. Circuit improvements. Fig. 40 is a revised block diagram of the X-band generator.

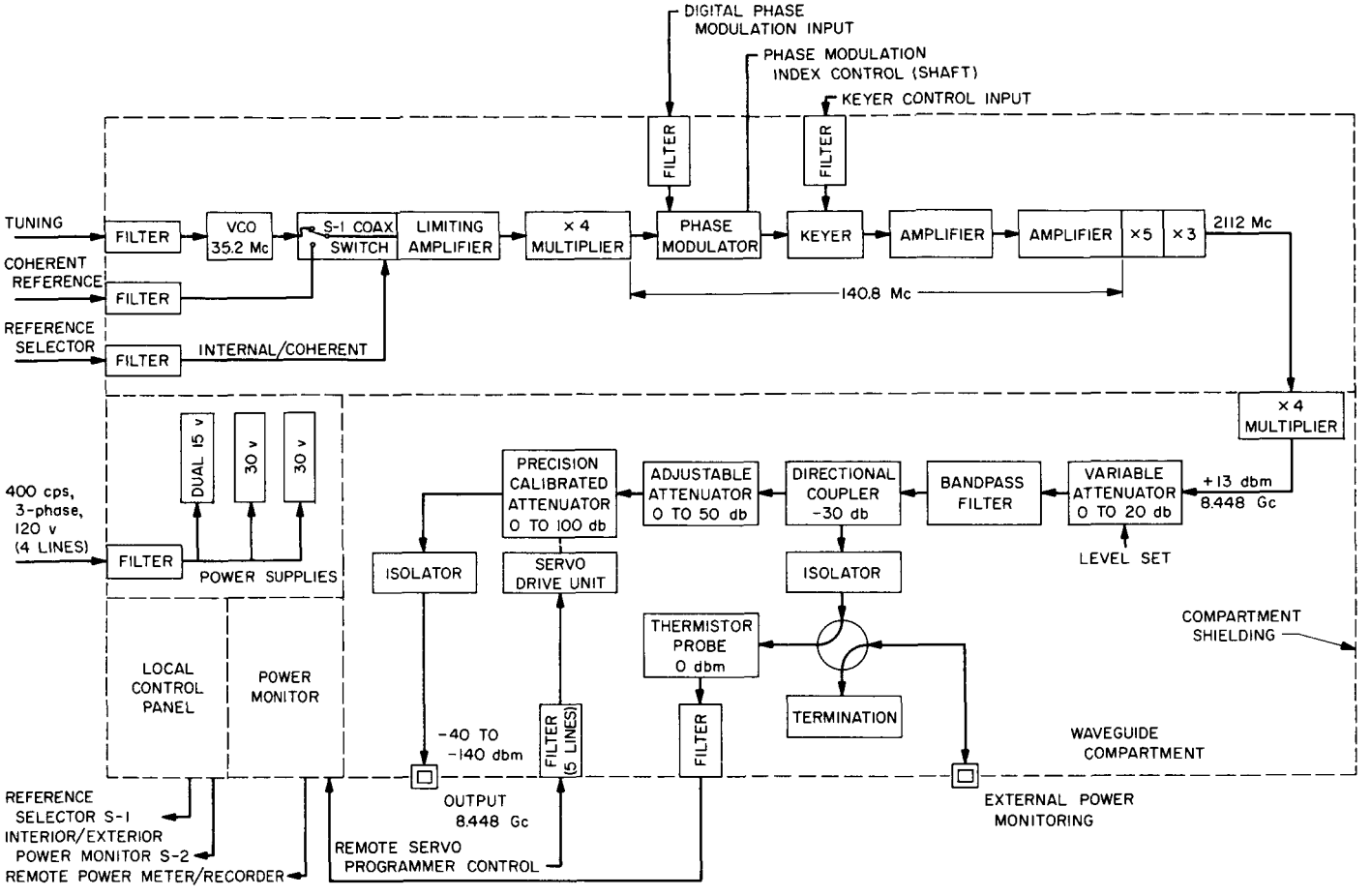

Fig. 40. 8.448-Gc standard signal generator block diagram

Note the rearrangement of the directional coupler. In the last report, this was shown feeding the signal directly to the output attenuator line, while the power monitoring picked off the signal via the attenuating arm of the coupler. In the revised circuit of Fig. 40, the signal is fed directly to the power monitoring branch. This results in attainment of 1 mw (0 dbm) at the thermistor probe, which is the optimum level for minimum drift power monitoring.

Simultaneously, this rearrangement eliminates a precision fixed attenuator in the output chain. The 30-db attenuation of the directional coupler, together with a 50-db adjustable attenuator and 100-db calibrated variable attenuator, provide all the necessary output range and range adjustment to permit use of any 100-db range between −30 and −180 dbm. Both the 0- to 100-db calibrated and 0- to 50-db attenuators are of the precision rotary vane type, which have maximum stability. They were selected because the output branch of the circuit is beyond the power monitoring point and any change of characteristic would occur undetected.

A ferrite isolator of high quality at the output maintains accuracy by isolating any mismatch reflections emanating from the external load. A similar isolator also protects against inaccuracy due to mismatch when switching from internal to external monitor for calibration checks.

The internal power monitor is shown in Fig. 40 removed from its former location in the compartment containing the waveguide output control components. Mounted on a separate panel in the equipment, the need for a meter window opening in the shielded compartment is eliminated, an important step in reducing radiated leakage.

Since the last report, provisions have been made for the addition of a remote controller for the output attenuator.

This will enable operation from the control room as well as directly at the signal generator, located on the antenna or at the collimation tower. In addition, provision has been made for remote indication of signal generator output power.

d. Status of signal generator program. All of the principal components have been specified, suppliers selected, and orders placed.

Packaging layout, and fabrication and assembly of the housing, panels, shield compartment boxes, and internal assemblies are being performed by a local contractor, under direction of the JPL cognizant engineer.

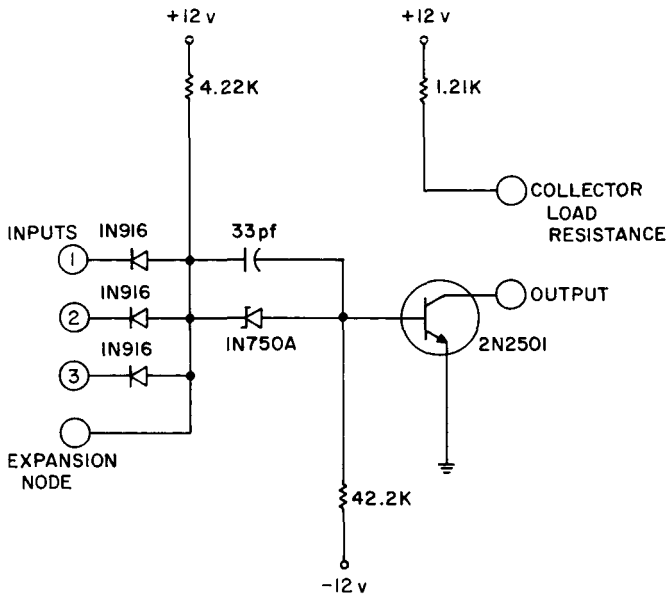

Fig. 41. *Nand* gate schematic

E. Digital Development

1. Development of Digital Circuit Modules

Continuing effort in the development of digital circuit modules previously described (Ref. 17) has resulted in the detailed design of three basic logic circuits. These are the decision or gate circuit, the memory or flip-flop circuit, and the power amplifier circuit. The use of detailed circuit specifications for procurement purposes, as opposed to envelope or black-box specifications, has the following advantages:

(1) Differences in the performance of modules purchased from alternate manufacturers due to the use of "proprietary design techniques" are avoided.

(2) Control of reliability through the use of JPL qualified components is facilitated.

(3) Circuit refinements to keep pace with improved technology can be initiated at JPL's convenience.

(4) Selection of vendors can be made on the basis of quality of workmanship, delivery, and manufacturing economy; rather than availability of a proprietary item.

a. Nand gate. Fig. 41 is the schematic of the gate circuit. It consists of a three input *and* diode gate followed by a transistor inverter. The diode node is brought out for expansion purposes. A separate collector resistance is used to permit the parallel connection of several gate outputs while still using only one collector resistance.

Calculations have been made to determine the fan-out or driving capability of the gate under worst-case conditions. Fan-out depends upon the ability of the transistor to stay in saturation when connected to the diode inputs of other gates and holding these gates at the zero logic level. Worst-case conditions include the following:

(1) $\pm 10\%$ variation of power supply voltages.

(2) $\pm 2\%$ variation of resistance values. 1% resistances are used.

(3) Module operation at a temperature range from 0 to $+100°C$. At 0, the transistor dc current gain (β) is taken to be 83.3% of the value at 25°C as interpolated from manufacturers curves.

(4) Transistor gain is taken to be 143% of minimum calculated required gain. This includes protection against ground-loop noise currents which might add to the normal gate load.

(5) Minimum values of transistor gain as interpolated from discrete specification points given by the manufacturer.

The minimum calculated fan-out using these worst-case conditions is six. Actual tests of 12 transistors randomly obtained from a commercial distributor show that the transistor with the lowest gain could provide a minimum calculated fan-out of 11. This would seem to indicate that a modest transistor selection process could be used if a minimum fan-out capability greater than six is desired.

Measurements have also been made on actual circuits to determine typical noise margins and pulse propagation delay times. These tests show that the transistor is held in saturation by all input voltages greater than +4 v and is cut off by all input voltages less than +3 v. Thus, if the inputs to a gate are at a high logic level of 10 v, the gate will be insensitive to noise spikes up to 6 v in the negative direction. Conversely, a low level input of 0.5 v will provide insensitivity to ground noise spikes up to 2.5 v in the positive direction.

Pulse propagation delay was measured at a voltage level of ±3.5 v, the voltage at which transition takes place. This delay was measured by cascading an even number of stages and measuring the total delay. The average delay per stage was then calculated by dividing the total delay by the number of stages. The average pulse propagation delay thus measured was less than 20 nsec per stage.

b. Flip-flop. A schematic of the flip-flop is shown in Fig. 42. The flip-flop changes state when a negative going waveform is applied to the proper trigger terminal, while the associated enable terminal is held at the zero logic level. This causes the conducting transistor to be cut off, which in turn causes the cutoff transistor to become conducting. Thus, when a positive clock pulse is applied to the trigger terminals, the flip-flop will assume its new state immediately following the trailing edge of the clock pulse. The required pulse width for triggering depends upon the fall time. Fig. 43 is a graph of this triggering dependence measured on a typical flip-flop circuit. The applied clock pulse was +10 v high and the base width was measured at the 1-v level. The fall time was measured between the 9- and 1-v levels. These measurements were independent of rise time. From the graph, it can be seen that a 3-Mc clock with trapezoidal symmetry and base width of 200 nsec lies well within the triggering region.

The dc inputs permit asynchronous set or reset when brought to the *zero* logic level. Normal flip-flop action resumes when the dc input is either disconnected or returned to the logic *one* level.

Fan-out for the flip-flop is the number of gates which may be driven under the same conditions as discussed for gate fan-out. Using these same worst-case conditions, the minimum calculated fan-out for the flip-flop circuit is twelve. Of the randomly selected transistors, the same low-gain transistor which provided a calculated fan-out of 11 for the gates would provide a minimum calculated fan-out of 21 for the flip-flop. Thus, a transistor selection process could be used to increase the minimum rated fan-out figure for flip-flops as well as gates.

The relatively large flip-flop fan-out has been deliberately provided at a small expense in gate fan-out. This resulted from system considerations which require flip-flops to drive heavy loads to a much greater degree than gates. For heavy loading on a gate, the power amplifier may be used.

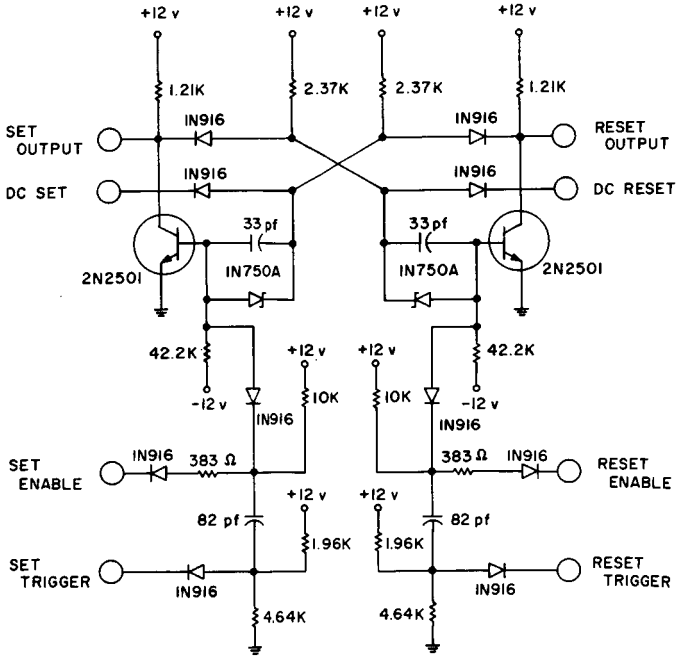

Fig. 42. Flip-flop schematic

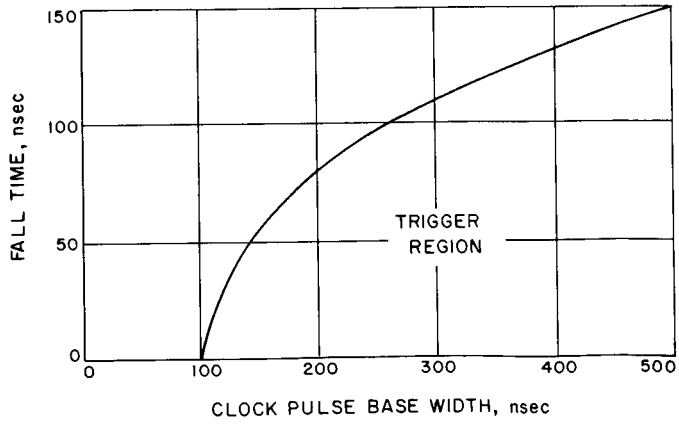

Fig. 43. Flip-flop triggering characteristic

c. Power amplifier. The power amplifier has been designed to drive long lines with relatively high capacitance, drive heavy logic loads, and as a clock pulse driver when connected to the trigger inputs of flip-flops. Fig. 44 shows the schematic of the power amplifier, which is logically equivalent to the gate circuit except for the parallel output feature. The outputs of power amplifiers may not be directly connected either to each other or to the outputs of other logic circuits.

Drive capability under worst-case conditions has been calculated to be 18 flip-flop trigger loads, 28 flip-flop dc inputs, or 41 gate loads. The input loading of the power amplifier is equal to one gate load, and the measured pulse delay is 30 nsec.

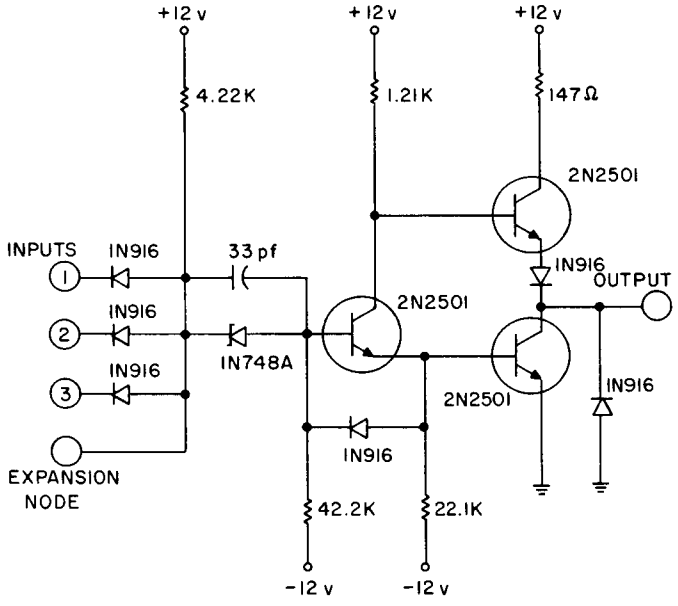

Fig. 44. Power amplifier schematic

2. Cooling System for Frames of the New Line of Digital Modules

a. Summary. This article describes the cooling system being developed for cooling frames of modules of the new line of digital circuit modules currently under development in Section 331. It is shown that a low-pressure water cooling system of 3/16-in. outside-diameter copper tubing with input water temperature equal to the maximum Goldstone air temperature of 140°F is adequate to remove the heat generated by cabinets full of the new line of modules. Thus,fans, blowers, and air conditioners will not be necessary.

b. Background. In Refs. 17 and 18, the development of a new line of digital circuit modules by Section 331 was described. These modules are built with silicon transistors, and thus can operate, as the specifications demand, at ambient temperatures of up to 100°C.

However, the modules have for example four flip-flops on a flip-flop card. Also, the connector is integral to the card. Thus, a high packing density is attainable. For example, in a 6-ft Venus site cabinet of four frames with 12 rows of 25 cards per frame, 1200 cards can be packed. Suppose these cards are all of the highest wattage card in the new line. That card is the flip-flop card, which dissipates 0.35 w per flip-flop, or a total of 1.4 w per card. The total dissipation for a frame of 300 cards is therefore 420 w. For a cabinet of four frames, 1680 w are thus dissipated. Consequently, even though operating temperatures of up to 100°C are permissible with the new line of silicon modules, there still is a cooling problem. We now discuss a solution to the cooling problem which is inexpensive and requires little equipment.

c. Requirements on a water cooling system. Let us consider desirable features in a water cooling system for digital circuit modules. Ideally, a water cooling system should allow adequate cooling with no refrigeration. The cooling in the system under consideration would be done by cooling the circulating water in an outdoor radiator. The cooling would be down to ambient air temperature. Another desirable feature in a cooling system is that of low water pressure, so that large pumps will not be necessary. Somewhat at variance with this feature, however, is the requirement that the pipes that carry the water to the vicinity of the modules be thin, in fact, be tubing rather than pipes. This feature allows cheap and easy fabrication, and in addition allows the cooling to be done with no change in dimensions of frames or cards. It will now be shown that all these requirements can be met in a system which cools a frame entirely full of the most power-dissipating card in the new line of digital circuit modules.

d. Numerical assumptions for cooling system. Let us state the numerical assumptions upon which subsequent calculations will be based. The maximum air temperature ambient must be known. This maximum of 140°F (or 60°C) occurs at the Goldstone Tracking Station with frequency about 1 day/yr. We shall do a worst-case analysis and assume that the temperature of the incoming water is 60°C (140°F). We shall assume a 5°C temperature rise from the input end of the cooling system to the output end. This rise is large enough to allow all the heat to be removed, and small enough so that air temperature conditions at all sections of the frame are nearly constant.

This approximate constancy means that each card operates at essentially the same temperature as every other card. The length of the cooling tubing in one frame of a 6-ft cabinet is 29 ft. (We do calculations on a per frame basis, even though a cabinet has four frames. The four cooling systems for each frame would be in parallel.) Tubing of ⅛-in. inside-diameter is considered. We shall calculate the flow necessary to remove 420 w, and convert to pressure drop. We shall then determine the wall thickness of tubing necessary to sustain sufficient pressure to support this drop. The effect of bends in the tubing will also be considered.

e. Flow-rate calculations for cooling system. The specific heat of water in the range of 60 to 65°C is essentially 1 Btu/°F lb. Since 1 Btu = 1.05 kw sec and 1°F = (5/9)°C, the specific heat in ad hoc units is 1.05 kw sec/(5/9)°C lb, or 1.89 kw sec/°C lb.

Now 420 w must be removed by 5°C rise in water temperature. How many pounds of water per second of flow are required? That is, (0.42/5) kw/°C are to be removed in 1 sec; how many pounds of water are required? The answer is 0.084/1.89 lb. Thus, a flow rate of 2/45 lb/sec, or 2⅔ lb/min, is needed.

To convert 2⅔ lb/min into gallons per minute, note that one gallon of water weighs 8.21 lb at 140°F. Thus, only 2⅔/8.21 = 0.325 gal/min of flow are needed for one frame. Consequently, 4 × 0.325 = 1.29 gal/min are needed to cool each four-frame cabinet.

f. Pressure calculations for cooling system. We must now convert the above flow rate to a pressure drop. There is a flow of 0.325 gal/min through 29 ft of ⅛-in. inside-diameter tubing. How much of a pressure drop is there between the input end and the output end? We use the standard formula (pp. 3–14) from Streeter's "Handbook of Fluid Dynamics" (Ref. 19):

$$P = 128\,\eta\,LQ/D^4,$$

where P is the pressure drop in lb/ft^2; η is the viscosity of the water in lb sec/ft^2; Q is flow rate in ft^3/sec; D is inside diameter in ft. We use: $\eta = 9.3 \times 10^{-6}$ lb sec/ft^2 at 140°F (Ref. 19, pp. 1–9); L = 29 ft; Q = 2/45 lb/sec = ((2/45)/(61.4))ft^3/sec; thus, in more familiar units, P = 4.36 psi. Since each separate frame has a paralleled cooling system, 4.36 psi is indeed the pressure drop to be supported.

However, to avoid collapse of the tubing when the pressure momentarily drops, and to keep the flow unidirectional, the water should be run through at a higher pressure. A convenient input pressure is 50 psi; the returning pressure is then 45.64 psi. The pump necessary to maintain 50-psi pressure at a flow of 1.29 gal/min per cabinet in, say, 10 cabinets is still small in size and modest in price (especially when compared with an air-conditioning system!).

g. Selection of tubing. The pressure in the tubing for the module cooling system has now been determined to be a maximum of 50 psi. A tubing easy to work with and to bond to the plates on back of the frames is soft annealed seamless copper tubing. The inside diameter has already been fixed at ⅛ in. What outside diameter is necessary to ensure that a pressure of 50 psi does not rupture the tubing wall?

Section 515, p. 1237, of Crocker's "Piping Handbook" (Ref. 20) is used. For copper tubing, the formula giving the minimum wall thickness t_m in. necessary to sustain an internal pressure of P psi in tubing of outside diameter D in. is $t_m = (PD/2S) + 0.8P$, where S is the allowable stress in the copper due to internal pressure, expressed in psi. From Table VII, p. 1239, of Ref. 20, S for seamless copper tubing is 6000 psi. Furthermore, P is to be taken at least 100 psi even if the service pressure is less than 100 psi. The pressure used is to be 50 psi, but 100 psi must therefore be used in the formula. Solving for t_m with $D = ⅛ + 2t_m$ yields t_m = 0.00105 in. as the minimum wall thickness necessary.

However, tubing with such thin walls is not made. The standard tubing that meets requirements minimally is 3/16-in. outside-diameter, 0.32-in. wall thickness, tubing. The inside diameter is 0.1235 in., which is slightly less than the original ⅛-in. inside diameter. Using the fourth power law of Part *c* of this article, the pressure drop will increase by a factor of only $0.1250^4/0.1235 = 1.05$. Hence, the pressure drop is 1.05 × 4.36 = 4.58 psi. This increase in pressure drop is of no consequence and still allows a cooling system with pressure of 50 psi.

h. Effects of bends on pressure drop. Another slight increase in the pressure drop which we now consider is the increase due to the bends in the tubing. The tubing will snake along the metal plate at the back of the frame, with 13 2-ft-horizontal runs and 12 4-in.-vertical runs, to give the total length of 29 ft. The curvature at the bends is the cause of the increased pressure drop. Now there are 2 × 12 = 24 such bends. The extra drop at one such bend shall be computed and multiplied by 24; again Ref. 19, p. 100, will be used.

A 90-deg smooth elbow bend will be considered. The effect of a bend on pressure drop is to add an equivalent length to the tubing for the purpose of computing pressure drop. For an elbow bend of radius R, inside diameter D, with $R/D = 4$, the length added by the bend is $7D$, from Table XIV, p. 100, of Ref. 19. (This factor of 7 is approximately the minimum over all R/D, as Table XIV of Ref. 19 indicates.) Since $D = 0.1235$ in., the extra length added is 0.8635 in./bend. Since there are 24 bends, a total extra length of $24 \times 0.8635 = 20.72$ in. is added to the length of the tubing. That is, an additional 1.73 ft of length shall be used in computing the pressure drop in the tubing. The total L that should be used in Part *c* is therefore 30.73 ft, instead of 29 ft. Since the pressure drop is a linear function of the length, however, the actual pressure drop, instead of being 4.58 psi, is $30.73/29 \times 4.58 = 4.86$ psi. Thus, the pressure drop is only 4.86 psi, even taking into account the bends in the tubing. The 50-psi system is still quite adequate.

i. Conclusions. A cooling system for the new line of digital circuit modules can be implemented with copper tubing of 3/16-in. outside diameter and 0.1235-in. inside diameter. The 420 w in one frame of 300 of the 1.4-w four flip-flop cards can then be removed by running 0.325 gal/min per frame of water at incoming temperature of 140°F, and outgoing temperature of 149°F. The water is then cooled in an outdoor radiator to ambient air temperature. In such a system with 29 ft of soft copper tubing bent into 13 horizontal runs of 2 ft and 12 vertical runs of 4 in. with 24-hr 4:1 90-deg elbow bends, the pressure drop is 4.86 lb/in.^{2}. Using 50-psi high pressure is well within the rated pressure for the copper tubing used.

However, to show that this cooling system is entirely feasible, the final operating temperature of the modules must be determined. The next article shows that the resulting maximum module temperature is low enough for operation of the new line of silicon digital circuit modules.

3. Steady-State Temperature Experiments for the New Line of Digital Circuit Modules

a. Summary. This article describes experiments to determine the steady-state operating temperature of modules of the new line of digital circuits being developed by Section 331. The qualitative conclusion is that the cooling system described in Sect. VI-E-2 of this report (the previous article) allows these silicon modules to operate more than 13°C below their rated maximum temperature of 100°C. Thus, a cheap and efficient cooling system is available for these silicon modules. Such a cooling system would not have been available for germanium ones, since germanium semiconductors must operate at lower temperatures.

b. Idea of experiment. The cooling system described in the previous article removes all the power generated by a cabinet full of 1200 of the 1.4-w four flip-flop silicon cards of the type currently under development by Sect. 331. But this fact alone does not determine what the steady-state temperature is on the cards. This steady-state temperature distribution inside the cabinet is determined by the distribution of heat sources (modules) within the cabinet, and by the steady-state temperature distribution on the back plates of the frames which hold the cards. The steady-state distribution is in effect a boundary condition for the heat equation. Radiation and convection to the ambient air around the cabinets also provide cooling.

An experiment was performed to estimate the temperatures of the cards when the cooling system of the previous article is used. This experiment was not a full scale mock-up of cabinet with cooling system, although such an experiment would provide better estimates of the card temperature. Instead, an oven was used, with a sealed metal box inside. The temperature on the inside lid of the box corresponds to the cooling plate temperature. The cards were allowed to run at full operating voltage, and temperatures on lid and card were determined. When steady-state was reached, the temperature on the inside lid and the temperature of the cards were determined. The temperature on the cards is then an estimate of what the temperature on the cards will be when the cooling system cools the plate down to the lid temperature that was recorded in the experiment.

c. Description of experiments. Thermocouples were placed on the cards, inside the lid of the box, on the outside of the box, and in back of the card cage. Fig. 45 shows the location of the thermocouples placed on the two cards that had thermocouples. The hottest portion of the card appears *a priori* to be H in Fig. 45. The point H

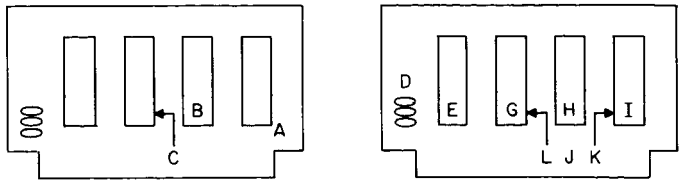

Fig. 45. Location of thermocouples on two cards

is right above the silicon transistor in one of the encapsulated flip-flop modules. Experiment bore out the fact that H was indeed the hottest.

Actually, the cards used in this experiment were of a previous design that dissipates 2.8 w per flip-flop card. As explained in Ref. 18, the ultimate set will dissipate half as much power, 1.4 w per card. Since this new design has not yet been delivered, it was decided to fill the card cage that went into the metal box with 12 cards at 2.8 w, and 12 blank cards, alternately spaced. The same total power is generated inside the box as if it were full of 24 of the 1.4-w cards. In fact, the temperature at H in the simulation is, if anything, higher than the temperature at the same point H would be if 24 of the 1.4-w cards were used, for the steady-state temperature at a point source of twice the heat output is greater than the steady-state temperature at each of two separated point sources, each of half the power as the single point source, provided the boundary conditions remain the same. Therefore, estimates of operating temperatures in this experiment are conservatively high.

Temperature measurements were actually made on two cards in the box, namely, the two most central ones. The card used for point H was the most central card. The relevant information to be obtained is a plot of steady-state temperature on the inside lid versus steady-state temperature at H, for a range of steady-state lid temperatures.

In order to improve radiation from the cards to the box, the inside of the box lid was coated with a black heat-absorbing coating. The other five inside surfaces of the box were left uncoated to simulate conditions in the cabinet, where only the cooling plate would be so coated, and only the cooling plate would be at the water temperature. In the experiments, the entire outside of the box was also black coated. This outside coating does not affect the relation between the various steady-state temperatures, but allows steady-state to be reached faster.

In order to determine the effect of coating the inside lid, however, experiments were first run without the black coating on the inside lid. The resulting steady-state temperatures on the cards were found to be indeed lower with the black coating than without the coating.

d. Results of experiment. The main qualitative result of the series of experiments described in this article is this: With the cooling system described in the preceding article, the operating temperatures of the modules will be well below the rated maximum operating temperature. Furthermore, it can be concluded that the use of black coating helps materially in keeping these operating temperatures low.

The experimental results will now be given in quantitative detail. Fig. 46 shows the thermal history of the

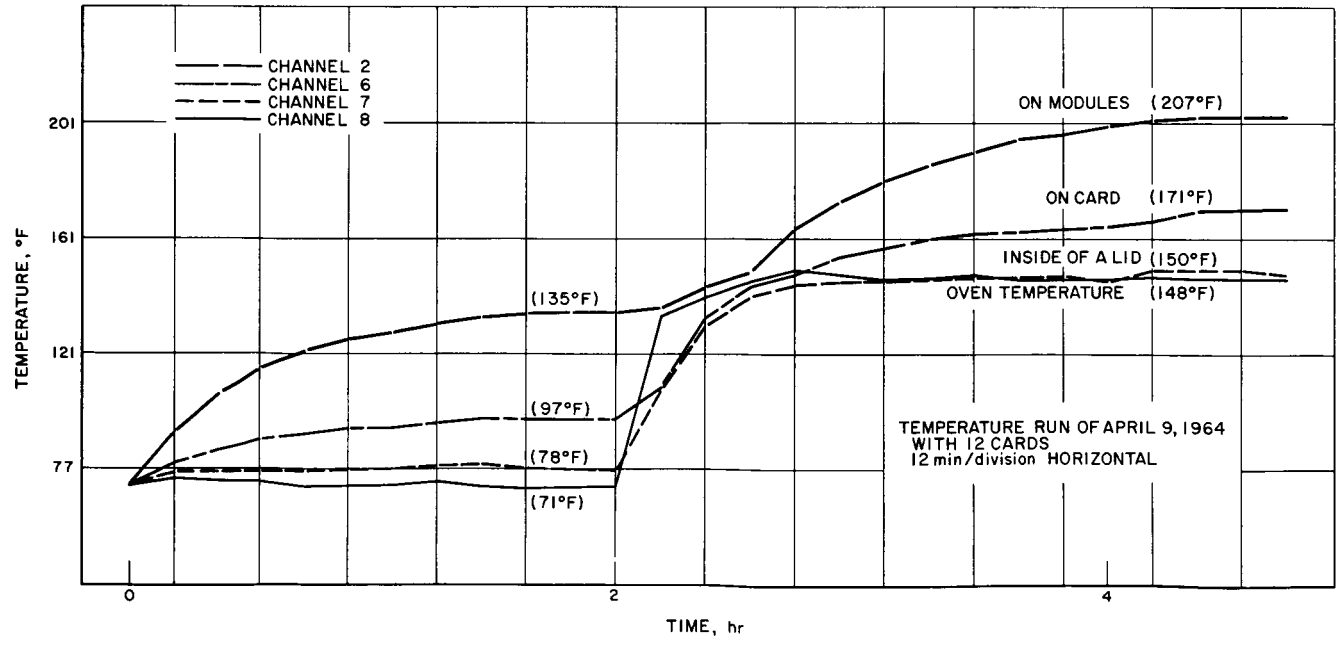

Fig. 46. Thermal history of four temperatures, no coating

temperatures at four sites for a 4¾-hr run, without the black coating on the inside lid. Equilibrium was first reached after 2 hr, with an oven temperature of 71°F. The temperature at point H was then 135°F, with an inside lid temperature of 78°F. That is, with the inside lid cooled at 71°F, the operating temperature would be 78°F. The oven temperature was then increased to a steady-state value of 148°F; steady-state took 2 hr 36 min to be reached from the moment the oven temperature started rising. The new steady-state inside lid temperature was then 150°F, and the point H temperature was then 208°F. That is, a 150°F plate temperature would result in a maximum operating temperature of 98°C, which is within specified operating temperature of the silicon modules. From this one run, then, we can conclude that the cooling system described in the preceding article would be effective even without black coating.

However, to obtain information about the increase in efficiency when the black coating was used on the inside lid, a similar experiment was performed with the coating (Fig. 47). The first equilibrium had 78°F inside lid versus 125°F card, instead of 78 and 135°F. That is, coating reduced the point H temperature 10°F for the same lid temperature. The second equilibrium was reached with a 162°F inside lid temperature versus 207°F card temperature. Thus, a 12°F increase in lid temperature, with the black coating, resulted in an actual decrease in maximum card temperature of 1°F. We conclude that the presence of the black coating gives a significant improvement in cooling performance, and such coating should be done in the ultimate system.

Finally, more points on the curve of point H temperature versus what would be incoming water temperature were obtained by running the above experiment at differing oven temperatures, with the black coating. These data are necessary so that operating temperatures will be predictable from knowledge of outside air temperature.

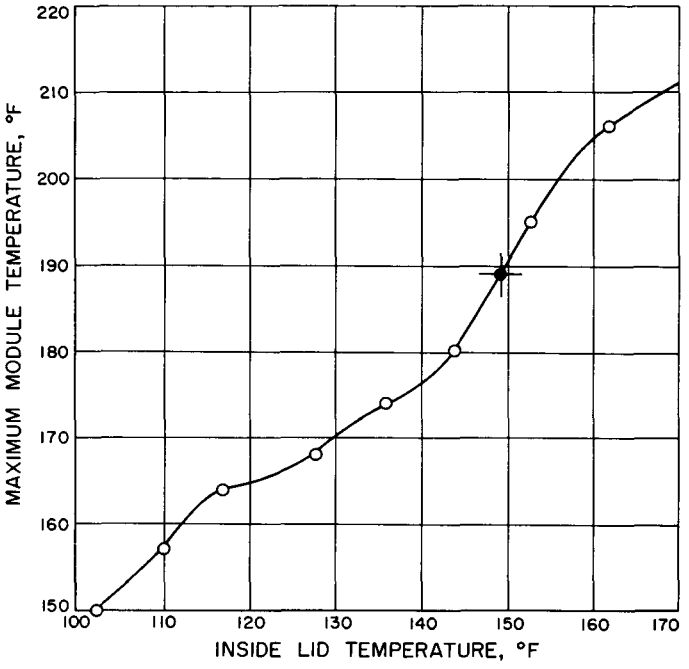

Fig. 48. Maximum module temperature versus inside lid temperature

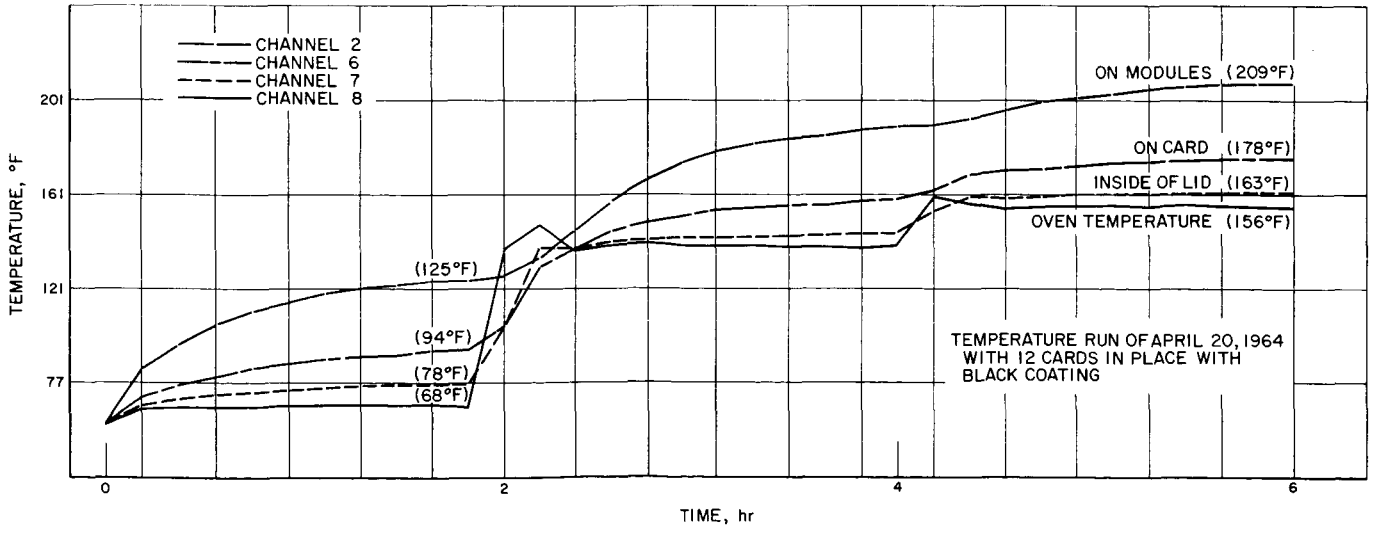

Fig. 47. Thermal history of four temperatures, black coating

(It may be desirable, on the other hand, to keep the water temperature at 140°F even in cool weather, so that the modules would always operate in the same temperature environment.) Data were obtained for inside lid temperatures ranging from 102 to 162°F, in varying environments. The point H temperature then varied from 150 to 211°F. Fig. 48 is the graph of the point H temperature versus lid temperature in this range.

One observes by interpolation from Fig. 48 that when the inside lid temperature is kept at the constant 149°F, which is in fact the maximum water temperature throughout the cooling system, then the point H temperature will be a rather cool 189°F. Thus, with the cooling system of the preceding article, the modules will indeed operate at a rather low maximum temperature at, or somewhat below, 87°C.

References

1. "Precision Drive System for 30-ft Antenna," *SPS 37-26*, Vol. III, pp. 23–24, Jet Propulsion Laboratory, Pasadena, California, March 31, 1964.
2. "Antenna Instrumentation," *SPS 37-20*, Vol. III, pp. 31–34, Jet Propulsion Laboratory, Pasadena, California, March 31, 1963.
3. "Antenna Instrumentation," *SPS 37-27*, Vol. III, Fig. 1, p. 54, Jet Propulsion Laboratory, Pasadena, California, May 31, 1964.
4. Seidel, B., "Simultaneous Lobing Radiometric Tracking System," *SPS 37-26*, Vol. IV, pp. 216–220, Jet Propulsion Laboratory, Pasadena, California.
5. "Simultaneous Lobing Radiometric Tracking System," *SPS 37-27*, Vol. III, Jet Propulsion Laboratory, Pasadena, California, May 21, 1964.
6. Manasse, Roger, "Maximum Angular Accuracy of Tracking a Radio Star by Lobe Comparison," *Transactions of the IRE*, PGAP, pp. 50–56, January 1960.
7. "Venus Site Experimental Activities," *SPS 37-27*, Vol. III, p. 62, Jet Propulsion Laboratory, Pasadena, California, May 31, 1964.
8. "Range-Gated Lunar Radar Experiment," *SPS 37-25*, Vol. III, pp. 38–47, Jet Propulsion Laboratory, Pasadena, California, January 31, 1964.
9. "High-Power 100-kw S-band Transmitter, Measurement of incidental phase modulation" *SPS 37-25*, Vol. III, pp. 31–32, January 31, 1964.
10. "Optimum Transmitter Power for Klystron Drive-Keyed Radar," *SPS 37-23*, Vol. III, pp. 52–55, September 30, 1963.
11. Stelzried, C. T., "Evaluation of H-band Maser Amplifier with Cascaded Cavity Amplifiers and Isolators," Technical Report No. 32-598, Jet Propulsion Laboratory, Pasadena, California, (to be published).
12. Potter, P. D., "A New Horn Antenna with Suppressed Sidelobes and Equal Beamwidth," *The Microwave Journal*, Vol. VI, June 1963.
13. "S- and X-Band Interim Frequency Synthesizer," *SPS 37-27*, Vol. III, pp. 90–92, Jet Propulsion Laboratory, Pasadena, California, May 31, 1964.
14. "30.455-Mc Balanced Mixer," *SPS 37-27*, Vol. III, pp. 92–94, Jet Propulsion Laboratory, Pasadena, California, May 31, 1964.

References (Cont'd)

15. "Multiplier Chains," *SPS 37-27*, Vol. III, pp. 86–89, Jet Propulsion Laboratory, Pasadena, California, May 31, 1964.

16. "8.448-Gc Standard Signal Generator," *SPS 37-27*, Vol. III, pp. 94–96, Jet Propulsion Laboratory, Pasadena, California, May 31, 1964.

17. "Development of Digital Circuit Modules," *SPS 37-27*, Vol. III, pp. 83–95, Jet Propulsion Laboratory, Pasadena, California, November 30, 1963.

18. "Evaluation of Digital Circuit Modules Procured under JPL-Owned Design," *SPS 37-27*, Vol. III, pp. 123–127, Jet Propulsion Laboratory, Pasadena, California, May 31, 1964.

19. Streeter, Victor L. (Editor), "Handbook of Fluid Dynamics," McGraw-Hill, New York, 1961.

20. Crocker, Sabin, "Piping Handbook," Revised Fourth Edition, McGraw-Hill, New York, 1945.

VII. Advanced Antenna System

A. Introduction

A 210-ft-diameter Advanced Antenna System (AAS) is being designed and constructed for the Mars site of the Goldstone Tracking Station. This AAS is designed specifically for deep space communications and will be integrated with related systems and equipment at the Goldstone Station of the Deep Space Instrumentation Facility (DSIF).

The work on the AAS Project has been reported regularly in previous issues of *SPS*, Vol. III. Since the last report, the concrete structural portions of the antenna pedestal have been completed. The final design of the basic antenna has been essentially completed by the major subcontractor (Rohr Corporation). Detail engineering procurement, fabrication, and manufacturing are in progress.

System integration studies, and final and detail designs for the structural components of the antenna are being carefully reviewed to assure compliance with all design requirements established by JPL. Clean-up work in the areas of documentation, quality control, and test and measurement procedures is in progress.

B. Supporting Studies

The dynamic analysis of the system presently shows the four lowest poles and zeros of the important transfer functions as follows:

(1) Azimuth motion.

Poles, cps	Transfer function zeros from drive motor, cps	
	To intermediate reference structure	To pinion drive
1.58	1.64	1.59
1.88	2.18	1.96
2.16	2.27	2.16
2.57	3.21	2.59

(2) Elevation motion.

Poles, cps	Transfer function zeros from drive motor, cps	
	To intermediate reference structure	To pinion drive
1.65	1.89	1.66
2.86	3.62	2.90
3.93	4.11	3.34
4.13	4.19	4.11

The final stresses for the primary reflector and backup structure, obtained through computer analysis, have been reviewed and checked against the reflector detail design. The reflector backup detailing is in progress.

C. Construction and Fabrication Progress

The azimuth motion components are being fabricated. The azimuth radial bearing runner fabrication is nearing completion and is scheduled for on-site installation in the near future. The target month for the first azimuth rotation is December 1964.

Detail engineering of elevation motion components is in progress and initial fabrication has begun. The first elevation rotation is scheduled for February 1965.

On-site work at the Mars site continues generally on schedule. Fig. 1 is a photograph of the azimuth radial bearing collar during concrete placement on May 11, 1964. The collar is a 4-ft-high by 4-ft-thick reinforced concrete ring with an inside radius of 11 ft. The top of the collar is 35 ft above ground floor level. The radial bearing runner, which is a steel ring about 4 in. thick by 20 in. high, will be grouted to the concrete collar. Six radial bearing rollers, mounted in pairs on three equally spaced trucks, will bear against a wear strip mounted on the runner. The trucks are mounted on the antenna alidade with preload devices to assure contact of all rollers in any wind condition.

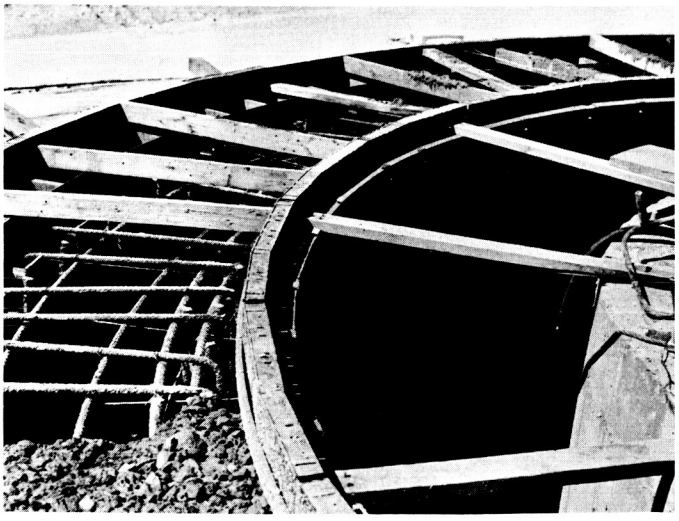

Fig. 1. Concrete placement for the azimuth radial bearing collar

Fig. 2 is a photograph of the inside of the pedestal at the second floor level prior to placement of a 6-in.-thick concrete floor slab. Concrete was mixed on-site and pumped up to the second floor. This placement completed the concrete structural work for the antenna pedestal.

A total of 2605 yd^3 of concrete has been placed for the pedestal and instrument tower. Water curing and Aquapon paint have been applied to the pedestal concrete. All emplaced concrete has met, or exceeded, specifications. The pedestal top deck exceeded 4000 psi in 14 days, and the azimuth radial bearing collar exceeded 3000 psi in 8 days. The design strength in 28 days is 4000 psi.

All cribbing has been removed from the pedestal top deck and azimuth radial bearing collar. Strain gages were monitored during the removal of the cribbing under the radial collar and no movement was observed. The total sag of the 3½-ft-thick pedestal top deck, at the centermost position, was 0.014 in. upon removal of cribbing.

Architect and engineering drawings for the Diesel Electric Power System have been completed, and on-site construction of the generator building is in progress. Excavations for the building and two 12,000-gal capacity fuel tanks have been completed. Foundation forming is in progress and the fuel tanks have been placed.

Construction work has begun on the antenna pump house and cooling tower. Fig. 3 depicts the start of cooling tower construction.

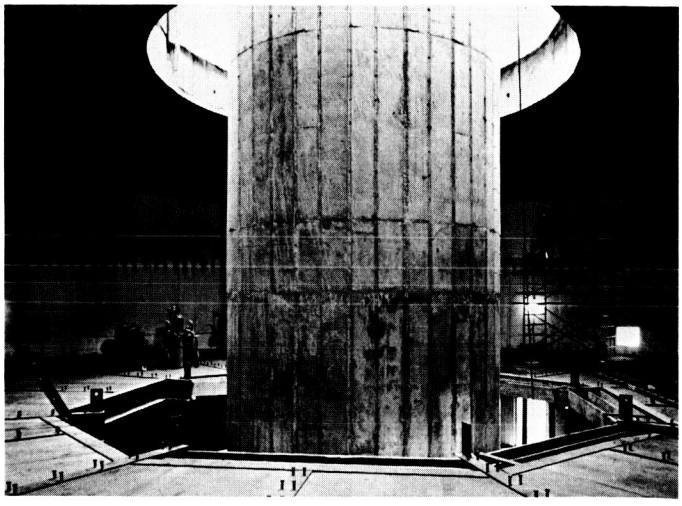

Fig. 2. Inside of the pedestal at the second floor level

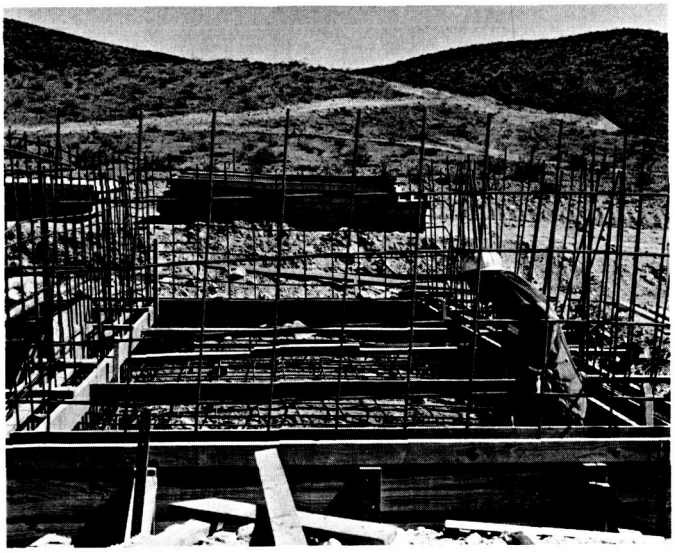

Fig. 3. Construction of the cooling tower begins

Preliminary design and specification work continues on the precision angle data system of the antenna, and contract negotiations for the precision optical instrument mount are in progress.

Planning and preparatory work on inter- and intra-site communications, ancillary equipment for the AAS, and the DSIF Station equipment continues.

D. Hydrostatic Thrust Bearing

A cross-sectional drawing and brief description of the major components of the AAS were included in Ref. 1. The following is a more detailed description of the AAS hydrostatic thrust bearing.

1. Introduction

The design efforts on the AAS azimuth hydrostatic thrust bearing are now essentially complete and the components are being manufactured. This bearing supports the rotating parts of the AAS on three bearing pads, one at each corner of the alidade base triangle. Other components of the bearing are the hydraulic power supply system and the runner and oil reservoir. The general configuration is shown in Fig. 4.

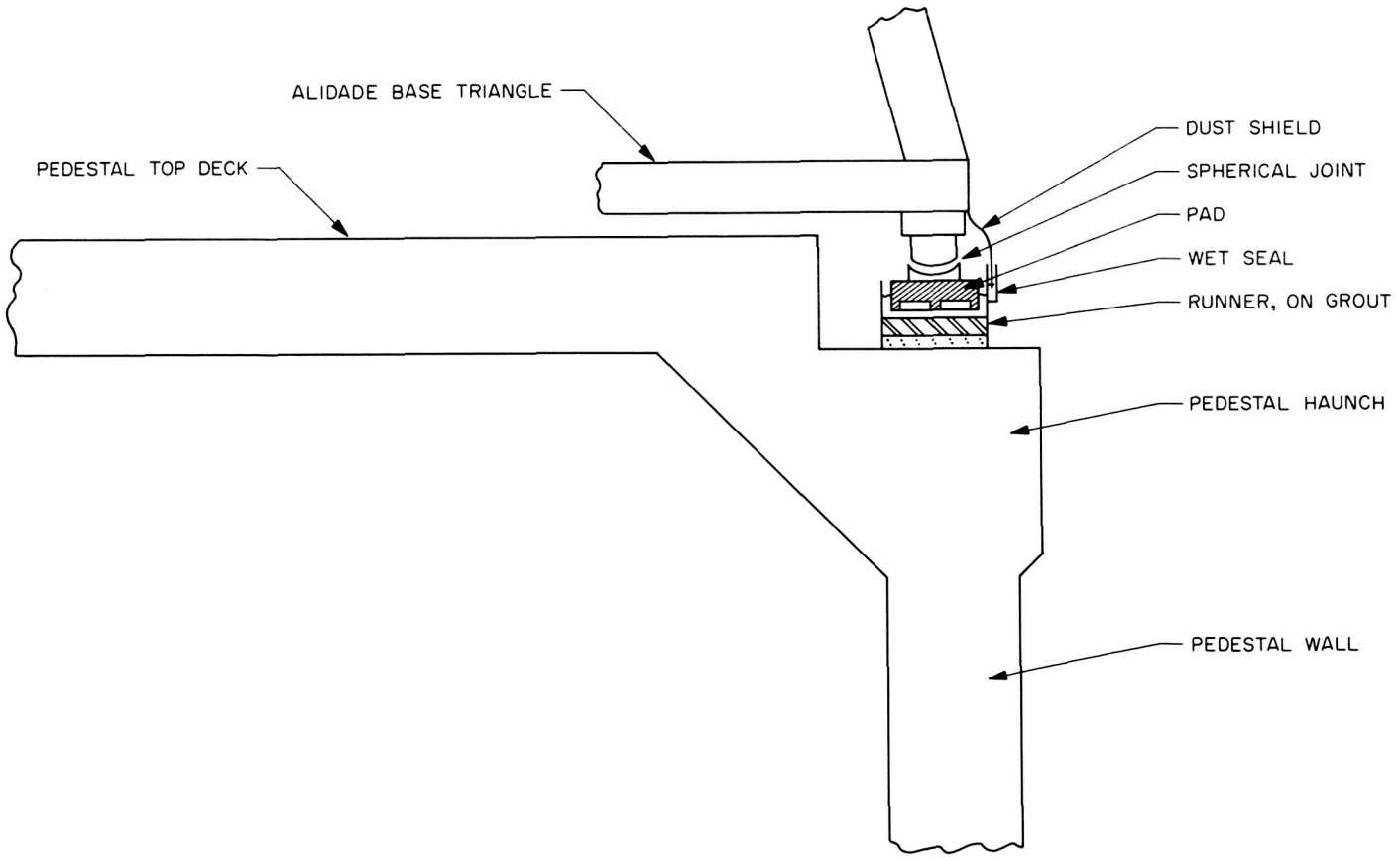

Fig. 4. Azimuth hydrostatic thrust bearing, general arrangement

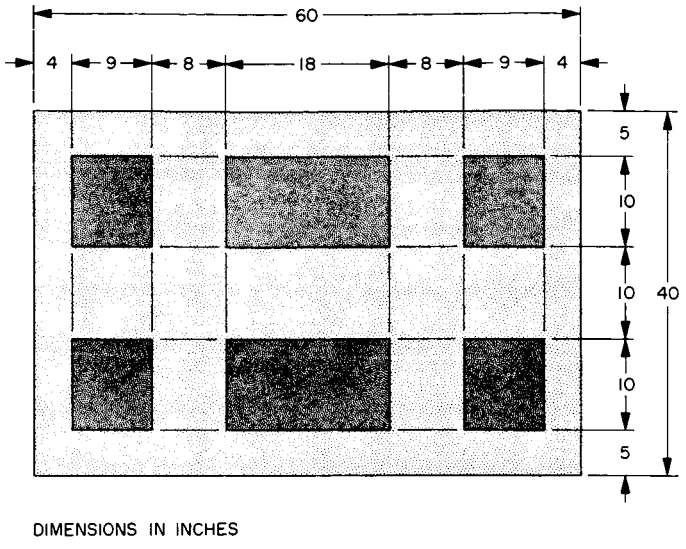

Fig. 5. Recess pattern of hydrostatic thrust bearing pad

2. Bearing Pads

The bearing pads are carbon steel forgings 60 × 40 × 20 in. thick. Each pad has six recesses in the pressure side through which oil is supplied for bearing operation (Fig. 5). A spherical seat is provided in the connection to the alidade to minimize the moment reaction on the pads.

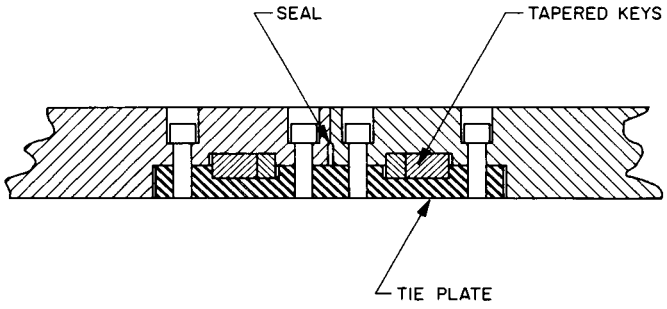

Fig. 6. Hydrostatic thrust bearing runner joint

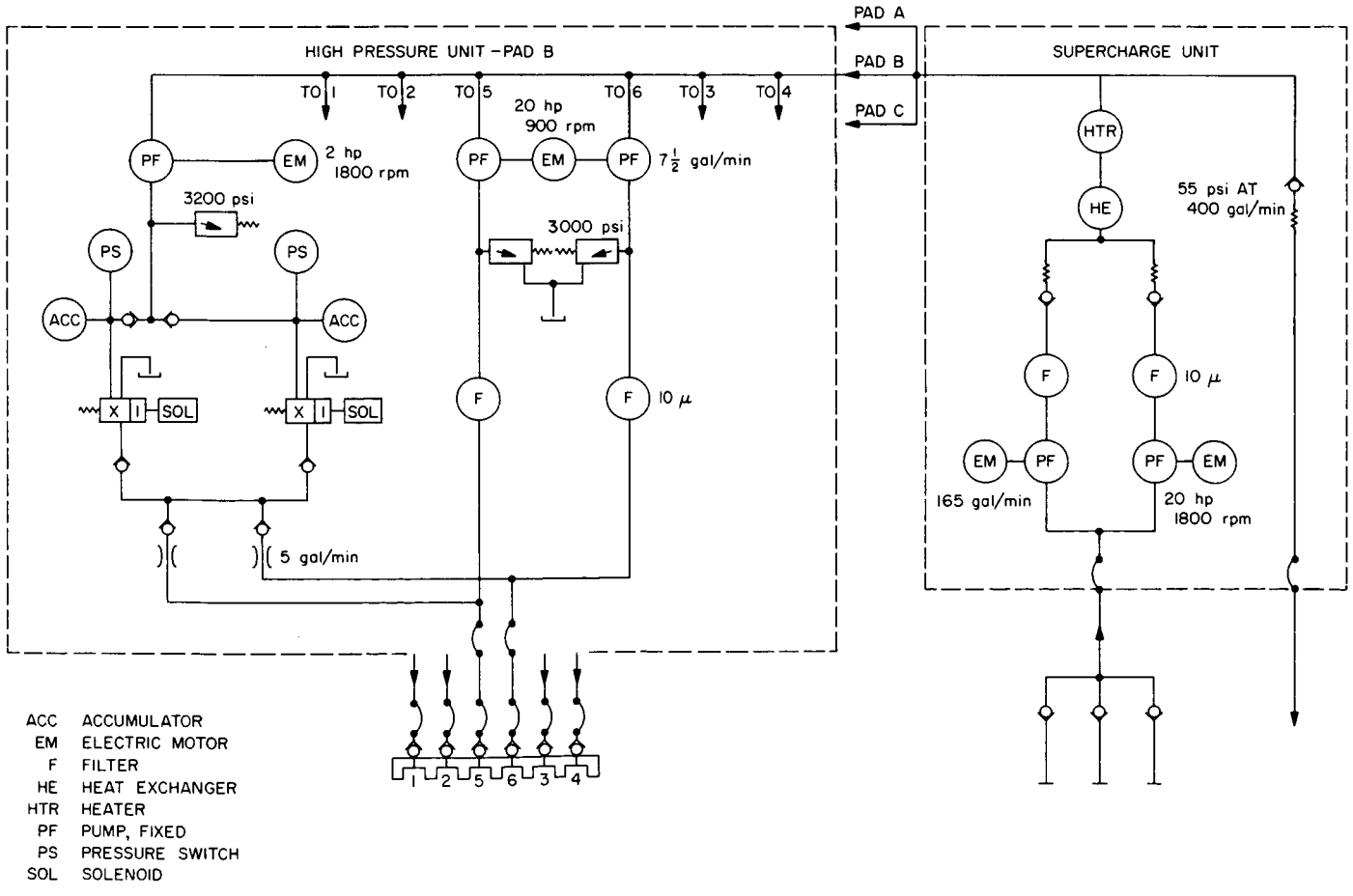

Fig. 7. Hydrostatic thrust bearing hydraulic power system

The spherical members will be an alloy steel (AISI 8620) case hardened to Rockwell C40-45 with a phosphate treatment to prevent galling.

3. Bearing Runner and Oil Reservoir

The bearing runner is made in 11 segments of low carbon (ASTM A36) steel 5 in. thick and 44 in. wide. A special joint has been designed to provide maximum stiffness against the bending under the pads and to provide an adequate seal against the oil film pressure (Fig. 6). The runner rests on a steel sole plate on nonshrinking grout. It is free to move radially to permit thermal expansion, but is restrained tangentially by stops embedded in the pedestal concrete. The reservoir is formed by walls fastened and sealed to the edges of the runner. The oil level in the reservoir will be approximately 9 in. deep to permit suction recovery of oil by the hydraulic power supply system. The entire bearing system is enclosed by a shield mounted on the alidade. This shield joins the outer reservoir wall in a wet type seal providing complete isolation from the outside atmosphere.

4. Hydraulic Power Supply System

The hydraulic power supply system (Fig. 7) consists of a precharge system, which draws oil from the reservoir and supplies it to the high-pressure units, and a high-pressure system, which supplies the high-pressure oil to the pad recesses. The precharge system consists of two 165-gal/min gear pumps, either of which can supply the entire flow requirements, two 10-μ filters, and a heat exchanger and heater to maintain the oil temperature at approximately 100°F. There are three high-pressure units, one for each pad. Each unit includes three electric motors driving six pumps. The pumps are arranged so that one motor drives pumps serving opposite recesses on the pad. In this manner, a balanced pressure pattern is maintained under the pad in the event of failure of one motor. A separate accumulator system is included with each unit which can maintain bearing operation for a period of several seconds after a power failure. This will assure that the azimuth drive has brought the antenna to a stop before the bearing touches down.

5. Operating Characteristics

The bearing operating characteristics were developed by the Franklin Institute. A computer program, which Franklin Institute had previously developed for JPL, was used for the analysis of hydrostatic bearings with a non-uniform film height resulting from elastic deflections of the pad and runner. The program was further developed in this effort to include the deflection of the pad and a more rigorous analysis of the runner and pad deflections. Using this program, the pad was designed to match the runner deflection with a 0.001-in. maximum film height variation under the pad. The nominal film height under dead load (1.5×10^6 lb per pad) and full hydraulic system operation is 0.010 in. The bearing will remain fully operational after loss of flow to any two recesses and marginally operational with loss of flow to any three recesses. Fig. 8 shows the film height along the center of the pad for various combinations of recess flows.

The hydraulic fluid will be Mobil DTE extra heavy with a viscosity of 590 ssu at 100°F.

6. Tests

During the design phase of the project, a test stand (Fig. 9) was built at the Franklin Institute to simulate the bearing and spherical joint. The bearing pad model was a one-fifth reproduction of the actual pad. An aluminum

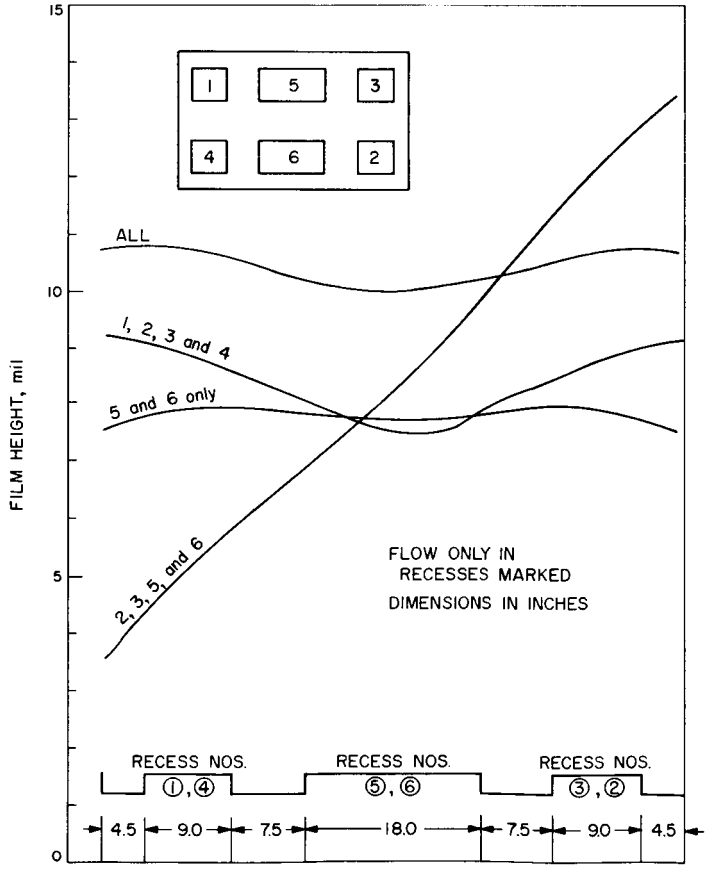

Fig. 8. Film height pattern for various flow combinations

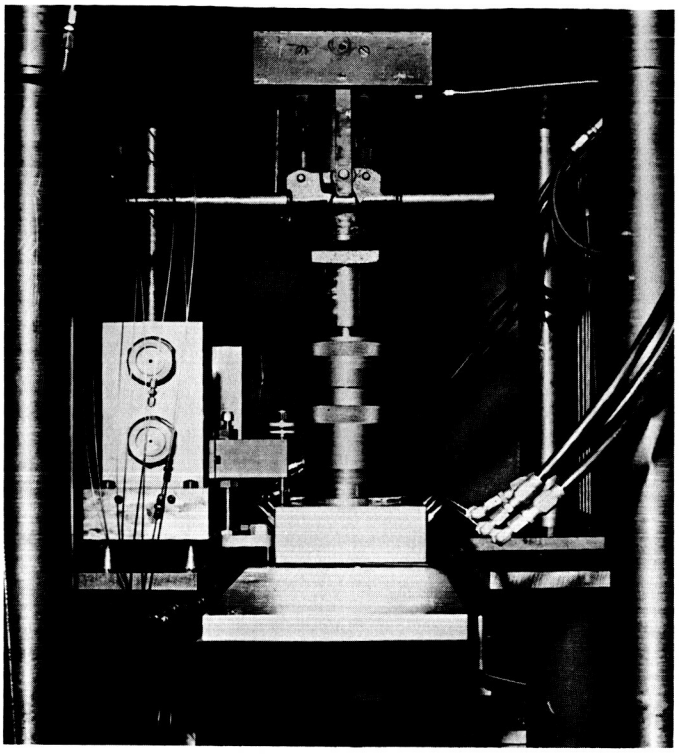

Fig. 9. Hydrostatic thrust bearing test stand

runner on a plexiglass base was used to simulate the actual runner and foundation. The model was used to develop the lubrication characteristics of the spherical joint and to verify the predicted performance of the bearing as a whole. The detail results of these tests will be described in a subsequent *SPS*.

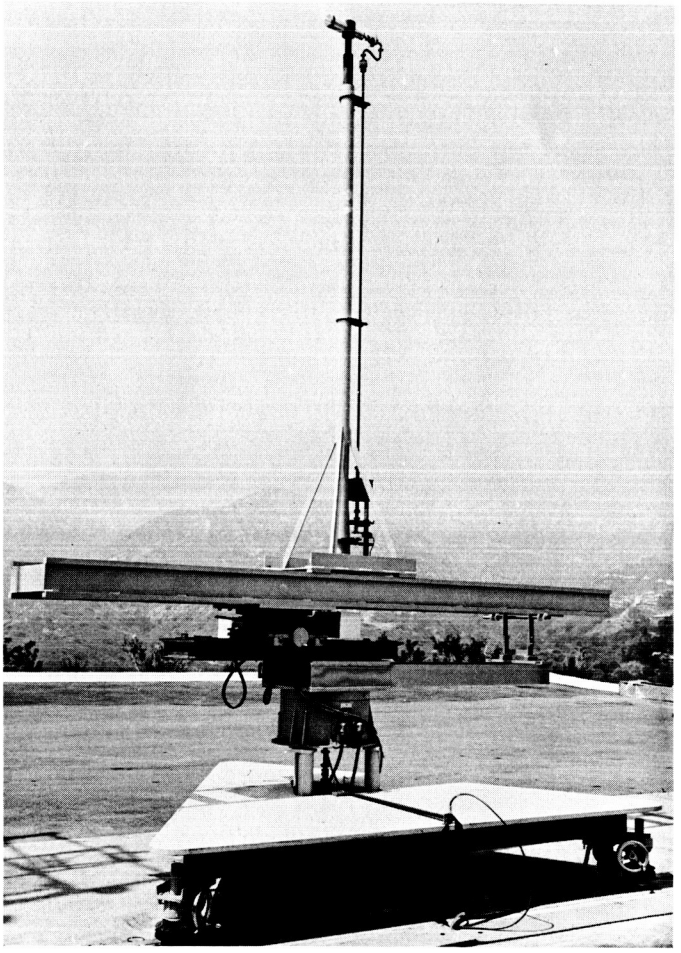

Fig. 10. Cassegrain feed rotator

E. 1/7-Scale Model Feed

a. Summary. During the months of May and June, preparations for the K_u-band scale model studies of the feed for the 210-ft Advanced Antenna System (AAS) continued. The Mesa K_u-band antenna range, 30-ft antenna Cassegrain feed cone and listening feed, and the 4-ft-diameter gain standard-illuminator antenna have been completed. The simultaneous lobing feed is 90% complete.

b. Recent work. As described in Ref. 2, the Goldstone Venus site 30-ft antenna will be used as an AAS model for feed design work. A firm scale factor has been established as the ratio of focal lengths of the two reflectors; thus, the operating frequency has been set.

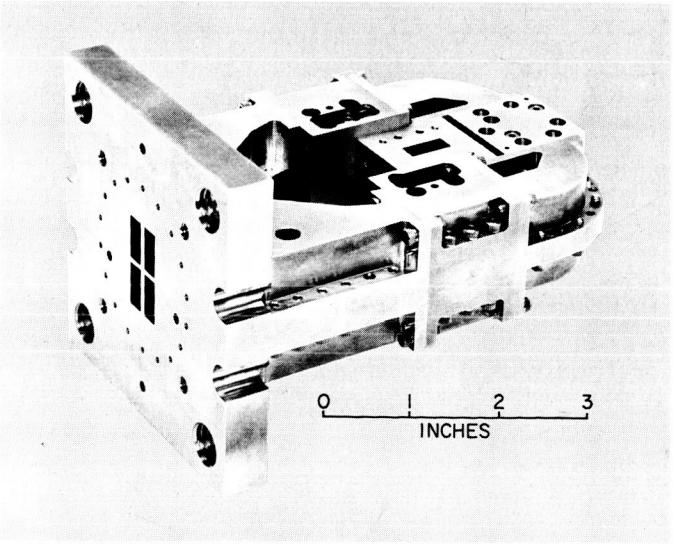

Fig. 11. K_u-band monopulse bridge

Fig. 10 shows the medium duty pedestal installed on the Mesa range, fitted with an x-y table and 16-ft support for rotating the Cassegrain assemblies. Amplitude and phase primary patterns are currently being obtained for the listening feed configuration; similar data will be taken on the simultaneous lobing feed configuration.

The linearly polarized monopulse bridge is shown in Fig. 11. A variety of mode generation/control sections and horns can be attached at the planar, four-port face as future developments in high efficiency feeds become available. The entire bridge is precision machined, using no castings nor extrusions, and is a model of an earlier X-band monopulse bridge developed at JPL.

Microwave hardware installation within the Cassegrain feed cone and on the 4-ft-diameter antenna has begun.

The decision has been made to operate the K_u-band equipment on the 30-ft antenna prior to delivery of the AAS scale quadripod in order to obtain preliminary data on the feeds. We anticipate that the measurements with the precise scale model configuration of the AAS quadripod will be conducted late this year.

References

1. "Advanced Antenna System," *SPS 37-27*, Vol. III, pp. 66–80, Jet Propulsion Laboratory, Pasadena, California, March 31, 1964.
2. "Scale Model Feed For AAS," *SPS 37-26*, Vol. III, pp. 72–75, Jet Propulsion Laboratory, Pasadena, California, March 31, 1964.

Erratum

The following correction should be noted for *SPS 37-27*, Vol. III: Page 26, Fig. 36 should appear as

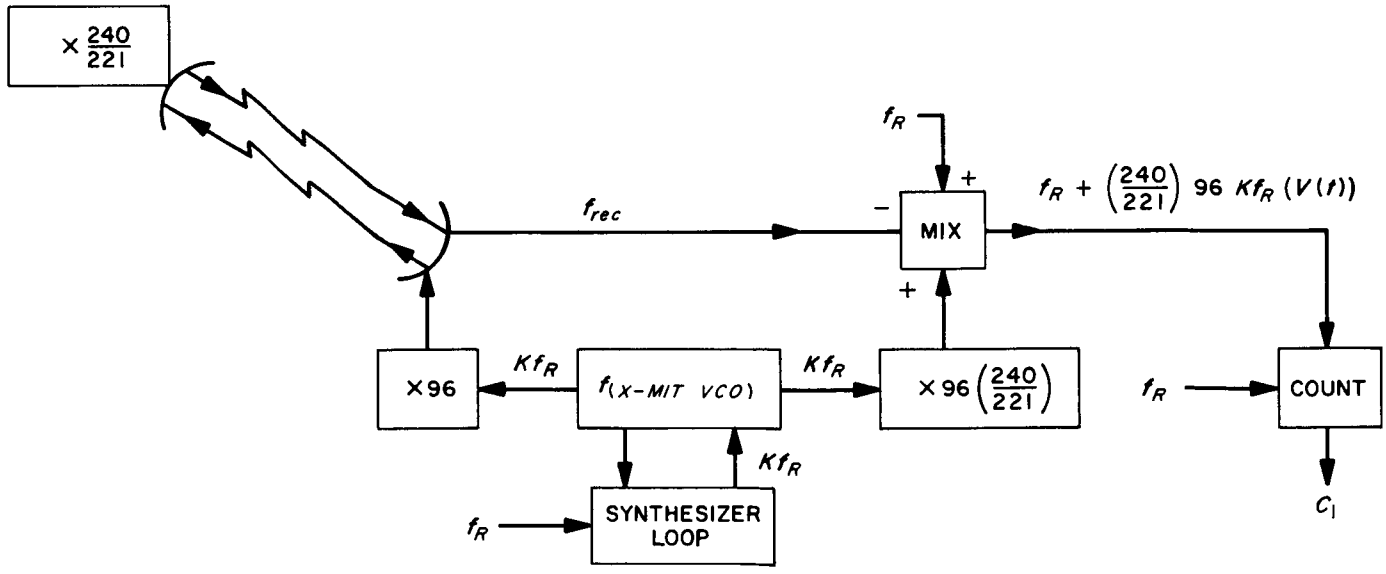

Fig. 36. S-band two-way mode